Photox and Certhrax: The characterization of novel mono-ADP-ribosyltransferase toxins

by

Danielle D. Visschedyk

A Thesis
presented to
The University of Guelph

In partial fulfilment of requirements
for the degree of

Doctor of Philosophy
in
Biophysics

Guelph, Ontario, Canada

ABSTRACT

PHOTOX AND CERTHRAX:
THE CHARACTERIZATION OF NOVEL MONO-ADP-RIBOSYLTRANSFERASE TOXINS

Danielle D. Visschedyk   **Advisor:**
University of Guelph, 2012   **Prof. Rod Merrill**

Pathogenic bacteria use an arsenal of toxic protein virulence factors to cause disease in host cells. The mono-ADP-ribosyltransferase (mART) toxins are a family of exotoxins produced by pathogens which contribute to a wide range of diseases including cholera, diphtheria and whooping cough. Specifically, mART toxins act by transferring ADP-ribose from NAD^+ to target proteins in host cells, altering or inhibiting target activity with deleterious downstream effects. Recently, *in silico* analyses have revealed two novel mARTs, Photox and Certhrax, from pathogenic organisms. Photox, from *Photorhabdus luminescens* was successfully expressed and purified from *E. coli* and was shown to target actin, specifically at Arg177. This covalent modification inhibits actin polymerization and leads to observed cytotoxicity in yeast cells. Photox has 35% identity with SpvB from *Salmonella enterica*, which allowed for a structural model to be built, showing the location of all characteristic mART active site components, and the binding site for potential inhibitors. Certhrax originates from *Bacillus cereus* G9241, implicated in a number of severe pneumonia cases. Certhrax shares 31% sequence identity with anthrax lethal factor from *Bacillus anthracis*; however, we demonstrated that the toxicity of Certhrax resides in the mART domain, whereas anthrax uses a metalloprotease mechanism. *In vivo* tests employing toxin gene expression in yeast, and receptor-mediated infection of mammalian, cells showed the extreme cytotoxicity of Certhrax

(LD$_{50}$ = 100 pg/mL against mouse macrophage cells), making it 60 times more toxic than its infamous counterpart, anthrax lethal factor. *In vitro* analysis indicated that Certhrax possesses NAD$^+$ glycohydrolase activity, characteristic of many mART toxins, but we continue to search for the natural host protein target of this toxic enzyme. We determined the crystal structure of Certhrax to 2.2 Å, which illustrates a close structural similarity with anthrax lethal factor. Furthermore, we identified several small molecule inhibitors which show protection against Certhrax both *in vitro* and *in vivo*. We determined a 1.9 Å crystal structure of one inhibitor in complex with Certhrax. Through identification and characterization of novel mART enzymes, we seek to better understand this family of toxic enzymes to aid in the discovery and development of more potent therapeutics.

Acknowledgements

Declaration of work performed

In some cases, it was necessary to include areas of a project where experiments were carried out by another scientist in order to write a complete story. All of the work contained in this thesis is my own, with the following exceptions: D. White performed all mutagenesis and cloning, except for the Photox-GFP fusions. Z. Turgeon and A. Rochon carried out the *in vivo* yeast and mammalian cell cytotoxicity assays. The β- and γ-actin were purified and provided by the Dawson lab. *In silico* modeling of Photox was done by R. Fieldhouse, but all analysis and figures were prepared by myself. The gel band-shift assay was done by A. Perieteanu. The Certhrax-PJ34 and apo-Certhrax structures were solved by members of the Structural Genomics Consortium, Toronto, but all analysis and preparation of figures was done by myself.

TABLE OF CONTENTS

LIST OF TABLES

LIST OF FIGURES

ABBREVIATIONS

ADP-ribose	Adenosine diphosphate-ribose
AMP	Adenosine monophosphate
ARTT motif	ADP-ribosyl-turn-turn motif
ATP	Adenosine triphosphate
BCIP/NBT	5-Bromo-4-chloro-3-indolyl phosphate/Nitro blue tetrazolium
BiFC	Bimolecular fluorescence complementation
BLAST	Basic local alignment search tool
βME	Beta-mercaptoethanol
βTAD	Beta-methylene-thiazole-4-carboxyamide-adenine dinucleotide
CDT	*Clostridium difficile* toxin
CHO	Chinese hamster ovary
CT	Cholera toxin
DAPI	4,6-diamidino-2-phenylindole
DEAE	Diethylaminoethyl
DIC	Differential interference contrast
DMEM	Dulbecco's modification of Eagle's medium
DNA	Deoxyribonucleic acid
DT	Diphtheria toxin
eEF2	Eukaryotic elongation factor 2
EF	Edema factor
εNAD+	Etheno-nicotinamide adenine dinucleotide
ExE motif	Catalytic Glu-x-Glu motif

F-actin	Filamentous actin
FBS	Fetal bovine serum
FDA	Food and Drug Administration (USA)
FITC	Fluorescein isothiocyanate
G-actin	Globular actin
GAP	GTPase activating protein
GDI	Guanine nucleotide dissociation inhibitor
GDP	Guanosine diphosphate
GEF	Guanine nucleotide exchange factor
GFP	Green fluorescent protein
GMP	Guanosine monophosphate
GTP	Guanosine triphosphate
IPTG	Isopropyl-1-thio-β-D-galactopyranoside
LC/MS/MS	Liquid chromatography/tandem mass spectrometry
LD50	Median lethal dose
LF	Lethal factor
MAPKK	Mitogen-activated protein kinase kinase
mART	Mono-ADP-ribosyltransferase
Mcf	Makes caterpillars floppy
MRSA	Methicillin-resistant *Staphylococcus aureus*
MTT	3-(4,5-Dimethylthiazol-2-yl)-2,5-diphenyltetrazolium bromide
NAD$^+$	Nicotinamide adenine dinucleotide
PA	Protective antigen

PARP	Poly-ADP-ribose polymerase
PBS	Phosphate-buffered saline
PEM	PIPES, EDTA, MgCl$_2$ buffer
PJ34	N-(6-Oxo-5,6-dihydrophenanthridin-2-yl)-(N,N-dimethylamino)acetamide hydrochloride
PKR	Protein kinase R
PN loop	Phosphate-nicotinamide loop
Q-TOF	Quadrupole time-of-flight
QxE motif	Catalytic glutamine-x-Glu motif
RNA	Ribonucleic acid
SDS-PAGE	Sodium dodecyl sulfate polyacrylamide gel electrophoresis
S$_N$1	Unimolecular nucleophilic substitution
S$_N$2	Bimolecular nucleophilic substitution
STRING	Search tool for the retrieval of interacting genes/proteins
STS motif	Serine-threonine-serine motif
T3SS	Type three secretion system
TB	Terrific broth
Tc	Toxin complex
TCEP	Tris-(2-carboxyethyl)-phosphine
TEV	Tobacco etch virus
UV	Ultraviolet
v$_{max}$	Maximum velocity
VIP2	Vegetative insecticidal protein

WT   Wild type

YFP   Yellow fluorescent protein

CHAPTER 1 - INTRODUCTION

According to the American National Institutes of Health, infectious diseases caused by microbes are responsible for more deaths worldwide than any other single cause (Fauci, 2001). In the United States alone, treatment of such infections costs approximately $120 billion annually. These microbes have an arsenal of toxic proteins to assist in invasion and dissemination. They work to modify host cell proteins to escape the immune system of a host organism and ensure their own survival, often killing the host cell. Clearly, pathogenic bacteria represent an important area of study in the context of human health. Here, we focus on a specific family of toxic enzymes produced by a wide variety of pathogenic bacteria, and contributing to a range of human diseases.

1.1 ANTIBIOTICS AND ANTIBIOTIC RESISTANCE

Bacterial infections are the primary cause of death in hospitals worldwide, and comprise a large fraction of infectious diseases. For decades, we have relied on traditional antibiotics to combat these bacteria, and the use of such compounds has led to a dramatic decrease in instances of death caused by bacterial infection. Since their discovery, these compounds have been improved for higher potency and better pharmacological properties, increasing the number of antibiotics available (Crowley & Martini, 2001). However, our toolkit of antibiotics consists of several variations on a small number of core compounds, while development and commercialization of novel broad-spectrum antibiotics is lacking (Fernandes, 2006, Projan, 2003, Talbot et al, 2006). The compounds in current use target a select few metabolic processes in the bacterium. For example, most current antibiotics target cell wall synthesis (β-lactams and glycopeptides), DNA replication (quinolones), or protein synthesis (macrolides). This

places the bacteria under immense selective pressure, and resistance to these drugs is increasing rapidly.

In addition to evolving resistance through environment challenge, bacteria may also acquire resistance genes to protect them from the drugs. When penicillin was introduced in 1943, nearly all bacterial infections were susceptible (Palumbi, 2001) and it was very effective as a therapeutic. By 1946, signs of resistance were observed, and higher doses or more potent drugs were required to control severe infections. Today, the vast majority of bacterial infections in a hospital setting do not respond to penicillin. More potent drugs have been developed in place of penicillin, but these have not been immune to resistance problems. This is best illustrated in the case of *Staphylococcus aureus* infection. Upon its discovery, penicillin readily killed *S. aureus*. In fact, it was on a petri dish of *S. aureus* cells that Sir Alexander Fleming first observed the antibacterial properties of *Penicillum* fungus. However, by 1950, more than half of *S. aureus* hospital infections were resistant to penicillin, and by 1960 this increased to 80% (Chambers & Deleo, 2009). This resistance is mediated by the production of penicillinase, which cleaves the β-lactam ring of the antibiotic. Consequently, in 1960, penicillinase-resistant antibiotics such as methicillin were introduced which would not be degraded. Yet, by 1961, resistance to methicillin was caused by an acquired *mec* operon, which encodes an alternative low-affinity penicillin-binding protein, allowing for resistance to all β-lactams. The prevalence of methicillin-resistant strains (MRSA) grew exponentially in the 1990s leading to the endemic state of today's hospitals. As a last resort, the glycopeptide antibiotic, vancomycin, is often used for its ability to disrupt cell wall synthesis in Gram-positive bacteria. Unfortunately, resistance to vancomycin was seen in

increasing numbers of bacterial species beginning in 1986, highlighting the need for new and immediate approaches to deal with bacterial infections (Palumbi, 2001). We can only assume that as new antibiotics are discovered and introduced into clinical practice, resistance will follow.

As a society, we contribute to this problem through the overuse of antibiotics in the form of unnecessary prescriptions and agricultural use. The indiscriminate environmental increase of these compounds leads environmental and zoonotic bacteria to harbour resistance genes. While this may not directly impact humans, these commensal organisms may transfer resistance genes horizontally to pathogenic bacteria. In fact, some experts predict that without radically new ways to deal with bacterial infections, we may be entering into a "pre-antibiotic era". Compounding the problem, the relative ease with which bacteria acquire resistance eliminates the incentive for large pharmaceutical companies to tackle research into new antibiotics (Projan, 2003). Profits cannot be generated if bacteria are resistant to a drug within a few years, and companies gain greater profit by working on treatment of more chronic illnesses.

1.2 VIRULENCE FACTORS AND ANTIVIRULENCE THERAPIES

By contrast, antivirulence therapies aim to disarm or inactivate the pathogen without introducing selective pressure for the organism's survival. Consequently, bacterial resistance should be much less prevalent than with traditional antibiotics, and the bacteria less toxic to humans. Several specific mechanisms that promote infection are commonly targeted. Firstly, adhesion of the bacteria to a host cell is a crucial first step in most infection processes. Bacterial adhesin proteins, often complexed into

4

heteropolymeric extracellular pili or fimbriae, bind to ligands or receptors of a target cell. Strategies to disrupt this initial bottleneck step include using derivatives of the host ligand to block the bacterial adhesion proteins, or using inhibitors to block pili biogenesis by chaperones; a broader-range tactic. Second, specific secretion systems such as Type III secretion (T3SS) are elements which can be disrupted to decrease infection rates. This system coordinates the delivery of virulence factors from the bacterial cytoplasm directly into the host cell cytoplasm via a molecular syringe. Some components of the T3SS machinery are conserved, making them ideal targets for broad-range therapeutics. Indeed, several small-molecule inhibitors of the T3SS have been described for *Yersinia pseudotuberculosis*, and also show inhibition in *Chlamydia trachomatis* (Kauppi et al, 2003, Nordfelth et al, 2005, Wolf et al, 2006). Third, bacteria use quorum sensing as a mechanism of determining their cell density. This chemical signaling by production and recognition of small molecule autoinducers helps to regulate bacterial group behaviours such as motility and biofilm formation. Quorum sensing may also regulate the release of virulence factors, and in *Pseudomonas aeruginosa*, more than 30 quorum sensing-regulated virulence factors are known. Recent work to inhibit quorum sensing determined several compounds that caused increased susceptibility of the bacteria to antibacterial agents and host defenses, indicating that further development of these compounds may be helpful as an early treatment of individuals with a *P. aeruginosa* infection (Bjarnsholt & Givskov, 2007, Hentzer et al, 2003). Lastly, the bacterial virulence factors themselves are attractive targets for antivirulence therapeutics. These bacterial toxins are often extremely toxic and the major cause of cellular failure and morbidity in affected individuals. They may be inhibited at several steps along their infection pathway including inhibition of

toxin gene transcription, as in the case of virstatin and *Vibrio cholerae* (Hung et al, 2005), neutralization by treatment with antibodies, as in the case of adult cases of botulism, caused by *Clostridium botulinum*, or the use of small molecule inhibitors to bind intracellularly and arrest toxin function. Each of these methods presents antivirulence approaches that will not challenge bacterial survival in the same way as traditional antibiotics. Most of these approaches are in the early stages of development, and have either not yet passed clinical trials, or have serious side effects for humans. The work to date shows that the problem of treating bacterial infections using this approach is not trivial, as all virulence factors have different mechanisms of entry and toxicity. It is evident that a more thorough understanding of toxin biochemistry and pathogenesis is necessary for development of more effective therapeutics.

1.3 BACTERIAL TOXINS

In general, bacterial toxins are soluble proteins which modify the natural metabolism of host cells with harmful effects on the host (Schmitt et al, 1999). Multiple modes of action exist for these toxins, making them an important area of study in order to understand their function and to determine methods of prevention and treatment. In the case of pore-forming toxins, such as streptolysin O from *Streptococcus pyogenes* and many hydrolyzing enzymes, the toxins damage the plasma membrane or extracellular matrix of eukaryotic cells, leading to host cell lysis and ease of toxin spread among other tissues (Bhakdi et al, 1996). Other toxins inhibit protein synthesis by targeting elongation factors and ribosomal RNA. Examples include diphtheria toxin and *Pseudomonas aeruginosa* exotoxin A, and this inhibition eventually results in host cell death (Jorgensen

et al, 2006). In some cases, bacterial toxins may not be directly responsible for cell death, but may instead disrupt signal transduction pathways to cause malfunction of cellular events or machinery. Heat-stable toxin from enterotoxinogenic *Escherichia coli* causes stimulation of membrane-bound guanylate cyclase, leading to an increase in intracellular cyclic GMP, which affects electrolyte flux in the bowel causing diarrhea (Sack, 2011). These few examples serve to illustrate that microbial toxins have many ways to interrupt essential functions of eukaryotic cells, and research on these bacterial enzymes is crucial work on the path to treating bacterial infections more efficiently.

1.4 MONO-ADP-RIBOSYLTRANSFERASE TOXINS

The mono-ADP-ribosyltransferase toxins (mARTS) are principle causative agents in a number of diseases including whooping cough, diphtheria, and cholera, and a contributing factor in many others. In general, these toxins act by cleaving intracellular NAD^+ and facilitating the covalent attachment of the ADP-ribose group of NAD^+ to a cellular target, impairing target function. Often, the host target is a major regulatory protein and its modification by toxin will disrupt cellular signaling or other processes. Although the general reaction remains the same, a number of different targets are used by mART toxins, resulting in various cellular consequences. For example, in the cases of cholera toxin and *E. coli* heat-labile enterotoxin, $G_{\alpha S}$ of the adenylate cyclase system is ADP-ribosylated, trapping it in its GTP-bound state (Galloway et al, 1987). This leads to a huge up-regulation of adenylate cylase, an increase in cytosolic cyclic AMP, and a massive loss of fluids and ions from affected intestinal cells (Field et al, 1989, Peterson & Ochoa, 1989). Pertussis toxin from *Bordetella pertussis* also targets small G-proteins,

resulting in uncoupling from their effectors and a corresponding increase in adenylate cyclase and cyclic AMP levels (Katada et al, 2005, Katada & Ui, 1982, West et al, 1985). Pertussis toxin receptors are found on many cell types and the resulting physiological effects vary in each tissue.

Traditionally, mART toxins have been divided into the diphtheria-like (DT) and cholera-like (CT) groups. The DT group of toxins includes diphtheria toxin (DT) from *Corynebacterium diphtheriae*, exotoxin A of *Pseudomonas aeruginosa* and cholix toxin from *Vibrio cholerae* which covalently modify eukaryotic elongation factor 2 (eEF2). Specifically, they modify a diphthamide residue in eEF2 to disrupt protein synthesis leading to cell death (Jorgensen et al, 2006, Van Ness et al, 1980). The CT group includes all other mART toxins and is commonly subdivided further. This study is primarily concerned with two specific subgroups of CT toxins: the C2-like toxins, and the C3-like toxins, which are further described below. These subgroups are formed based on host protein target, as well as structural characteristics of the toxins.

1.4.1 The mART reaction

All functionally characterized mART toxins facilitate the covalent attachment of an ADP-ribose group from NAD^+ to a host target protein (Figure 1.1). In addition, some mARTs also have a residual glycohydrolase activity, by which the cleavage of NAD^+ into nicotinamide and ADP-ribose occurs in the absence of the target protein, instead using water as a substrate. This glycohydrolase activity is not strictly conserved among the family of mART toxins, but in cases where the host substrate is not known, it may be useful in the characterization of a toxin.
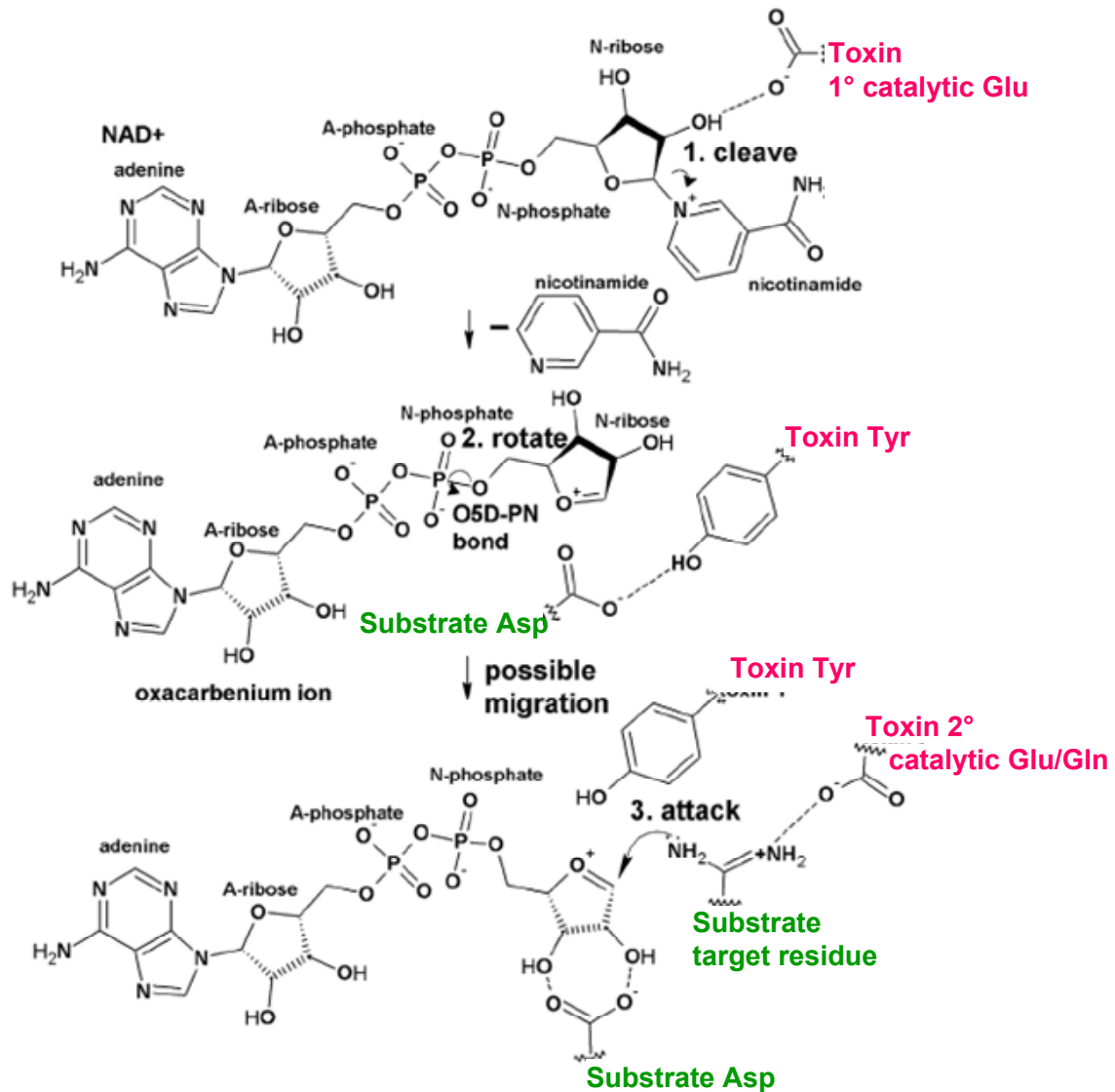
Figure 1.1. Basic reaction mechanism of mART toxins. Toxin residues are annotated in pink, while substrate residues are in green. First, the nicotinamide group is cleaved and represents the leaving group (Step 1). The remaining oxacarbenium ion is stabilized by the primary catalytic Glu, and is open to nucleophilic attack from a protein target. Rotation about the O-P bond of the nicotinamide phosphate relieves strain and brings the ADP-ribose in closer proximity to the target substrate residue (Step 2). The subsequent nucleophilic attack (step 3) results in the covalent modification of the protein with an ADP-ribose moiety (modified from Fieldhouse et al, 2010).

Although both S_N1- and S_N2-type reactions have been proposed for the mART toxin reaction, the most recent biochemical data suggest that it follows an S_N1 reaction mechanism. In this reaction, the nicotinamide of NAD^+ represents the leaving group, and the cleavage of the glycosidic bond between ADP-ribose and nicotinamide results in a positively charged oxacarbenium ion intermediate. A rotation of the intermediate around an O-P bond at the nicotinamide phosphate relieves strain, and forms a second intermediate. Nucleophilic attack by a target residue results in covalent ADP-ribose modification at this residue. A number of key catalytic toxin residues play a role in this reaction mechanism. The conserved primary catalytic Glu H-bonds to the nicotinamide ribose and the conserved Region 1 Arg forms phosphate electrostatic interactions to hold together the NAD^+ in a conformation that favours the oxacarbenium ion intermediate. This intermediate is further stabilized by a Ser residue of the STS motif. The ADP-ribose stays bound to the toxin until the nucleophilic attack has occurred. A conserved Tyr may induce the rotation of the nicotinamide ribose ring to alleviate strain and to bring the electrophile in closer proximity to the nucleophile. The secondary catalytic Glu is in place to stabilize the target nucleophile, while a target Glu or Asp may help to stabilize the nearby ribose group.

Some researchers have argued that an S_N2 reaction mechanism is also possible (Bell & Eisenberg, 1997a, Wilson et al, 1990), whereby a deprotonated nucleophile attacks the carbon of the ribose ring, forming a pentacoordinate oxacarbenium transition-state intermediate. However, the S_N1 mechanism seems to be favoured by available biochemical data (Bell & Eisenberg, 1997a; Armstrong and Merrill, 2004; Jorgensen et al, 2005; Jorgensen et al, 2008; Zhou et al, 2004) as well as a Michaelis complex crystal

structure involving exotoxin A, eEF2, and an NAD$^+$ analogue, βTAD (Jorgensen et al, 2005). A thorough understanding of the reaction mechanism will allow for clear identification of transition states involved, and the ability to develop transition-state analogues as small-molecule inhibitors.

1.4.2 Structural mART family characteristics

mART toxins are often difficult to identify by popular *in silico* methods due to the low primary sequence similarity within the family. A simple BLAST search generally fails to identify all but the most closely related mARTs. However despite the lack of overall sequence similarity, the toxins share a core three-dimensional fold. Throughout each mART subgroup, the core catalytic domain consists of a mixed α/β structure with dimensions of approximately 35 × 40 × 55 Å. This core structure consists of two main β-sheets flanked by a varying number of α-helices. The NAD$^+$ binding site is contained within this core structure and is always bordered on one side by a β-sheet, and by either an α-helix or a loop on the other side (Holbourn et al, 2006). Even within this mART core of roughly 100 residues, sequence identity is low. However, a number of active site residues are highly conserved, and have been shown to play specific crucial roles in the reaction (Figure 1.2). Several of these key regions are highlighted below:

i. The ARTT motif

The so-called ADP-ribosyltransferase turn-turn (ARTT) motif is a loop region connecting either two β-sheets in the active site, or a β-sheet with an α-helix. It contains the primary catalytic Glu residue, required for activity by all mART toxins. In addition, all but the
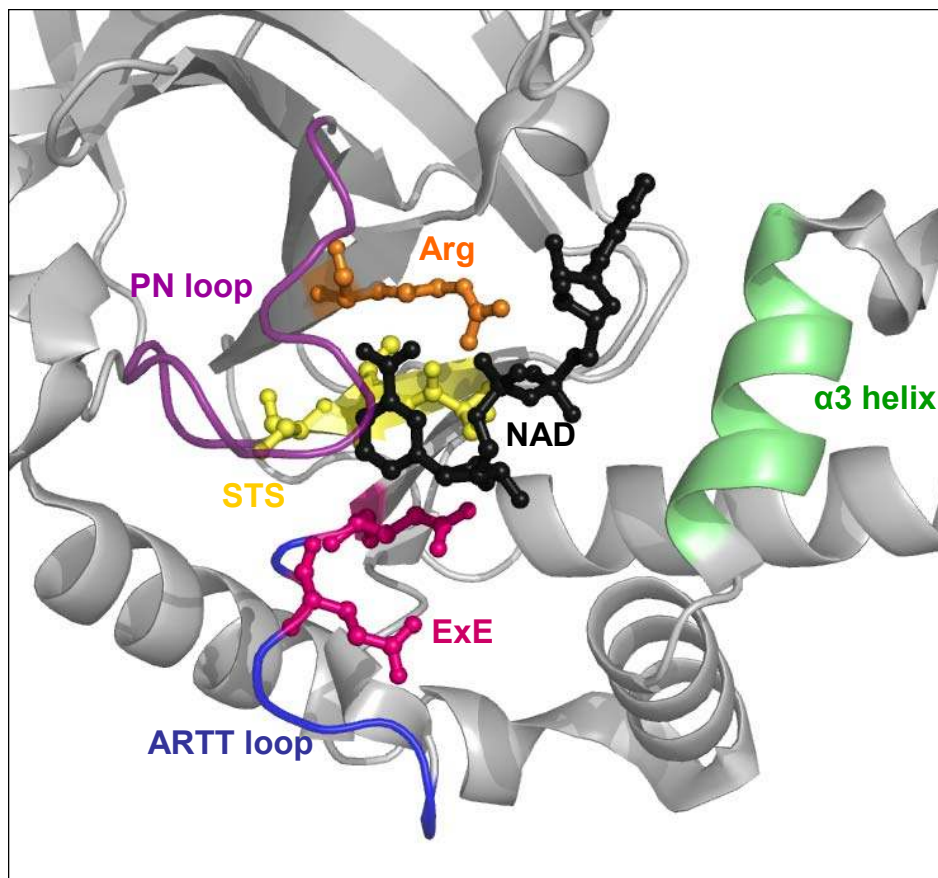
Figure 1.2. Representative active site of mART toxins. The Iota toxin active site (PDB: 3BUZ) is shown in grey in cartoon format, with conserved catalytic residues shown in ball-and-stick format in colour. The catalytic Arg (orange), STS motif (yellow), and catalytic Glus (pink) border NADH (black). The ARTT loop (blue), PN loop (purple) and α3 helix (green) flank the active site.   .

DT-like mARTs contain a secondary catalytic Glu or Gln two positions upstream of the primary Glu. This secondary residue has been shown to be required for transferase activity, but not necessary for glycohydrolase activity (Nagahama et al, 2000, Wilde et al, 2002). In addition, this loop is expected to play a substantial role in substrate recognition. Indeed, the single point mutation of this secondary Gln residue to a Glu resulted in the change of the C3lim toxin target from an Asn to an Arg residue (Vogelsgesang & Aktories, 2006). A sequence alignment shows that toxins which modify an Arg residue contain a Glu at this position, while those that target an Asn residue include a Gln at the site. Furthermore, the C2- and C3-like toxins include an aromatic residue in the ARTT loop that is required for binding of Rho to the toxin, and may play a role in other toxins as well (Han et al, 2001, Wilde et al, 2002).

ii. The STS motif

Within the NAD^+ binding site, CT group mART toxins contain a pattern of *aromatic-hydrophobic-Ser-Thr-Ser* which forms the scaffold of the binding site (Domenighini & Rappuoli, 1996). The first Ser residue is required for mART activity and hydrogen bonds with the catalytic Glu and a Tyr residue to hold the Glu in place for the reaction (Evans et al, 2003, Han et al, 1999, Han et al, 2001). The threonine residue forms additional hydrogen bonds with neighbouring β-strands to brace the active site, while the latter Ser forms hydrogen bonds with a subsequent loop and with the secondary catalytic Gln (Han et al, 2001). In DT group members only, the STS motif is replaced by a pair of Tyrs which interact through π ring stacking to scaffold the active site (Bell & Eisenberg, 1997b, Li et al, 1996).

iii. The catalytic Arg

A conserved Arg residue is found in all CT group toxins, preceded by a Val/Leu and an aromatic residue. Although this Arg does not play a direct role in transferase activity, mutation of this residue decreases or abolishes activity due to its role in binding NAD^+ and other active site elements (Domenighini & Rappuoli, 1996, O'Neal et al, 2005, Tsuge et al, 2003).

iv. The PN loop

The C2- and C3-like toxins include a phosphate-nicotinamide (PN) loop directly following the STS motif. It contains an Arg which bonds with a phosphate group of NAD^+ and an aromatic residue involved in ring stacking with the nicotinamide of NAD^+ (Menetrey et al, 2002). The loop often undergoes a large movement upon NAD^+-binding to allow these contacts. The DT group toxins contain a homologous aromatic residue, but lack the Arg, whereas the remaining CT toxins function without either of the PN loop elements.

v. The α-3 motif

The C2- and C3-like mARTs contain an α-3 helix flanking the NAD^+ binding pocket (Evans et al, 2003, Han et al, 1999, Han et al, 2001, Tsuge et al, 2003). The conserved sequence, *Y-$X_{6/7}$-N-X_2-L-R/I*, aids in active site stabilization with conserved residues forming hydrogen bonds with the STS motif, the catalytic Glu, and NAD^+ (Holbourn et al, 2006). Mutations in several of these residues have led to a decrease in both glycohydrolase and mART activity (Tsuge et al, 2003). Other mART toxins contain a loop region in place of the α-3 motif.

1.5 ACTIN-TARGETING MART TOXINS

A large subgroup of mART toxins covalently modify actin within host cells, disrupting actin's cellular functions. These ten mARTs are classically divided into binary and non-binary actin-targeting toxins, each of which is described below. Actin's dynamic reversal between globular and filamentous states allow it to fulfill a variety of roles within the cell, including involvement in innate immunity (Irving et al, 2012). Consequently, actin is an attractive target for invading bacteria.

1.5.1 Introduction to actin

The cytoskeletal protein, actin, is a highly conserved eukaryotic protein with a role in a multitude of cellular processes. Actin commonly exists as both a monomer (globular, or G-actin), and as a filament (filamentous, or F-actin). Its ability to self-associate into long double-stranded helical polymers is crucial for the protein's diverse functions such as intracellular trafficking, cell motility, and muscle contraction (Aktories et al, 2011). The formation of an actin dimer from two free monomers is the rate-limiting step in actin filament formation, followed by the addition of a third monomer to form a trimer nucleus. F-actin filaments are elongated from this nucleus in an ATP-dependent process until a steady-state is reached (Sept & McCammon, 2001). It is this ability to self-associate that also makes the structure of actin quite difficult to study. The numerous different filament lengths which may exist at any one time preclude any efforts to crystallize F-actin. Instead, polymerization-deficient actin variants have been used to determine the structure of the actin monomer (Kabsch et al, 1990, Margarit et al, 2006,

Otterbein et al, 2001), and X-ray fibre diffraction has been used to obtain the most recent model of the actin filament (Oda et al, 2009).

1.5.2 Mono-ADP-ribosylation of actin

Actin-targeting mART toxins modify actin at Arg177 which is found at the interaction site between actin monomers in an F-actin filament. The ADP-ribosylated actin effectively becomes a "capping protein", disrupting the classical polymerization/ depolymerization cycle of actin within a host cell (Wegner & Aktories, 1988, Weigt et al, 1989). Several studies have shown that the modification is reversible, and in the presence of excess nicotinamide, the ADP-ribosylation can be removed and actin can regain its ability to polymerize (Just et al, 1990, Perieteanu et al, 2010). Recent work with *Clostridium difficile* toxin (CDT) has shown that the toxin's ADP-ribosylation of actin has an effect on the dynamic regulation of microtubules and associated proteins. These changes in microtubule formation lead to increased binding of invading bacteria to a host cell, and may indicate a role in host-pathogen interaction for these toxins (Schwan et al, 2009). Studies with an antiviral protein kinase R (PKR) showed that the regulation of actin-modifying proteins during the innate immune response can change the level of cellular defense against intracellular pathogens (Irving et al, 2012). Since a major component of resistance is based on structural defense, actin plays a key role. The actin cytoskeleton is crucial for the reorganization of the cell membrane, arrangement of receptors, recruitment of cell-signalling intermediates, endocytosis and phagocytosis, so it seems obvious that the disruption of actin function by a mART toxin may have a distinct role in altering host-pathogen interactions as well.

Each actin-targeting mART toxin includes the conserved catalytic Arg residue and the STS motif (Figure 1.3). Furthermore, the catalytic Glu is always preceded two residues upstream by a second Glu to give an E-x-E motif. The first Glu is part of the ARTT motif involved in substrate recognition and is required for ADP-ribosylation of the actin Arg residue. This differs from the QxE motif found in the same location in other mART toxins, which do not target an Arg residue.

The exception to the actin modification at Arg177 is TccC3, part of a toxin complex from *P. luminescens*. This bacterium produces many toxins which have not all been characterized. TccC3 ADP-ribosylates actin at Thr148 to increase polymerization, instead of forcing depolymerization like other mART toxins (Lang et al, 2010). The location of this ADP-ribosylation disrupts the binding of the peptide, β-thymosin, which generally sequesters G-actin to inhibit the usual salt-induced actin polymerization. As a result, an increase in actin polymerization is observed in TccC3-treated cells (Lang et al, 2010). Since it does not function in the same way as the other actin-targeting toxins, this is not considered a classical C2-like mART toxin, and may be a unique actin-targeting toxin, or part of a subgroup not yet described.

1.5.3 Binary actin-targeting mARTs

To date, ten mART toxins have been identified that mono-ADP-ribosylate actin and disrupt actin polymerization. Most of these are binary toxins consisting of an A subunit with mART enzymatic activity and a B subunit responsible for binding/translocation. The clostridial binary actin-targeting toxins were among the first mARTs studied. *C. perfringens* Iota (Vandekerckhove et al, 1987), *C. botulinum* C2

α8   α9   α10

C2I

```
         10              20                          30            40          50
C2I    LGALEGYLHSDYKAINSYLRNN......................R..VPNNDBLNKKIELISSAL....SV
Iota   LADVNDYMRGGYTAINNYLISN....................GPLNNPNPBLDSKVNNIENAL....KL
Sa     LAGVNDYMRGRYTAINNYLIAN....................GPTNNPNABLDAKINNIENAL....KR
CdtA   LADVNDYMRGGYTAINNYLISN....................GPVNNPNPBLDSKITNIENAL....KR
Vip2   REALDGYARQDYKEINNYLRNQ....................GG..NGNEKLDAQIKNISDAL....GK
SpvB   ..........KYLRGDDYPETQAKETLLSRDYLSTNEPSDEEFKNAMSVYINDIAEGL....SS
Photox LQALRYYSAQGYNLINTYLRGGEYVKHQAIETLLSRNYLHSNEPTPQEFDAGMRAYIQDVTEGL....NE
AexT   VMALGLYTNGEYQHLNRSLRQ.............................EKQLDAGQALIDQGMSAAFEK
VgrG1  DEALRYYSAQGYTLLNNYLRDRPYKQREAIDTLLSRSYLNDEPTSASEFDQAMKAYVADVEAGL....AK
```
α3

β9   η5   TT   β10   β11   α11   β12   β13

C2I

```
         60              70              80         90         100        110
C2I    K.PIPQTLIAYRRVDGIPFDLPSDFSPDKKENGEIIADKQKLNEFIDKWTGKBIENLSFSSTSLKST.PS
Iota   T.PIPSNLIVYRRSGPQEFGLTLTSPEYDF......NKIENIDAFKEKWEGKVITYPNFISTSIGSVNMS
Sa     E.PIPANLVVYRRSGPQEFGLTLSSPEYDF......NKVENIDAFKEKWEGQTLSYPNFVSTSIGSVNMS
CdtA   E.PIPTNLTVYRRSGPQEFGLTLTSPEYDF......NKLENIDAFKSKWEGQALSYPNFISTSIGSVNMS
Vip2   K.PIPENITVYRWCGMPEFGYQISDP..........LPSLKDFEEQFLNTIKEDKGYMSTSLSSERLA
SpvB   L.PETDHRVVYRGLKLDKPA................LSDVLKEYTTIGNIIIDKAFMSTSPDKAW..
Photox L.AITDHKKVYRGLKFDKSE................LKNLLDQYTTEGNIIAEKGFLSTSPDKAW..
AexT   STPAEQLVKTFRGTHG....................GDAFSGVTEGQVGHDTAYFSTSRDPKVAT
VgrG1  LPASPDLDFVYRGLALDKPE................LAALKDQFTGVGNIIVEPGFMSTSPDKAW..
```
↑ Arg   STS ↑   PN

η6   β14   TT   β15   TT   TT   β16

C2I

```
        120         130         140         150
C2I    SFSKSRFIPRLRLSEGAICAPIYGFSGPQDEQEILLNKN.............
Iota   AFAKRKIILRINIPKDSPGAYLSAIPGYAGEYFVVLNHG.............
Sa     AFAKRKIVLRISIPKNSPGAYLSAIPGYAGEYFVVLNHG.............
CdtA   AFAKRKIVLRITIPKGSPGAYLSAIPGYAGEYFVVLNHG.............
Vip2   AFGSRKIIILRLQVPKGSTGAYLSAIGGFANEKEILLDKD.............
SpvB   ...INDTILNIYLBKGHKGRILGDVAHPKGEALMFFPPN.............
Photox ...VNDTILVINLESGHKGRILGDAAHPKGEALMFFPPESKMLVEKVLNRDDKEFDSHFSNLRLTDDASA
AexT   SFGGSG...TISTVFGRSGIDVSDISVEGDEQEILYNKA.............
VgrG1  ...VNDTLLRIRLPAGHGGRLLGEAAHPKGEALMFFPTQTRLRVDRVVSSMSGDFDSLLNTIPTSDN.A.
```
ARTT   ↑↑ExE

β17

C2I

```
        160
C2I    ..STF...........K
Iota   ..SKF...........K
Sa     ..SKF...........K
CdtA   ..SKF...........K
Vip2   ..SKY...........H
SpvB   ..TKL...........K
Photox DTTRI..KRIINIKMLNE
AexT   ..TDM...........R
VgrG1  ..SDNRSRIKRLIEVSVL
```

Figure 1.3. Multiple sequence alignment of catalytic domains of C2-like mART toxins. Alignment was done using Expresso (Armougom et al, 2006) and visualized using ESPript (Gouet et al, 1999). Identical residues are highlighted in red, and homologous residues in red text, including the ARTT motif (blue box), ExE motif (pink arrows), STS motif (yellow arrows), PN loop (purple box) and α3 motif (green box). Colours correspond to the corresponding regions in Figure 1.2.

(Aktories et al, 1986), *C. spiroforme* Sa (Popoff & Boquet, 1988), and *C. difficile* CDTa (Gulke et al, 2001) along with *Bacillus cereus* vegetative insecticidal protein (VIP2) (Han et al, 1999) function in this binary fashion. Structurally, the enzymatic component resembles two structurally similar domains, but lacks the catalytic residues in the N-terminal domain. C2 serves as the prototypical actin-targeting mART toxin, and has been well studied. The binding component (C2II) requires proteolytic cleavage for activation before the formation of heptamers, which bind at the cell surface (Barth et al, 2000, Ohishi, 1987). The mART enzyme component C2I binds to the heptameric C2II to allow endocytosis. A conformational change is triggered by the low pH of the endosome and several loops form a β-barrel through which the mART domain can pass through to the cytoplasm to undertake its toxic function. The binding components of Iota, Sa and CDT are highly similar and can be exchanged to carry out their binding and translocation function with one another's toxic subunits, while the C2 toxins specifically require their own binding component for proper translocation (Richard et al, 1999). A recent structure of Iota toxin in complex with NAD^+ and actin showed that Iota toxin binds to actin through five loops of the enzyme including the PN loop and ARTT loop. Interestingly, the N-terminal domain of the toxin was also found to be involved in the interaction with actin (Tsuge et al, 2008). The structural similarity among binary actin-targeting toxins provides hope that small molecule inhibitors of one enzyme might be effective against other toxins of this group.

1.5.4 Non-binary actin-targeting mARTs

The remaining actin-targeting mARTs do not fit this architecture. Since they do not have the separate enzymatic A and B subunits, these non-binary mARTs must have alternative mechanisms of host cell entry. SpvB of *Salmonella enterica* is a 594 residue protein which gains entry to target cells by the type III secretion system (T3SS). SpvB modifies actin at Arg177, and was shown to be required for *Salmonella* virulence (Lesnick et al, 2001, Margarit et al, 2006). Likewise, *Aeromonas salmonicida* AexT uses a T3SS for invasion of host fish cells. This mART toxin carries a second functional domain with Rho-GTPase activating (GAP) activity (Fehr et al, 2007, Vilches et al, 2008), reminiscent of the well-characterized ExoS expressed by *Pseudomonas aeruginosa*. Both enzymatic activities work in tandem to prevent actin polymerization. Although most non-binary mARTs share identity in key catalytic regions with other actin-targeting mARTs, AexT contains an extra residue in its catalytic Glu motif, with the sequence ExxE instead of the usual ExE for Arg-targeting mARTs. VgrG1 from *Aeromonas hydrophila* was first described as a mART toxin in 2010, and was shown to gain host cell entry via a type VI secretion system (Suarez et al, 2010), where it then targets actin and disrupts actin polymerization causing cell rounding and apoptosis. *Streptococcus pyogenes* SpyA (Coye & Collins, 2004) is a single-domain mART that does not fit neatly into either the C2- or C3-like subgroups of mART toxins. Like classical actin-targeting toxins, SpyA modifies actin, but also a variety of other substrates such as vimentin and tropomyosin. It modifies protein substrates at Arg residues like other C2-like toxins. However, its 25 kDa size, high pI (9.1), lack of a known eukaryotic binding protein, and highest sequence identity with C3 enzymes, make it a candidate for a

unique member of the C3-like subgroup as well. Overall, these non-binary actin-targeting toxins share less than 25% sequence identity with other actin-targeting mARTs (compared with up to 96% sequence identity for binary toxins with one another), but their conserved core catalytic domain may allow single therapeutics to be efficient across the actin-targeting family. Futher studies will be required to investigate this possibility. Enzymes such as SpyA and TccC3 remind us that classification of mART toxins is not always straightforward, and that this family of enzymes includes a number of variations which make them more difficult to study and inhibit.

1.6 C3-LIKE MART TOXINS

The C3 mART toxins are a second large subgroup of mARTs that target Rho proteins at a surface-accessible Asn residue (Sekine et al, 1989). To date seven C3-like exoenzymes target RhoA, B, and C at Asn 41, inhibiting the function of these low molecular weight GTPases. The prototype of this subgroup, C3bot1 from *C. botulinum* was first discovered over 20 years ago (Aktories et al, 1987, Aktories et al, 1988, Rubin et al, 1988), along with the highly similar C3bot2 (Nemoto et al, 1991). These toxins are not restricted to *C. botulinum*, and the rest of the subgroup includes C3lim from *C. limosum* (Just et al, 1992), C3cer from *B. cereus* (Just et al, 1995), and three exoenzymes from *S. aureus*, C3stau1, C3stau2, and C3stau3 (originally named EDIN-(A-C)) (Inoue et al, 1991, Wilde et al, 2001, Yamaguchi et al, 2001). These enzymes all share between 35-77 % identity with one another (Vogelsgesang & Aktories, 2006). A sequence alignment (Figure 1.4) shows that all components of the mART active site are highly conserved, including the catalytic Arg and the STS motif. Throughout this subgroup the ARTT loop
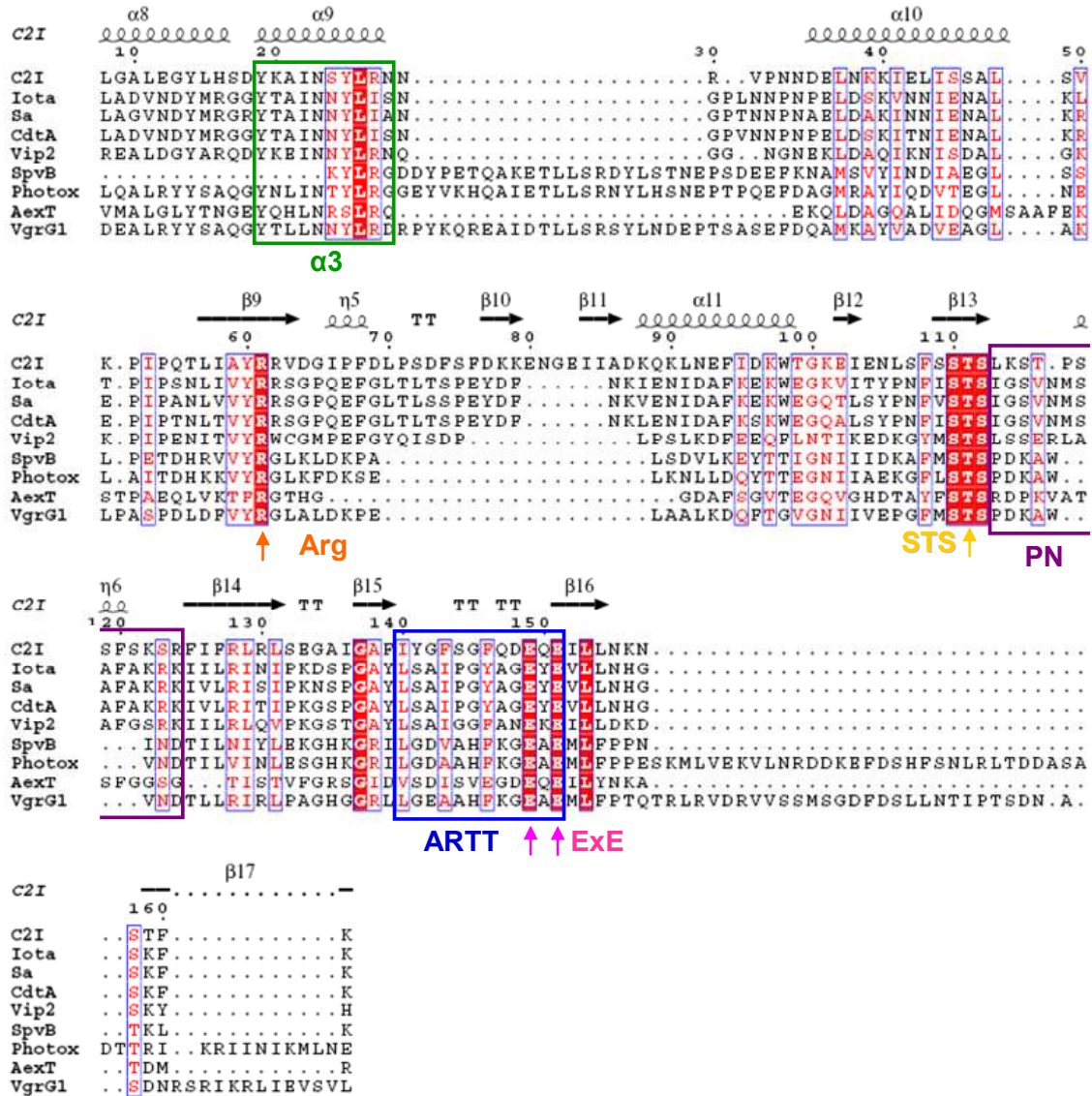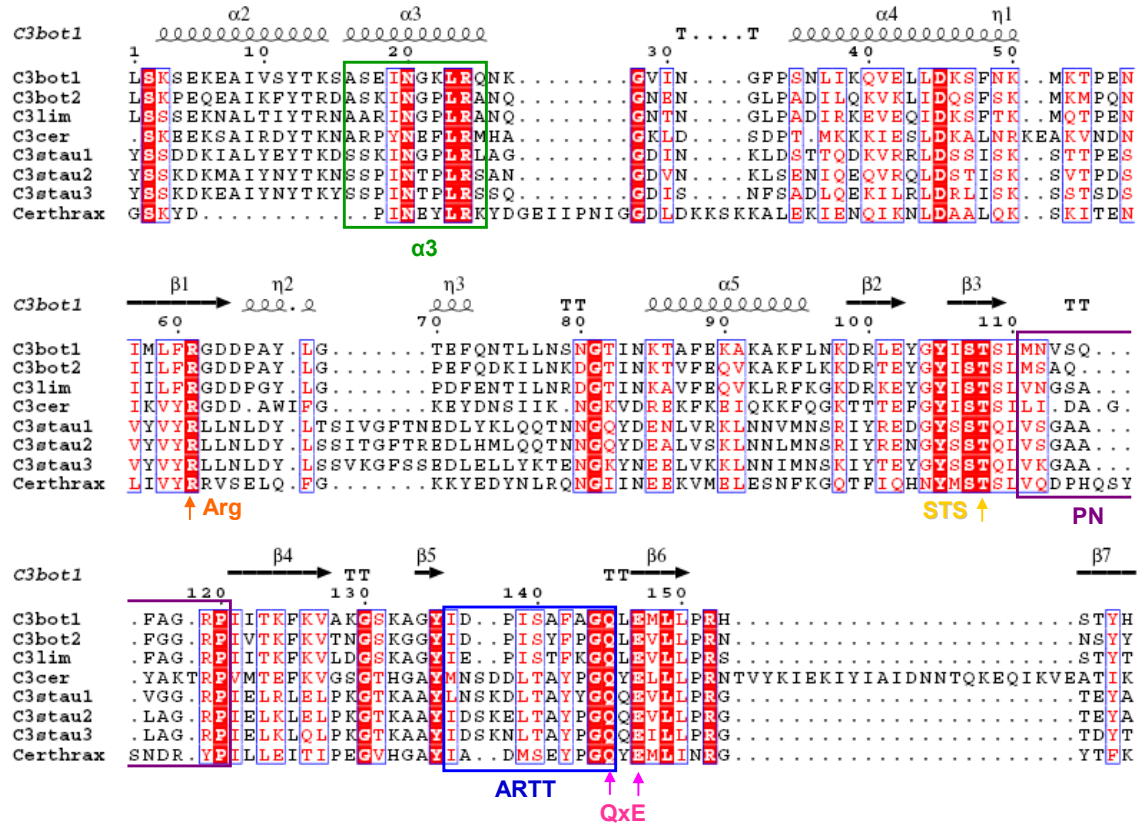
Figure 1.4. Multiple sequence alignment of catalytic domains of C3-like mART toxins. Alignment was done using TCoffee (Armougom et al, 2006) and visualized using ESPript (Gouet et al, 1999). Absolutely conserved residues are highlighted in red, and highly conserved residues in red text, including the ARTT motif (blue box), QxE motif (pink arrows), STS motif (yellow arrows), PN loop (purple box) and α3 motif (green box). Colours correspond to identical regions in Figure 1.2.

contains a QxE motif instead of the ExE pattern of actin-targeting toxins. This QxE motif is known to be preferred when the target residue is not an Arg. Unlike the actin-targeting subgroup, all C3-like mARTs exhibit NAD^+ glycohydrolase activity in the absence of a protein substrate.

1.6.1 Protein substrates of the C3 subgroup

All C3-like enzymes target RhoA, B, and C with high specificity, and some also ADP-ribosylate other Rho-family proteins with lower affinity. For example, Rac is targeted weakly by C3bot, Cdc42 by C3lim (Just et al, 1992, Wilde et al, 2003), and RhoE and Rnd3 by the C3stau toxins (Wilde et al, 2001). Rho proteins constitute a subset of more than 20 proteins of the Ras family of GTP-binding proteins. They act as molecular switches in the regulation of numerous signaling pathways. In particular, Rho proteins play a role in actin cytoskeleton regulation, contributing to smooth muscle contraction, phagocytosis, and other cellular processes (Bishop & Hall, 2000, Etienne-Manneville & Hall, 2002). A Rho protein is in its active form when bound to GTP. Hydrolysis of bound GTP to GDP by GTPase activating proteins (GAPs) renders the Rho inactive. The inactive Rho-GDP can then be sequestered out of the membrane by guanine nucleotide dissociation inhibitors (GDIs). Conversely, membrane bound Rho-GDP can be activated by the conversion of GDP to GTP by guanine nucleotide exchange factors (GEFs), and in its active form will interact with a number of effector proteins to fulfill its role in signaling. Mono-ADP-ribosylation of Rho by a C3 exoenzyme precludes the activation of RhoGDP to RhoGTP, trapping it in the inactive state (Figure 1.5). Crystal structures indicate that Asn41 in Rho is part of a conserved site for interaction with Rho
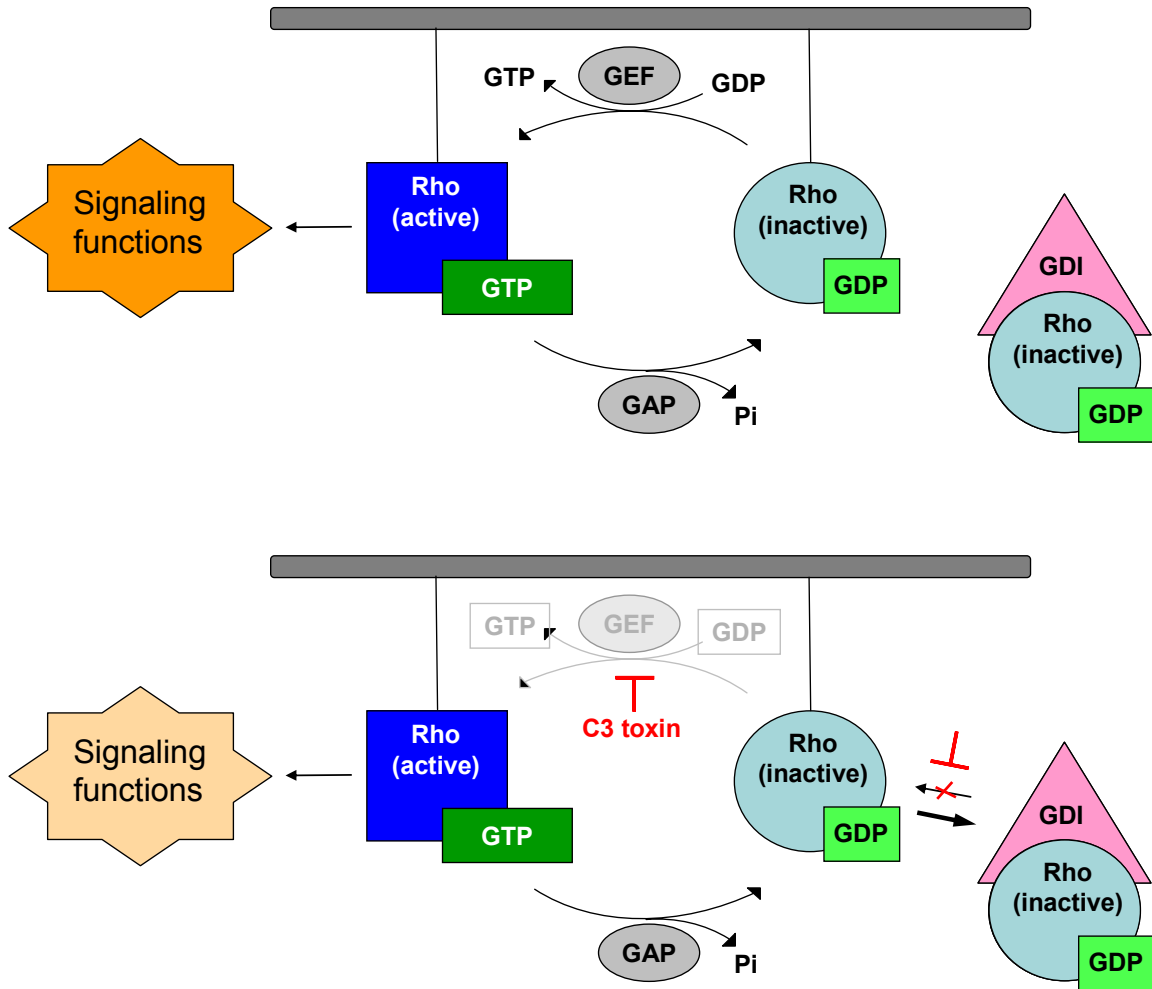
Figure 1.5. Rho inactivation by C3 mART toxins. Inactive GDP-bound Rho can be activated by the conversion of GDP to GTP by guanine nucleotide exchange factors (GEFs). Active GTP-Rho is inactivated by the hydrolysis of GTP. GDP-Rho can be sequestered to the cytosol by guanine nucleotide dissociation inhibitors (GDIs). In the presence of a C3 mART toxin (bottom half), the ADP-ribose modification at Asn41 causes inhibition of the GEF activation, trapping Rho in the inactive state, leading to an increase in sequestered GDI-Rho-GDP, and disruption of the usual Rho signaling functions. Adapted from Vogelsgesang & Aktories, 2006.

effectors and regulators. Modification at this residue serves the dual purpose of locking

Rho in the inactive state by preventing GDP-GTP conversion by GEFs (Sehr et al, 1998),

and inhibiting signaling roles through prevention of Rho interaction with downstream

effectors (Fujihara et al, 1997, Genth et al, 2003). The eventual consequence is a lethal

redistribution of actin within the cell (Chardin et al, 1989, Paterson et al, 1990, Wiegers

et al, 1991).

1.6.2 Structural characteristics of C3 mART toxins

While other mARTs comprise a typical AB structure, with an enzymatic domain

and a translocation domain, C3-like mARTs lack a specific transportation domain. In the

case of *S. aureus* C3 toxins, this does not seem to pose a problem. The whole bacterium

invades host cells, and can then excrete the toxins into the cytoplasm (Fahrer et al, 2010).

In other cases, C3lim and C3bot1 have been shown to enter host cells despite the lack of

a translocation domain. Originally this non-specific uptake was believed to occur due to

the high concentration of C3 enzyme surrounding the host cell. However, recent work

indicates that C3 toxins are selectively endocytosed by monocytes and macrophages,

even at low concentrations, while C2 clostridial toxins are not (Fahrer et al, 2010). This

suggests a specific mode of recognition which is not yet understood.

The first structure of a C3-like toxin was solved in 2001 by Han et al. (2001). Their

C3bot1 structure contained all of the hallmark mART active site regions. To date,

structures have been solved for four enzymes of this subgroup. The 2002 structure of

C3bot1 in complex with NADH allowed for comparison with the apo structure. The

NADH stretched between the ARTT motif and the PN loop, and was stabilized by

interactions of the PN loop with nicotinamide. Comparison with the apo- structure showed movement of the ARTT loop into the NAD-binding pocket when NADH is present. Concurrently, the secondary catalytic Gln of C3bot1 was drawn deeper into this pocket. Given its proposed role in Rho Asn41 recognition, this movement may help to position Rho in place for the transferase reaction to occur. A crystal structure of a C3 toxin in complex with a Rho protein would highlight which regions of the toxin are most important for substrate recognition and binding. Later structures of C3stau2 in the presence and absence of NADH did not show this ARTT loop movement upon NADH binding (Evans et al, 2003). The other notable difference from C3bot1 was the position of the α3 helix away from other helices. It was postulated that these changes may in part account for the increased number of substrates targeted by the *S. aureus* C3 toxins.

1.7 APPLICATIONS OF MART TOXINS

A number of current and future applications exist for mART toxins. Several of the most common are described here. Historically, their use in vaccines has been the most important, beginning with the development of the diphtheria vaccine in 1913. More recently, these toxins have created interest for their extreme toxicity and potential value in cancer therapies. Additionally, mART toxins have been studied from an antivirulence approach, and small molecule inhibitors are being developed to prevent their toxic effects. Continued understanding of the function of these toxins will expand our ability to use them for human therapeutics.

1.7.1 mART toxins as vaccines

Currently some mARTs are used for vaccinations, in order to prevent or lessen the severity of infections before they begin. Specifically, vaccines for diphtheria, cholera, and pertussis have been successfully created based on their respective mART toxins (Robbins et al, 2005). The vast majority of vaccines today are live attenuated or killed/inactive microorganisms (Plotkin & Plotkin, 2011); however, many diseases still lack a vaccine. Newer technology can now be applied to decrease the time required to produce new and safe vaccines. Currently, few vaccines are based on recombinant technologies, but our collective knowledge of genomics and structural biology now makes this a relevant option (Rappuoli et al, 2011). In the case of mART toxins, advanced knowledge of putative toxins contributing to disease may greatly decrease the time required to develop new vaccines. The identification of new protein toxins and the ability to make catalytic mutants or inactive domains recombinantly would allow these variants to be brought to clinical trials as vaccines more quickly. Additionally, the use of recombinant bacterial proteins is attractive, since they are generally more potent, safer, better characterized, and less reactogenic (Unnikrishnan et al, 2012). In this way, the human immune system could be prepared for future encounters with the active toxin. In some cases, such as the cholera vaccine, Dukoral^{TM}, the medication is delivered orally, making it accessible to a greater population. Perhaps in future years, we will see more vaccines based on mART toxins for the treatment of bacterial infections.

1.7.2 mART toxins in cancer therapies

mART toxins are also showing promise in the treatment of cancer. Toxins with an active catalytic domain and a mechanism of cell entry can be linked to antibodies to form an immunotoxin. This immunotoxin is directed to specific cells based on antibody recognition of cell-surface antigens in specific tissues. Once there, the mART toxin enters the cell by endocytosis and carries out its toxic function, killing the host cell. In this way, specific cells can be targeted for destruction without harming the neighbouring healthy cells. In particular, mART-based immunotoxins show promise in the treatment of blood cancers, where the immunotoxin has increased access to the cancer cells (Pastan et al, 2007, Weldon & Pastan, 2011). In many treatments, patient resistance to a drug is a common problem, and only short treatment periods are viable before the appearance of neutralizing antibodies. The use of mART toxins allows for a certain mART catalytic domain to be exchanged for another from a different mART toxin during each round of treatment. In this way, resistance cannot be acquired, as there are many different mechanisms by which a mART toxin can kill a cell. This technology has already been approved by the FDA for use with diphtheria toxin, and is now an available therapy called Ontak (denileukin diftitox) (Choudhary et al, 2011). Similar therapeutics using exotoxin A are now in clinical trials (Weldon & Pastan, 2011). Expansion of the number of characterized mART toxins may increase the breadth of options for the use of mART toxins in cancer therapy.

1.7.3 Small molecule inhibitors of mART toxins

As described above, antivirulence therapies provide a means of neutralizing toxic components of a bacterium's arsenal without directly challenging the survival of the bacterium. In this context, an antivirulence approach can be taken with mART toxins by using small molecule inhibitors to block the mART reaction and rescue the cell without pressuring the offending organism to develop resistance. Previous work in our laboratory in this area involved virtual screening of a library of small molecules combined with a site-directed library of poly-ADP-ribose polymerase (PARP) inhibitors. A number of compounds were found that demonstrated inhibition of mART toxins from *P. aeruginosa* and *V. cholerae*. *In vitro*, these small molecules gave IC_{50} values as low as 90 ± 10 nM, and the results were corroborated *in vivo* by EC_{50} values as low as 2.9 ± 0.8 nM upon infection of human lung epithelial cells (Turgeon et al, 2011). In cases where a mART toxin is a major contributing factor, or, as in the case of diphtheria toxin where the toxin is the sole cause of disease, small molecule inhibitors may be able to prevent infection or lessen its severity. This approach is even more promising given the fact that groups of mART toxins share active-site properties and host cell targets. Single small molecule inhibitors may be effective across a broad-range of related mART toxins. This antivirulence approach is further discussed in Chapter 4 with respect to Certhrax from *B. cereus* and the identification of several lead compounds for its inhibition.

1.8 IDENTIFICATION OF NEW MART TOXINS

As bacterial genomes continue to be sequenced, the list of potential new mART toxins continues to expand. Identification of new members of this enzyme family is not

trivial, and demands the use of several complementary approaches. Dozens of putative mART toxins have been discovered in the past five years, and we would even expect additional subgroups to be created based on the characterization of these toxins. As the family continues to grow, we enhance our knowledge of how these enzymes function, increase our understanding of the nature of protein-protein interactions, and how to disrupt them for therapeutic purposes.

1.8.1 *In silico* search strategies

Past efforts to identify new members of the mART family have included only a PSI-BLAST search and have led to the discovery of SpvB, from *Salmonella enterica* (Otto et al, 2000), SpyA from *Streptococcus pyogenes* (Coye and Collins, 2004), and HopU1 from *Pseudomonas syringae* (Fu et al, 2007). Further improvements matched a conserved mART sequence pattern in a small region with corresponding secondary structure and led to the identification of NarE of *Neisseria meningitides* (Masignani et al, 2003). Most recently, a pattern-based search was combined with structure prediction to identify new mARTs (Fieldhouse and Merrill, 2008). Fold-recognition databases of emerging genomes are searched based on the folds of known mART toxins. The hits are filtered to include only those produced and secreted by bacterial pathogens. They are further screened by the following consensus pattern, *[YFL]-R-X$_{27-60}$-[YF]-X-S-T-[SQT]-X$_{32-78}$-[QE]-X-E*, containing the most conserved mART residues. New putative mART toxins predicted in this manner can then be assessed *in vivo* to verify cytotoxicity.

1.8.2 Yeast assay for characterization of new mARTs

A well-characterized cell-based assay can be easily used to verify cytotoxicity of putative new mARTs. As previously described (Turgeon et al, 2009), the expression of putative mART toxin genes under the control of a copper-inducible promoter will lead to cell death in the presence of an active wildtype toxin. Similar assays with known mART toxins have shown that mild growth restoration is achieved with substitution of the secondary catalytic Glu/Gln residue to Ala. Increased growth restoration occurs when the primary catalytic Glu is converted to Ala, and near-complete growth restoration is seen when both of these residues are substituted. A similar pattern of growth upon substitution of homologous residues in putative mARTs is an indication that they are indeed responsible for observed cytotoxicity, and are functioning via a mART reaction. This verification method provides a rapid cell-based screen for a predicted toxin before embarking upon further biochemical, crystallographic or microscopic studies, which can be extremely laborious and time-consuming.

1.9 RESEARCH RATIONALE AND OBJECTIVES

The continued study of mART toxins is important to improve our understanding of how these enzymes work, to build a more complete library of this enzyme/toxin family, which will assist in the identification of important structural features necessary for function. This work will ultimately lead to the development of more potent therapeutics for the treatment of bacterial diseases in plants, animals and humans. Bacterial mART toxins are the causative agents, or contributing factors, of diseases around the globe. In many cases the responsible pathogenic bacteria are just now

emerging as human pathogens, making them more relevant than ever as organisms of study. **The goal of this research is to characterize novel members of the mART family of enzymes, to better understand their mechanism of action and to lay the groundwork for the development of effective inhibitors.** Herein, two toxins were biochemically characterized following *in silico* identification and *in vivo* verification by the above-mentioned methods. First, Photox is shown to be a novel mART from *Photorhabdus luminescens* that targets all actin isoforms at Arg177. *In vitro* work shows that although Photox lacks detectable glycohydrolase activity in the absence of substrate, mART enzymatic activity is higher than for a number of other mARTs, and comparable with the well-studied Iota toxin. Substitutions of catalytic residues resulted in decreased enzyme activity, giving clues as to their role in the mART reaction. The modification of actin by Photox is enough to disrupt actin polymerization and render actin unable to fulfill its crucial role within the cell. Photox becomes the 10th member of the C2-like toxins. Second, Certhrax from *Bacillus cereus* was found to be a new mART toxin closely related to anthrax lethal factor (LF). The presence of the active mART domain instead of an active metalloprotease domain sets Certhrax apart from its famous counterpart, but Certhrax confers 60-fold higher toxicity than anthrax LF. The crystal structure of Certhrax highlights similarities and differences between the two lethal toxins, and co-crystal structures with inhibitors combined with *in vitro* characterization led to the development of some lead compounds as therapeutic candidates against this new toxin. Each of these new enzymes increases our understanding of the mART family and contributes to a working knowledge required to render them less harmful to humans.

CHAPTER 2 - EXPERIMENTAL PROCEDURES

2.1 MATERIALS

Unless otherwise noted, chemicals were purchased from Sigma-Aldrich (St. Louis, MO). Purified α-, β-, and γ-actin were kindly donated by the lab of Dr. John Dawson (University of Guelph). The β/γ actin mixture was purchased from Cytoskeleton, Inc (Denver, CO). Protective antigen (PA) was a kind gift of Dr. Jeremy Mogridge (University of Toronto).

2.2 TOXIN EXPRESSION AND PURIFICATION

The mART toxins in this study were overexpressed and purified from *Escherichia coli*. Photox was purified from an insoluble fraction and refolded during chromatography, while Certhrax was purified in its soluble form. The expression and purification procedures for each toxin are described below.

2.2.1 Photox purification

The Photox gene was overexpressed in *Escherichia coli* cells and the protein was purified from inclusion bodies. In brief, the Photox gene was cloned into a pET-28b vector with an N-terminal His$_6$ tag and a tobacco etch virus protease (TEV; expressed and purified from a clone obtained from Detlef Brodersen Åarhus University, Denmark) site. *E. coli* Rosetta (DE3)pLysS cells were transformed with plasmid and plated onto 2×YT plates containing ampicillin to grow overnight at 37 °C. Cells were grown at 37 °C in 2 L cultures of 2×YT containing 100 μg/mL of ampicillin to an A$_{600}$ value of ~0.6 before induction with 1 mM isopropyl-1-thio-β-D-galactopyranoside (IPTG). Three hours post-induction cells were harvested by centrifugation at 5,000×g for 10 min. Cell pellets were

resuspended in 20 mM Tris-HCl, pH 7.5, 50 mM NaCl and the cells were lysed using a French press. Lysate was centrifuged for 25 min at 14,000×g and the pellet was resuspended in 20 mL of inclusion body wash buffer (50 mM Tris-HCl, pH 7.5, 2 mM EDTA, 100 mM NaCl, 0.05% (w/v) deoxycholate, 0.5 mg/mL of lysozyme). After further centrifugation at 10,000×g for 20 min the pellet was resuspended in 15 mL of denaturation buffer (50 mM Tris, pH 7.5, 500 mM NaCl, and 3 M guanidine hydrochloride). The supernatant from a spin at 20,000×g for 40 min was diluted to 30 mL with denaturation buffer with 5 mM imidazole. The sample was loaded to a 1 mL chelating Sepharose fast flow column (GE Healthcare, Uppsala) and eluted with 0-100 mM imidazole, without guanidine hydrochloride. The resulting protein was dialyzed into 10 mM Tris-HCl, pH 7.5, 100 mM NaCl and concentrated to 0.5-1.0 mg/mL using an Amicon Centriprep concentrator (Millipore, Billerica, MA).

2.2.2 Full-length Certhrax purification for *in vivo* and *in vitro* assays

Certhrax was overexpressed in *E. coli* Rosetta(DE3)pLysS cells (Novagen) and purified using immobilized metal affinity chromatography. In brief, the open reading frame encoding the 476-residue Certhrax (GI:122687420) or the catalytic domain (Asn242-Leu469) was cloned into a modified pET-28+ vector with an N-terminal hexa-His tag and a TEV protease site. *E. coli* Rosetta cells were transformed with plasmid and grown at 37 ºC in 2 L cultures of 2×YT containing kanamycin (30 µg/mL). After induction with 1 mM IPTG, expression occurred overnight at 15 ºC. Harvested cells were resuspended in 10 mM HEPES pH 7.5, 500 mM NaCl, and 10% (v/v) glycerol (Lysis buffer) and lysed using an Emulsiflex-C3 high pressure homogenizer (Avestin).

Following centrifugation at 14,000×g for 30 min, the supernatant was passed through an 8 mL diethylaminoethyl (DEAE) column. Column flow-through was loaded to a Zn^{2+}-charged HiTrap^{TM} Chelating HP column (GE Healthcare) equilibrated with Lysis buffer containing 10 mM imidazole, and was eluted with a 0-250 mM imidazole gradient. Certhrax was concentrated using an Amicon Ultra-15 10K filter to ~5 mg/mL in Lysis buffer.

2.2.3 Purification of Certhrax for crystallography

Certhrax for crystallization purposes was expressed and purified at the Structural Genomics Consortium facility in Toronto, ON. Truncated full-length Certhrax (residues 18-471) and catalytic domain (residues 242-469) were cloned into pNIC-CH (GenBank accession EF199843) and pET-MHL (GenBank accession EF456735) vectors, respectively, and the resulting plasmids were transformed into *E. coli* BL21 (DE3) for protein overexpression. Both *E. coli* transformants were cultured in terrific broth (TB) media at 37°C until OD_{600} of 2.5 to 3.0 and induced with 0.5 mM IPTG at 18 °C overnight. These proteins were purified as described above and truncated Certhrax was further purified on a Q anion-exchange column (elution with a linear gradient of 0 - 0.5 M NaCl) and by size-exclusion chromatography using a Superdex 75 gel filtration column equilibrated with 10 mM HEPES pH 7.5, 10% glycerol, 2.5 mM Tris-(2-carboxyethyl)-phosphine (TCEP). For the Certhrax catalytic domain, the N-terminal His tag was removed by TEV protease before dialysis and the dialyzed sample was directly loaded onto the Sephadex 75 gel filtration column. Both full-length and catalytic domain samples were concentrated to 25-30 mg/mL and stored at -80°C until further use.

2.3 FLUORESCENCE-BASED ASSAYS

Fluorescence-based techniques are popular in biochemistry for their high sensitivity and relative ease of use. In this study, both intrinsic and extrinsic fluorophores were used to characterize the toxins. Experimental procedures for these fluorescence-based assays are given below.

2.3.1 Mono-ADP-ribosyltransferase activity

In order to determine the initial reaction rate, Photox mono-ADP-ribosyltransferase activity was measured using a stopped-flow spectrometer (model SX20-MV, Applied Photophysics, Leatherhead, UK). Photox (80 nM) was mixed rapidly in a 1:1 (v/v) ratio with varying concentrations of etheno-nicotinamide adenine dinucleotide (ε-NAD$^+$) and actin after equilibration of all samples to ambient temperature. Increasing fluorescence intensity of the cleaved ε-NAD$^+$ was recorded as the reaction progressed (excitation 305 nm, emission 385 nm cuton filter). Individual reactions were repeated with actin concentrations ranging 0-15 μM and ε-NAD$^+$ concentrations ranging 0-300 μM. All reactions were performed in 10 mM Tris-HCl pH 7.5, 0.2 mM ATP, 0.2 mM CaCl$_2$, 0.2 mM β-mercaptoethanol (β-ME). Actin at 3.5 μM and εNAD$^+$ at 250 μM were chosen as saturating conditions for the collection of Michaelis-Menten data. A calibration curve was created by measuring fluorescence intensity changes upon completion of the reaction at various actin concentrations in the presence of excess ε-NAD$^+$, and by assuming the molar amounts of actin and ε-NAD$^+$ consumed by the reaction were equal. Data were fit using non-linear regression to the Michaelis-Menten equation ($v_o = v_{max}S/(K_M+S)$, where v_o is the initial velocity, v_{max} is the

maximum velocity, S is the substrate concentration, and K_M is the Michaelis constant indicating substrate concentration at half-maximal velocity) using GraphPad Prism 5 (La Jolla, CA) software. In the case of εNAD$^+$ variance, data were fit to a substrate inhibition model ($v_o = v_{max}S/(K_M+S(1+S/K_i))$), where K_i is the binding dissociation constant for substrate binding), which was statistically preferred over the Michaelis-Menten model (p = 0.004).

2.3.2 NAD$^+$ glycohydrolase activity

Since NAD$^+$ cleavage, or the glycohydrolase reaction is generally much slower than the mART reaction, it was easily measured using a Cary Eclipse fluorescence spectrophotometer (Varian). For both Photox and Certhrax, the toxin was mixed well with various concentrations of εNAD$^+$ (0-100 μM) in 20 mM Tris pH 7.9. Increasing fluorescence intensity of the cleaved ε-NAD+ was monitored at excitation and emission wavelengths of 305 nm and 405 nm, respectively, for 300 s, using excitation and emission slit widths of 5 nm each. Certhrax was used at a concentration of 5 μM and reactions were run for 5 min. Photox was used at a concentration of 10 μM and reactions were carried out for 4 h. Initial reaction slopes were measured and plotted against ε-NAD$^+$ concentration, and fitting to the Michaelis-Menten model was used to determine K_M and v_{max} using GraphPad Prism 5 software.

2.3.3 NAD$^+$ and inhibitor binding

Quenching of intrinsic tryptophan fluorescence was used to determine the binding dissociation constant, K_d, for both NAD$^+$ and the inhibitors as previously described

(Armstrong et al, 2002, Yates et al, 2005), with slight modifications. Toxin (1 μM) in 50 mM NaCl, 20 mM TrisHCl pH 7.9 was titrated with either NAD$^+$ or an inhibitor, while fluorescence was monitored using excitation and emission wavelengths of 295 nm and 340 nm, respectively, and slit widths of 5 nm each, on a Cary Eclipse fluorescence spectrophotometer. Data was analyzed by non-linear regression using GraphPad Prism 5 (La Jolla, CA) to determine the binding dissociation constant.

2.3.4 Tryptophan fluorescence for folding integrity

Intrinsic tryptophan fluorescence was measured for wild type Photox and each Photox mutant to observe changes in folding. Solutions containing 4 μM toxin in 50 mM NaH$_2$PO$_4$, pH 7.0 and 50 mM NaCl were analyzed in quartz cuvettes using a Photon Technology International Inc. (Birmingham, NJ) fluorometer. Excitation and emission (scan) wavelengths were 295 nm and 305-450 nm, respectively, and slit widths were 2.5 nm each. The wavelength of maximum fluorescence was recorded and compared with the wild type protein for each sample. Data were corrected by subtracting the spectrum of a buffer-only solution and smoothed using Felix software (Photon Technology International Inc, Birmingham, NJ) before determining the first derivative.

2.3.5 Inhibition of mono-ADP-ribosyltransferase activity

Inhibitors P1, P3, and P6 were a gift from Guilford Pharmaceuticals (Baltimore, MD), originally part of a small, directed poly(ADP-ribose) polymerase library. V23 and V30 were identified as potential inhibitors through a screen against a previously studied mART toxin (Turgeon et al, 2011), and purchased from Chembridge Corp. (San Diego,

39

CA). The P6 derivatives, P6C, P6D, P6F and P6G were designed and synthesized by Sinova Inc. (Bethesda, MD). Partition co-efficients for each inhibitor were calculated using ChemAxon software available at: http://intro.bio.umb.edu/111-112/OLLM/111F98/newclogp.html. LogP is the calculated $\log_{10}$(partition coefficient), where partition coefficient is [compound]$_{octanol}$/[compound]$_{water}$. LogD pH profiles represent the calculated $\log_{10}$(distribution coefficient), where distribution coefficient is [microspecies]$_{octanol}$/[microspecies]$_{water}$ including ionized and non-ionized microspecies. The inhibitors were characterized for their effectiveness against Certhrax activity. To determine the IC$_{50}$, the concentration of inhibitor which reduced enzyme activity by 50% was calculated from inhibition data sets; NAD$^+$ glycohydrolase activity was measured in the presence of various concentrations of inhibitor. Inhibitors P1, P3, P6, suramin, and PJ97A were assessed as described above using a Cary Eclipse fluorescence spectrophotometer. To accelerate the data collection process when sufficient stocks of inhibitor solutions were available, an automated FLUOstar Omega microplate reader (BMG Labtech) was employed for kinetic data acquisition. Various concentrations of inhibitor were injected into a 384-well plate containing 1 μM Certhrax and 100 μM ε-NAD$^+$ in 20 mM Tris, pH 7.9 for a final volume of 35 μL. Increasing fluorescence intensity was measured using excitation and emission bandpass filters of 300 nm and 405 nm, respectively (20 nm bandpass). In both cases, initial slopes were recorded and the IC$_{50}$ was calculated by non-linear regression curve fitting using GraphPad Prism 5. These values were converted to K_i values using the Cheng-Prusoff equation (Cheng & Prusoff, 1973), $K_i = \text{IC}_{50}/(1 + [S]/K_M)$, where [S] is the NAD$^+$ concentration and K_M is for the NAD$^+$ substrate. Experimental K$_i$ values were determined for inhibitors, PJ34 and P6F,

from Dixon plots of the kinetic inhibition data. A Dixon plot of $1/v_o$ vs. inhibitor concentration (0, 6, 12, or 24 µM) was plotted for four different concentrations of εNAD$^+$ (12.5, 25, 50, and 100 µM). Linear regression using GraphPad Prism 5 was employed to determine the slope of each line. These slopes were then plotted vs. $1/[εNAD^+]$, and the slope of the resulting line was used to determine Ki by the following equation:

Slope = $K_M/(v_{max} \times K_i)$.

2.4 PROTEIN CRYSTALLOGRAPHY

Full-length Certhrax was crystallized both ligand-free, and in complex with inhibitor P6. The catalytic domain of Certhrax was crystallized in complex with inhibitor PJ34. Description of the crystallization and data collection for each structure is given below.

2.4.1 Crystallization of Certhrax

Crystallization was performed by sitting-drop vapor diffusion at 18 ^{o}C. Full-length Certhrax was mixed with suramin (5 µM, Sigma) and incubated overnight at room temperature. Elastase was added (1:100 mol/mol, Sigma) to the protein solution immediately before crystallization trays were dispensed. Crystals were obtained against reservoirs containing 2.4 M sodium malonate and 10 mM HEPES pH 7.2. For the complex with inhibitor P6, the inhibitor was soaked into pre-formed crystals by first transferring the crystal to a 4 µL drop of reservoir solution for 5 min. Then, 2 µL of 10 mM P6 was added to the drop, and incubated for 30 min. Crystals were then rinsed in paratone for cryoprotection, and frozen with liquid nitrogen. Crystals of the catalytic

domain of Certhrax in complex with PJ34 were obtained after overnight incubation with an excess amount of PJ34 before crystallization in 2.9 M ammonium sulfate and 0.1 M Bis-Tris, pH 6.4 within 2 days.

2.4.2 Data collection and processing

Datasets were collected for each crystal at the Canadian Light Source (beamline 08ID, (Grochulski et al, 2011)). Data was processed using DENZO/SCALEPACK (Otwinowski & Minor, 1997) and XDS/SCALA (Evans, 2006, Kabsch, 2010). The Certhrax-PJ34 structure was built using molecular replacement with *Clostridium limosum* C3 exoenzyme as the model template (PDB: 3BW8). The Certhrax-apo and Certhrax-P6 structures were built using molecular replacement with the Certhrax-PJ34 structure as the model. Intermediate refinement of each structure was performed with PHENIX (Adams et al, 2010), before COOT (Emsley et al, 2010) and/or O (Jones et al, 1991) were used for interactive rebuilding. REFMAC (Murshudov et al, 2011) was used for final refinement of the Certhrax-apo and Certhrax-PJ34 structures, and Phenix.refine for the Certhrax-P6 structure. MolProbity (Chen et al, 2010) was used for validation of model geometry in all cases.

2.5 SUBSTRATE IDENTIFICATION

Numerous methods were used in attempts to identify the host protein target of these toxins, with varying success. Experimental procedures for the most promising of these methods are given below.

2.5.1 Biotin-NAD$^+$ blot

A blot with biotin-NAD$^+$ (Trevigen, Gaithersburg, MD) was used to detect potential substrates from a whole cell lysate or from a purified protein sample. As modified from a previous method (Jorgensen et al, 2008), biotin-NAD$^+$ was incubated with toxin, and a cell lysate or purified protein sample. Reaction mixtures were separated by sodium dodecyl sulfate-polyacrylamide gel electrophoresis (SDS-PAGE) and subsequently transferred to a nitrocellulose membrane. In some cases, the reaction mixture was separated by isoelectric focusing before SDS-PAGE to achieve greater separation. Potential substrates were then detected using a streptavidin-alkaline phosphatase and 5-bromo-4-chloro-3-indolyl phosphate/nitro blue tetrazolium (BCIP/NBT) colorimetric detection method.

2.5.2 Native PAGE

Native PAGE was used to assess a shift in mobility after ADP-ribosylation of actin. Actin (3 μg samples) was incubated for 1 h in the presence of 200 μM ε-NAD$^+$, and in the presence or absence of 1 nM Photox. Proteins were separated by native PAGE on 10% non-denaturing, non-reducing gels supplemented with 0.2 mM ATP and 0.2 mM CaCl$_2$. Native PAGE was run at low voltage (<80 V) on ice to prevent protein denaturation. Visualization was performed under UV in a FluorChem 8900 gel-doc instrument (Alpha Innotech, San Leandro, CA).

2.5.3 Fluorescently-labeled NAD$^+$ gel

NAD$^+$ labeled with a fluorophore was used in a similar manner to detect ADP-ribosylation of several actin isoforms. Fluorescein-ADP-ribose labeling of actin isoforms was obtained by incubating 19 μM fluorescein isothiocyanate-NAD$^+$ (FITC-NAD$^+$) (Trevigen) with 5 μM Photox and 2 μg purified β- or γ-actin for 1 h at 25ºC in the dark. Proteins were separated by SDS-PAGE and visualized using UV illumination and a fluorescein filter on a FluorChem 8900 instrument.

2.5.4 Mass spectrometric analysis of modified actin

ADP-ribosylated α-actin was analyzed by liquid chromatography/tandem mass spectrometry (LC/MS/MS) on a quadrupole time-of-flight (Q-TOF) mass spectrometer (Micromass) at the University of Western Ontario following proteolytic digestion using endoproteinase AspN, to determine the site of the 541 Da ADP-ribose group. Calibration was performed using myoglobin and mass error was < 0.5 Da.

2.6 TOXIN MICROSCOPY STUDIES

Microscopy was employed for the visualization of mART toxins *in vivo*. These studies allow insight into toxin localization within a host cell.

2.6.1 Co-localization of Photox and actin in yeast

The Photox E353A/E355A gene was cloned into a pRS-416-ADH1-GFP vector to give an N-terminal green fluorescent protein (GFP) tag. W303a yeast cells transformed with plasmid were grown with 150 μg/mL adenine to an OD_{600} value of 0.8, and were

fixed in 3.7% (v/v) formaldehyde. After centrifugation (5,000×g, 5 min) cells were washed twice with PEM buffer (0.4 M PIPES pH 6.9, 20 mM EGTA, 20 mM $MgCl_2$) and resuspended in 25 % (v/v) methanol in PEM buffer. After addition of 1.5 μM rhodamine-phalloidin, cells were stained in the dark for ~30 min before washing and resuspension in 100 μL PEM buffer. The 4 μL stained cell suspension was visualized with a Nikon Eclipse 6600 epifluorescent microscope.

2.6.2 Confocal microscopy of Certhrax cell entry

Certhrax was fluorescently labeled at primary amines with a DyLight 488 amine-reactive dye kit following the manufacturer's instructions (ThermoScientific, Rockford, IL). The ratio of protein to label was calculated and found to be 1.1 mol fluorophore per mol Certhrax. RAW264.7 murine macrophage cells (ATCC, Manassas, VA; catalogue number TIB-71) were cultured in Dulbecco's modification of Eagle's medium (DMEM) (Lonza, Basel, Switzerland) containing 10% fetal bovine serum (FBS) (Gibco, Life Technologies, Burlington, ON) and penicillin (100 U/mL)-streptomycin (100 μg/mL) mixture (Lonza) in a water-jacketed CO_2-incubator at 5% CO_2, 37 ^{o}C in 25-cm^2 culture flasks (Corning, Lowell, MA). Cells were grown to 90% confluency, scraped to lift, diluted with fresh supplemented DMEM to $2×10^4$ cells/mL, and seeded on glass cover slips in 6-well plates. The cells were incubated for various periods of time with Certhrax ($1×10^6$ pg/mL) in the absence or presence of *Bacillus anthracis* protective antigen (PA) (100 ng/mL). Cells infected with Certhrax for 0-60 min were pre-incubated with PA for 15 min before the addition of toxin. The cells were washed with PBS and fixed with 4% paraformaldehyde at room temperature for 20 min in the dark. Cells were immediately

stained with 0.1 µg/mL 4,6-diamidino-2-phenylindole DAPI and mounted on glass cover slips using a drop of Dako fluorescent mounting medium (Roche, S3023). Images were acquired using confocal microscopy (Leica Upright DM 6000B) at 63× magnification, a pinhole of 1 Airy unit, the FITC excitation and emission range (511-572 nm), and a pixel resolution of 1024×1024 (scanning speed of 400 Hz). Differential interference contrast (DIC) images were aquired concurrently with each set of fluorescent images at the same magnification. The acquisition software was Leica Applications Suite Advanced Fluorescence (LASAF) version 1.6.0. Images were taken as z-stacks, and ImageJ (version 1.44p/Java 1.6.0_20, http://imagej.nih.gov/ij) was used to generate 2D images using z-projection and average intensity.

2.7 STRUCTURAL MODELING

Despite several attempts, Photox proved to be recalcitrant to crystallization due to low solubility. A model of the Photox catalytic domain was built on the 1.9 Å X-ray structure of the NAD-bound catalytic domain of SpvB (PDB: 2GWL) using MODELLER (31), and quality was assessed by MetaMQAPII (32). The Photox-actin-NAD complex was prepared by the superposition of Photox-NAD in place of Iota toxin in the 2.8 Å Iota-actin-NAD Michaelis complex structure (PDB: 3BUZ) using Coot (33).

Certhrax was aligned with anthrax LF using the align function in the PyMol v.0.99 software. This produces a BLOSUM62-weighted dynamic sequence alignment followed by a series of refinement cycles to find the best alignment.

All protein structures in this thesis were visualized and prepared using PyMol v.0.99.

CHAPTER 3 - PHOTOX: SHEDDING LIGHT ON A NEW MART TOXIN

3.1 OVERVIEW

3.1.1 Abstract

Photorhabdus luminescens is a pathogenic bacterium that produces many toxic proteins. In this chapter, a novel mART from *P. luminescens*, named Photox, is characterized. Identified via *in silico* methods, this 46 kDa toxin shows high sequence identity to other actin-targeting mARTs in hallmark catalytic regions and retains a similar core catalytic fold. Furthermore, Photox shows *in vivo* cytotoxic activity against yeast, with protection occurring when catalytic residues are substituted with Ala. *In vitro,* enzymatic activity (k_{cat} =1680 ± 75 min^{-1}) is higher than that of the related Iota toxin, and diminishes by nearly 14,000-fold following substitution of the catalytic Glu (E355A). This toxin specifically ADP-ribosylates monomeric α-skeletal actin and nonmuscle β- and γ-actin at Arg-177, inhibiting regular polymerization of actin filaments. Yeast fluorescence microscopy studies indicate the co-localization of Photox with actin *in vivo* and a model of the Michaelis complex of Photox, actin, and NAD$^+$ demonstrates the location of catalytically important residues in the active site. Together these results indicate that Photox is indeed a mono-ADP-ribosyltransferase, making it the newest member of the actin-targeting mART family.

3.1.2 Introduction to *Photorhabdus luminescens*

Photorhabdus luminescens is a motile, bioluminescent, gram-negative bacterium belonging to the *Enterobacteriaceae* family, known to be an insect pathogen (Fischer-Le Saux et al, 1999). Sequenced in 2003 (Duchaud et al, 2003), the *P. luminescens* genome encodes an extensive variety of toxins and hydrolytic enzymes, many of which are being studied as potential virulence factors. These bacteria live in close symbiosis with soil-dwelling *Heterorhabditis* nematodes. After *Photorhabdus* colonization of the nematode intestinal tract, the nematodes invade an insect host, and migrate to the haemolymph. Within this open circulatory system, *Photorhabdus* bacteria are released by regurgitation. An array of toxic compounds released by the bacteria eventually kills the insect host. Both nematode and bacteria feed on the insect cadaver and reproduce to repeat the cycle, each benefiting from their close relation with the other (Waterfield et al, 2009).

Among other toxins, *Photorhabdus* bacteria produce toxin complexes (Tc's), high molecular weight, multi-subunit, insecticidal toxins (Waterfield et al, 2001), some of which show oral toxicity in the same range as *Bacillus thuringiensis* endotoxins (ffrench-Constant & Bowen, 2000), as well as the 'makes caterpillars floppy' (Mcf) toxin, responsible for insect midgut destruction (Daborn et al, 2002). Based on its pathogenesis and the high number of virulence factors that it produces, *P. luminescens* has garnered interest in the area of biopesticides due to increasing resistance against conventional pesticides (Ehlers, 2001). Recently, *Photorhabdus* has gained attention due to the emergence of a new species of human opportunistic pathogen, *P. asymbiotica*, which has been recovered as clinical isolates from human wounds in both North America and Australia (Wilkinson et al, 2009). A better understanding of the virulence factors of

Photorhabdus will allow for more efficient treatment of infections, or the effective use of the bacteria for insecticidal purposes.

3.1.3 *In silico* identification of Photox

The plu0822 gene of *Photorhabdus luminescens* strain TT01 was identified as a putative mART *in silico* and further confirmed using fold-recognition and pattern-based search methods. Although a simple BLAST search also identifies this protein as a putative mART, this search strategy alone is prone to false positives and benefits from further substantiation by fold-recognition and a pattern-based search. The gene encoding Photox was found after searching the Genomic Threading Database (McGuffin et al, 2004) using SCOP code d.166.1.1 (Murzin et al, 1995), which describes the mART fold. The predicted fold was confirmed by three independent protein prediction servers (3D-JURY (Ginalski et al, 2003), Genesilico (Kurowski & Bujnicki, 2003), and Pcons (Wallner et al, 2007)) and the characteristic mART primary sequence pattern was confirmed using ScanProsite (de Castro et al, 2006, Fieldhouse & Merrill, 2008) and multiple sequence alignments using 3D-Coffee (Armougom et al, 2006). This gene was found to encode a protein of 408 residues (45.9 kDa). The two-domain protein, named Photox, shares 39% primary structure identity overall with SpvB of *Salmonella enterica*. Specifically, the C-terminal 200 residues of Photox share 61% identity in primary sequence with the catalytic domain of SpvB. Identity in catalytic signature regions and a predicted mART fold indicate that *plu0822* encodes a putative mART enzyme, and that Photox is likely to have enzymatic activity akin to other toxins of this family. A primary sequence alignment of Photox with several known actin-targeting mART toxins is shown

in Figure 3.1. The alignment reveals strong primary sequence identity in Region 1 for the catalytic Arg288 preceded by a Tyr, the Region 2 Ser-Thr-Ser motif preceded by aromatic and hydrophobic residues, and Region 3 primary and secondary Glu residues, Glu355 and Glu353, respectively. Together these sequence characteristics provide strong evidence that Photox is a new mART toxin member, and like similar members of this mART subgroup, it is predicted to target the actin of a host cell.

3.1.4 Actin isoforms

Based on the *in silico* prediction of actin as a host protein target for Photox, actin became an important protein for subsequent characterization of the novel bacterial mART enzyme. At least 6 different actin isoforms have been identified in humans, which are divided into three classes: α, β, and γ (Herman, 1993, Vandekerckhove & Weber, 1978). In this study, we most often employ α-skeletal muscle actin, but also look at β- and γ-actin, which are classically cytoplasmic. The three classes of actin share >85% sequence identity, and this value increases to >98% within each class (Egelman, 2001). It is postulated that the large number of actin-binding proteins contribute to the strict conservation of sequence in order to preserve numerous different functions of the protein.

3.1.5 Yeast cytotoxicity of Photox

A yeast growth-deficiency assay was used to demonstrate that the mART activity of Photox is cytotoxic. The *plu0822* gene encoding Photox was cloned into a *S. cerevisiae* vector under the transcriptional control of the *CUP1* promoter on a low-copy number

Toxin, Organism	Region 1	Region 2	Region 3
	⟶	⟶	⟶
Photox, *P. luminescens*	KKV**YRG**LK(24)	**FLSTS**PD(29)	G**EAE**ML
SpvB, *S.typhimurium*	RVV**YRG**LK(24)	**FMSTS**PD(29)	G**EAE**ML
Sa, *C.spiroforme*	LVV**YRR**SG(37)	**FVSTS**IG(34)	G**EYE**VL
Iota toxin, *C.perfringens*	LIV**YRR**SG(37)	**FISTS**IG(34)	G**EYE**VL
Cdta, *C.difficile*	LTV**YRR**SG(37)	**FISTS**IG(34)	G**EYE**VL
Vip2, *B.thuringiensis*	ITV**YRW**CG(31)	**YMSTS**LS(34)	N**EKE**IL
C2 toxin, *C.botulinum*	LIA**YRR**VD(43)	**FSSTS**LK(33)	D**EQE**IL

Figure 3.1. Identification of Photox. Sequence alignment of several mARTs. Characteristic catalytic residues are indicated. Region 1 contains the catalytic Arg, region 2 includes the STS motif, and region 3 contains the catalytic and secondary Glu residues. General secondary structure for these regions is indicated above the sequences (arrow denotes β-sheet).

plasmid by homologous recombination, as described by Turgeon et al. (2009). Basal expression of Photox in yeast cells was sufficient to incur a severe growth-defective phenotype in yeast (Figure 3.2, red bars), demonstrating the highly toxic nature of this protein in a eukaryotic cell system. In contrast, expression of the E353A or E355A mutations partially suppress the lethal effects of the toxin (Figure 3.2, green and blue bars, respectively) except at the higher Cu^{2+} concentration, confirming their role in the catalytic activity of the enzyme. Importantly, the double mutations, E353A/E355A, almost completely abolished toxin cytotoxicity at all Cu^{2+}-induction levels (Figure 3.2, cyan bars), indicating that both residues are required for full mART activity *in vivo,* and that this activity is entirely responsible for the observed growth-defective phenotype observed in yeast. As a result of these studies, Photox from *Photorhabdus luminescens* was identified as a putative mART toxin, and shown to be cytotoxic in a eukaryotic system. Armed with this knowledge, this chapter discusses the biochemical characterization of this novel enzyme.
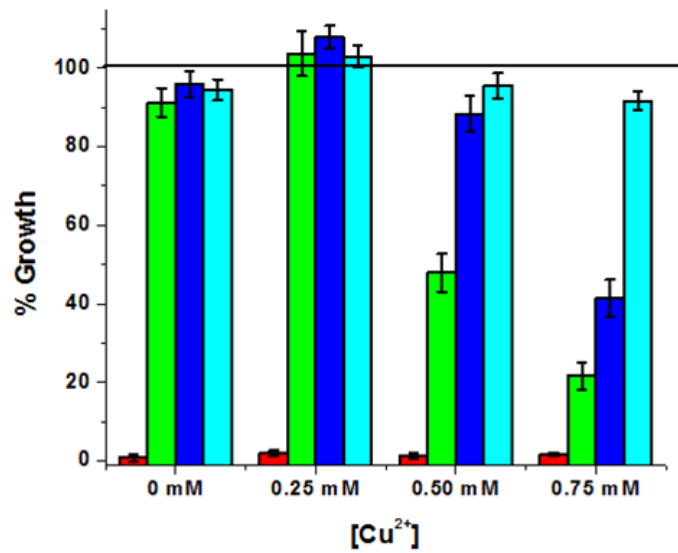
Figure 3.2 Effects of Photox expression on yeast growth. Growth of *S. cerevisiae* expressing WT or mutant Photox with point mutations to catalytic Glu residues. The WT (red), E353A (green), E355A (blue), or E353A/E355A (cyan) gene in pRS415 was induced with Cu^{2+} for 48 h. (Modified from Turgeon et al, 2009).

3.2 RESULTS AND DISCUSSION

3.2.1 Overexpression and purification of Photox

The *plu0822* gene was cloned into the *E. coli* pET 28b vector and overexpressed in *E. coli* Rosetta cells. Photox was successfully purified from an insoluble state by denaturation, followed by simultaneous renaturation during immobilized metal affinity chromatography. The purity level and the relative mobility of the protein by SDS-PAGE indicated that we had isolated the *plu0822* protein product. Photox was further identified as a His-tagged protein by Western blotting using a monoclonal antibody against the polyHis tag (Figure 3.3). The yield of purified Photox was approximately 10 mg/L of bacterial culture.

3.2.2 Photox ADP-ribosylates actin

The toxin was tested for *in vitro* mART activity by incubating Photox with biotin-NAD^+ and target cell lysate or a purified protein sample. ADP-ribosylated proteins carrying the biotin label (biotin-ADP-ribose) were detected on a nitrocellulose membrane following SDS-PAGE by a colorimetric reaction. The Photox-catalyzed mART activity in the presence of biotin-NAD^+ and purified α-actin resulted in the biotin-ADP-ribose labeling of actin. A similar reaction with Chinese hamster ovary (CHO) lysate resulted in a single band of the same molecular weight. The lack of other ADP-ribosylated proteins in the CHO lysate indicates that actin is the primary target of this mART toxin (Figure 3.4). This explains the lack of deleterious effects when Photox is expressed in *E. coli*, as bacteria do not possess actin.
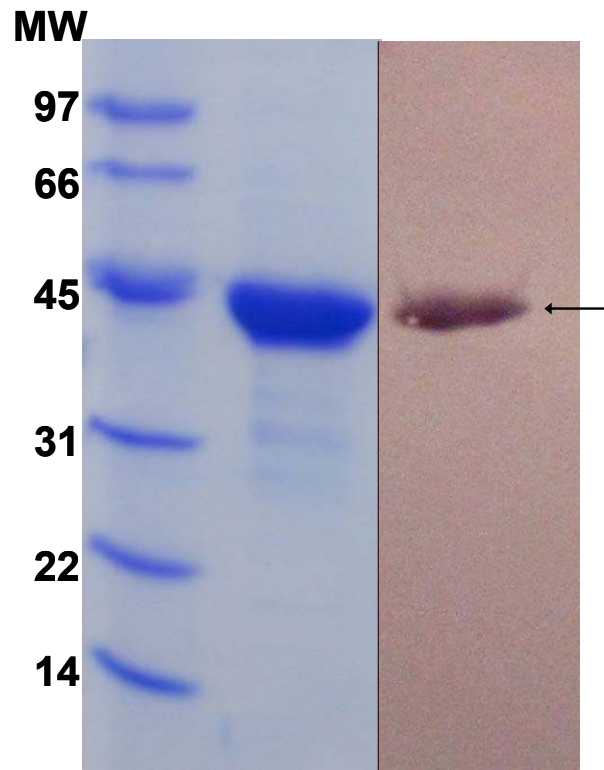
Figure 3.3 Purification of Photox. Purified Photox (black arrow) as analyzed by SDS-PAGE and Coomassie staining. It was confirmed by Western blotting using an antibody against the poly-His tag. Lane 1, protein molecular weight standards (Biorad) in kDa; lane 2, purified Photox; lane 3, Western blot of purified Photox.

	1	**2**	**3**	**4**	**5**
	Actin	Lysate	-	Actin	Lysate
Photox	+	+	+	-	-
BioNAD	+	+	+	+	+
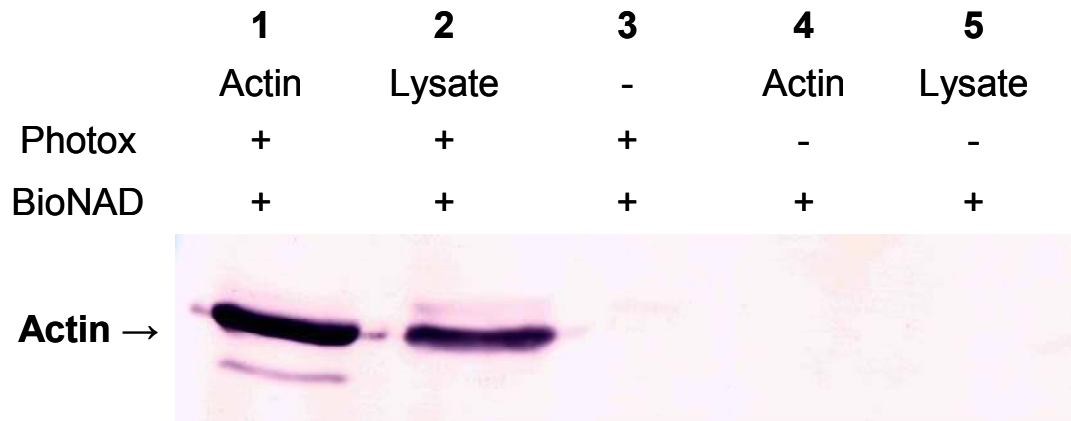
Actin →

Figure 3.4 ADP-ribosylation of actin by Photox. Modified Western blot from reactions of Photox with biotin-NAD$^+$ and potential protein substrates, showing biotin-ADP-ribose labeling of actin. Lane 1, 0.25 μg of purified actin labeled with Photox; lane 2, CHO lysate labeled by Photox; lanes 3-5, various controls.

The substrate specificity of Photox was qualified using various actin isoforms. Incubation of purified muscle α-actin or nonmuscle β- or γ-actin with Photox and FITC-NAD$^+$ allowed for fluorescent visualization of ADP-ribosylated actin following SDS-PAGE. Photox proved to target each of the three actin forms as substrates in the mART reaction (Figure 3.5). Although other actin-targeting mART enzymes have been characterized using a β- and γ-actin mixture (Hochmann et al, 2006, Sakurai et al, 2003, Schleberger et al, 2006), we show here that all three purified actin isoforms individually serve as targets of this reaction. Like Photox, SpvB, Iota, Sa, and CDTa toxins have each been shown to lack specificity towards actin isoforms, in sharp contrast to the activity of C2 toxin, which is specific for β- and γ- nonmuscle forms of actin (Gill & Meren, 1978). Preliminary kinetic characterizations using purified skeletal α-actin and a mixture of β- and γ-actin showed that mART activity of Photox was only slightly higher (approximately 3-fold, data not shown) with a non-muscle actin substrate. As a result, in-depth kinetic characterization was conducted with α-actin as a substrate due to its availability.

3.2.3 Photox ADP-ribosylates actin at Arg-177

The specific site of ADP-ribosylation on α-actin was confirmed by LC/MS/MS mass spectrometry of ADP-ribosylated actin following AspN digestion. A single site of modification on the protein was confirmed by mass spectrometric analysis of labeled and unlabeled actin showing a difference of 541.28 Da, equivalent to a single ADP-ribose group (Figure 3.6A). Greater than 99% ADP-ribosylation efficiency was also confirmed by mass spectrometry, and it was revealed that the only modification site was at Arg-177

	1	2	3	4	5	6	7
Actin	α	β	γ	-	α	β	γ
Photox	+	+	+	+	-	-	-
FITC-NAD	+	+	+	+	+	+	+
Actin →							
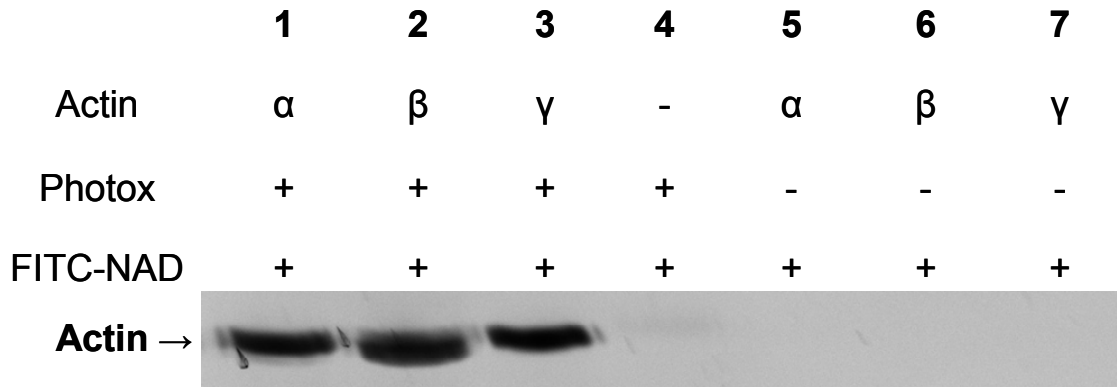
Figure 3.5 Mono-ADP-ribosylation of actin isoforms. Labeling of various actin isoforms by Photox using FITC-NAD$^+$. Lanes 1-3, 0.5 µg α-, β- or γ-actin incubated with Photox and FITC-NAD$^+$; Lanes 4-7, various controls. Proteins were separated by SDS-PAGE and visualized using UV illumination and a fluorescein filter on a FluorChem 8900 instrument.
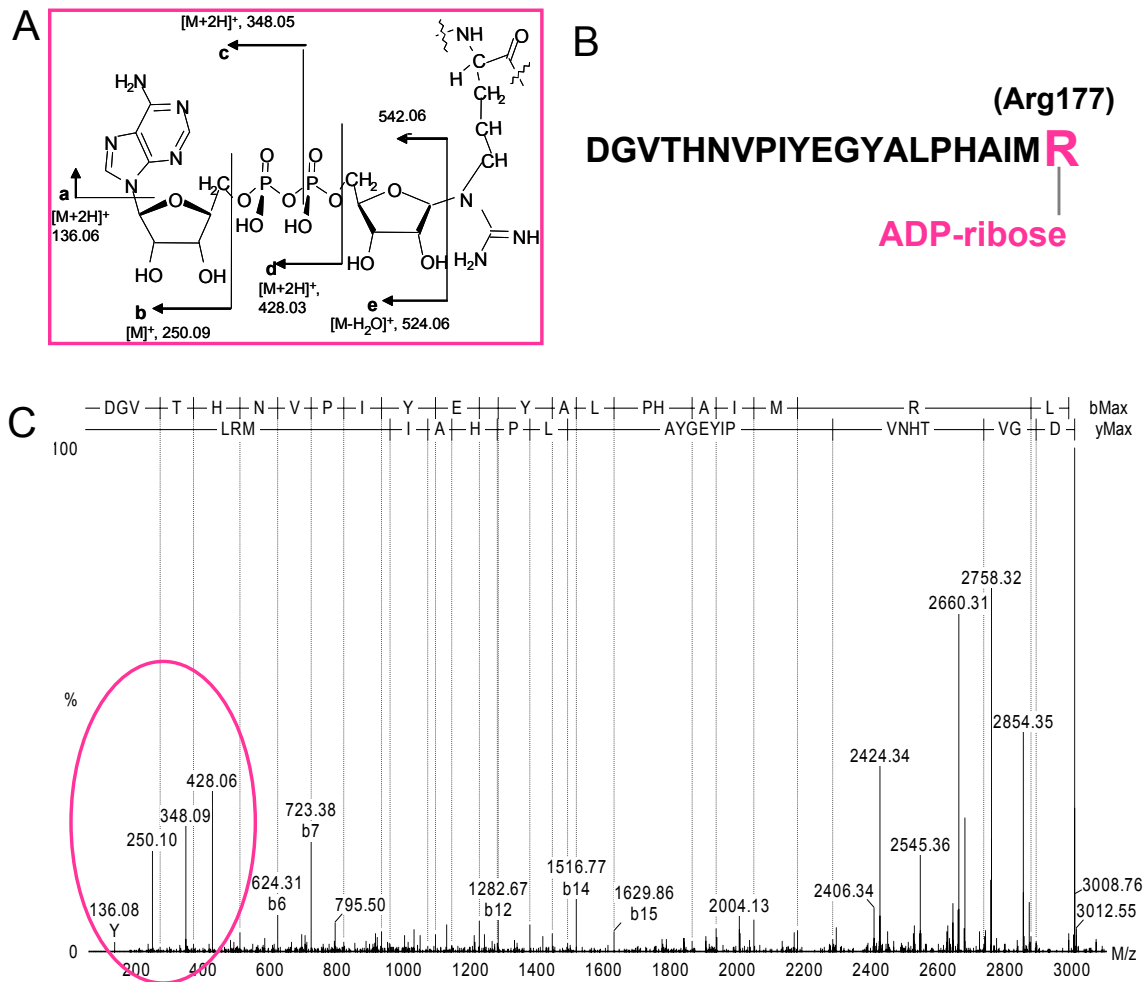
Figure 3.6 ADP-ribosylation of actin at Arg177. Mass spectrometer analysis of the ADP-ribosylation site on α-actin. (A) Fragmentation and resulting m/z ratios of the ADP-ribose. (B) Peptide sequence of actin indicating site of ADP-ribose modification. (C) Spectrum showing b- and y-ions of this peptide fragment containing the ADP-ribose modification. Fragments produced by the ADP-ribose group are circled in pink.

(Figure 3.6B,C). Figure 3.6C gives the fragmentation pattern of the ADP-ribose group and shows the b- and y-ions resulting from fragmentation of the peptide containing this modification. For this peptide, 20 fragments ("b" ions) of correct mass were easily identifiable with no mass changes that would indicate a site of modification. This left only Arg or Leu as the site of ADP-ribose modification on this peptide. Since Leu is not ionizable, the modification cannot exist there, confirming that the single ADP-ribose modification must be on Arg-177.

The specific site of actin modification was confirmed *in vivo* using a yeast assay. A mutant yeast strain expressing only an R177A mutant actin was employed, and was seen to confer resistance to Photox upon toxin gene induction (Figure 3.7). This supports the conclusion that Photox specifically ADP-ribosylates actin at Arg-177. Furthermore, this single point mutant of actin (R177A) is sufficient to completely reverse the cytotoxic effects of Photox, suggesting that ADP-ribosylation of actin at Arg-177 is the only cytotoxic activity linked with Photox.

3.2.4 Kinetic characterization of Photox mART activity.

A fluorescence-based assay was used to characterize the mART activity of Photox using highly purified α-actin as protein substrate. Photox (40 nM) was incubated with varying concentrations of actin and εNAD^+ and initial reaction rates were measured using a stopped-flow spectrophotometer. In the presence of excess εNAD^+, the reaction proceeded to completion in 30 min (Figure 3.8A), and a band-shift assay by native-PAGE revealed that at equilibrium nearly all of the actin is ADP-ribosylated (Figure 3.8B).
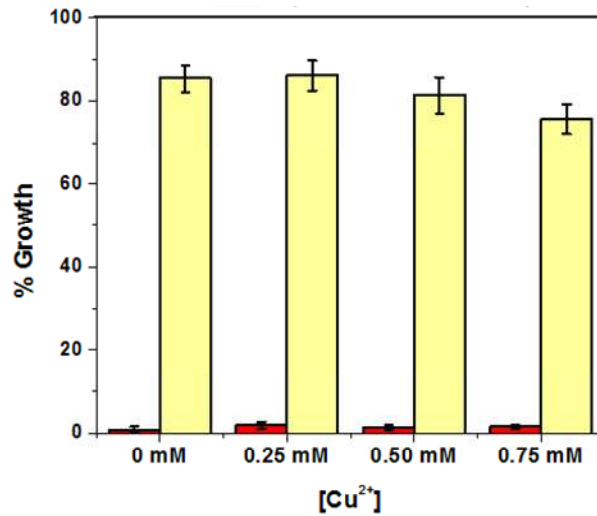
Figure 3.7 *In vivo* **effect of Arg177 mutation.** Growth recovery in yeast producing R177A mutant actin (yellow) as compared to wild-type actin (red) when treated with Photox. Error bars show the standard deviation of 8 replicates. The 100% horizontal line represents growth of yeast expressing a non-toxic aminotransferase protein, as described earlier (Turgeon et al, 2009).
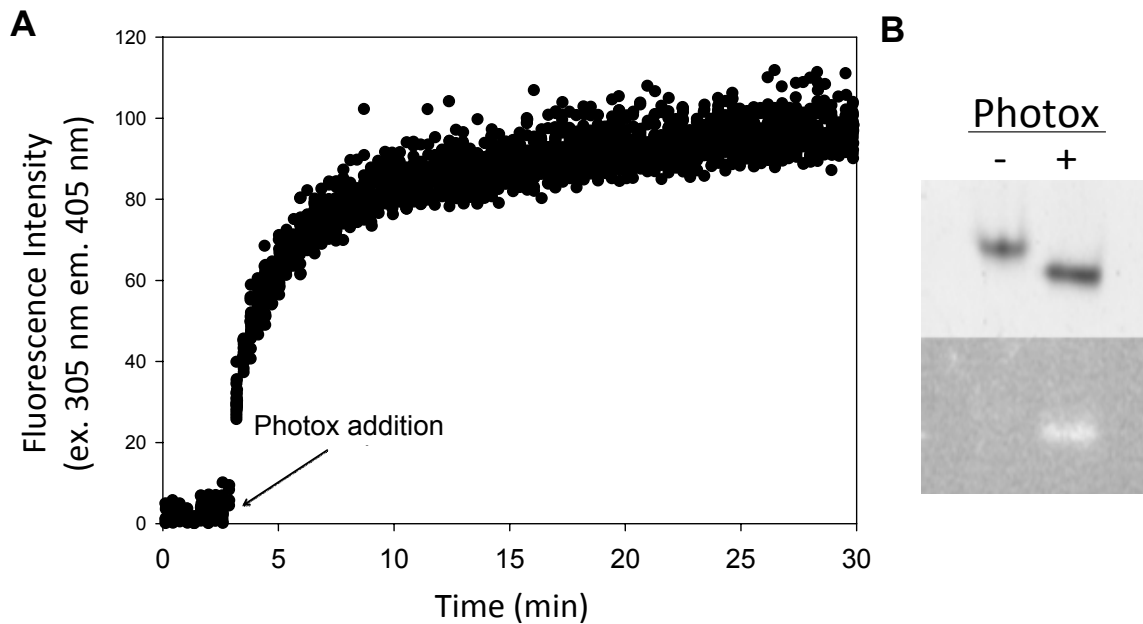
Figure 3.8 ADP-ribosylation of actin by Photox. (A) Fluorescence intensity trace of the reaction of α-skeletal actin, ε-NAD$^+$ and Photox, showing increasing fluorescence intensity following the addition of Photox. (B) Native-PAGE analysis of actin in the presence of εNAD$^+$, with or without the addition of Photox, shows a shift in relative mobility upon ADP-ribosylation. Ultra-violet visualization (lower panel) shows detectable fluorescence only in the presence of Photox.

Photox mART activity exhibited Michaelis-Menten kinetic behaviour with respect to the actin substrate (Figure 3.9A). The Michaelis constant, K_M, was found to be 0.60 ± 0.08 μM for the α-actin substrate. The initial reaction rates at various ε-NAD$^+$ concentrations were also fitted to the Michaelis-Menten model, and the K_M with respect to ε-NAD$^+$ was found to be 27.4 ± 4.4 μM (Figure 3.9B). This is only marginally higher than that observed for the closely related Iota toxin ($K_M = 6.0$ μM) (Barth et al, 1998). As shown in Table 3.1, Photox is a highly efficient and active mART enzyme ($k_{cat}/K_M = 10^7$-10^9 M^{-1}min^{-1}) with a substrate turnover number, k_{cat}, of 1680 ± 75 min^{-1}. This measure of activity is again comparable to that of Iota toxin ($k_{cat} = 2200$ min^{-1}) (Barth et al, 1998).

Single point mutations for Photox were employed to identify key catalytic residues. Trp fluorescence wavelength emission maximum ($\lambda_{em,max}$) values were measured to assess the folded integrity of WT and mutant Photox enzymes. Resulting data indicated that all of the mutants were folded similarly to the WT enzyme ($\lambda_{em,max} = 343$-344 nm; Table 3.2). Significant impairment in Photox mART activity was observed when signature catalytic residues were replaced with Ala. The greatest change was evident when the Region 1 conserved Arg was substituted with Ala. Although the concentration of Photox was increased by nearly 200-fold, a slope could not be accurately measured since it was below the limit of detection of the instrument, which was at least 100-fold slower than the initial velocity of wild type Photox. It is therefore safe to say that the R177A mutant shows at least a 20,000-fold decrease in k_{cat} (Table 3.2). Replacement of the primary and secondary Region 3 Glu residues with Ala resulted in 13,000- and 600-fold reductions in mART activity, respectively, while the conversion of the Region 2 Ser-
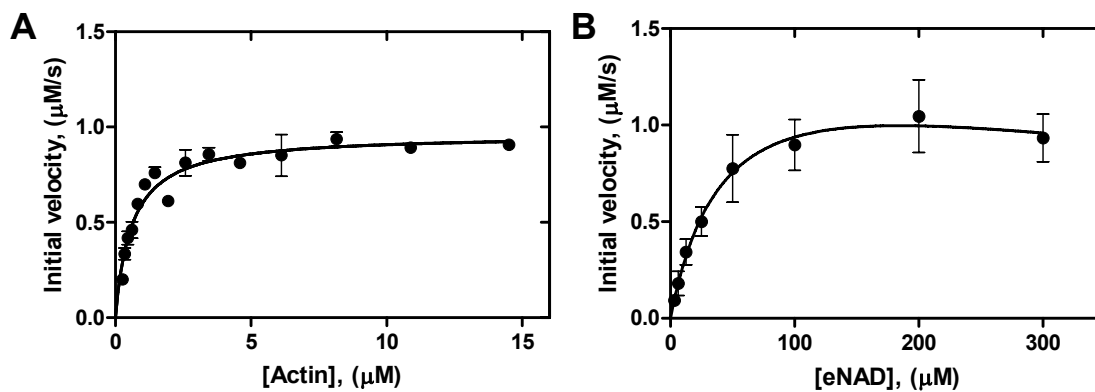
Figure 3.9 Michaelis-Menten plots of Photox mART activity. (A) Photox activity as a function of actin concentration. Initial velocity measurements were obtained using 200 μM ε-NAD$^+$ (saturating) and 40 nM Photox at 25°C, and fit to a standard Michaelis-Menten model. (B) Dependence of initial velocity on ε-NAD$^+$ concentration. Measurements were obtained using 3.5 μM actin and 40 nM Photox at 25°C, and were fitted to a substrate inhibition model.

TABLE 3.1

Kinetic Parameters for Photox mART Activity

Parameter	Varied Substrate	
	NAD^+	Actin
K_M (μM)	27.4 ± 4.4	0.60 ± 0.08
V_{max} (μM min^{-1})	67.2 ± 3.0	57.6 ± 1.86
k_{cat} (min^{-1})	1680 ± 75	-*
k_{cat}/K_M (M^{-1} min^{-1})	6.13×10^7	2.4×10^9

Note: Kinetic parameters were measured as described in Experimental Procedures section. All measurements represent the mean ± standard deviation of at least 5 replicates. When [εNAD$^+$] was varied, actin was held constant at 3.5 μM. When [actin] was varied, εNAD$^+$ was held constant at 250 μM. Photox was held constant at 40 nM. *k_{cat} could not be accurately determined using varied concentrations of actin due to the propensity of actin to polymerize at high concentration under the conditions required for this reaction.

TABLE 3.2

Tryptophan Emission, Activity, and Substrate Affinity of Photox Mutants

Photox mutant	Trp λ emission maximum (nm)	Relative k_{cat} (mART activity)	Relative K_d (NAD$^+$)[a]
Wildtype	344 ± 1	1.00	1.00 ± 0.03
E353A	343 ± 1	0.00156	1.22 ± 0.08
E355A	344 ± 0	0.0000737	3.67 ± 0.14
R288A	343 ± 0	≈ 0[b]	4.28 ± 0.45
STS/ATA	343 ± 0	0.000470	5.41 ± 1.07

Note: Measurements were obtained as described in *Experimental Procedures* section and represent the mean ± standard deviation. Trp λ emission measurements represent at least 3 replicates; mART activity, at least 5 replicates.

[a]Based on a K_d value for wildtype Photox of 11.2 + 0.3 μM.

[b]Measurements of initial slopes were below the limit of detection of the instrument, at approximately 0.0001 FI/s.

Thr-Ser motif to Ala-Thr-Ala decreased the activity by 2000-fold. These noteworthy decreases in mART activity indicate that these residues do indeed play important catalytic roles in the enzymatic activity of Photox, which strongly correlates with observations made for other actin-targeting members of this toxin family. Previous studies have shown comparable relative activity changes for mutations in these signature catalytic residues of C2I from *C. botulinum* and Iota toxin from *C. perfringens* (Barth et al, 1998, Otto et al, 2000).

Notably, NAD^+-glycohydrolase activity was not detectable for WT or mutant Photox enzymes, although most mARTs are known to possess this residual activity, which hydrolyzes the NAD^+ in the absence of a protein substrate. Among actin-targeting mARTs, both C2I and Iota toxin show NAD^+-glycohydrolase activity (Otto et al, 2000, Schleberger et al, 2006) whereas SpvB does not (Sakurai et al, 2003, Sun et al, 2004) further highlighting the similarity of SpvB to Photox.

A simultaneous kinetic characterization of modified actin by our collaborators revealed that actin polymerization is inhibited by ADP-ribosylation at Arg-177 (Visschedyk et al, 2010). By several different techniques, ADP-ribosylated actin was found to be polymerization-deficient, even under ionic conditions which would favour actin's complete polymerization. Furthermore, F-actin treated with Photox was found to depolymerize, and remain in the G-actin form, indicating that Photox ribosylated G-actin, and sequestered it from the G-F equilibrium. Given the importance of actin within a cell, it is not surprising that this disruption of the G- and F-actin equilibrium would have serious deleterious effects.

3.2.5 Photox NAD$^+$ binding

NAD$^+$ binding was measured using a fluorescence assay based on the quenching of the intrinsic tryptophan fluorescence. The NAD$^+$ binding constant (K_d) was determined to be 11.2 ± 0.3 μM for wild type Photox. This is only slightly tighter binding than other mART toxins, including Certhrax (K_d = 52.3 ± 12.2 μM), (Visschedyk et al, 2012), and C3 toxin (K_d = 60 ± 6 μM) (Menetrey et al, 2002). The binding constant of each Photox catalytic mutant for NAD$^+$ was measured in the same way, and the results are given in Table 3.2. Importantly, none of these mutations affected the NAD$^+$-binding ability of Photox in the absence of the actin protein substrate, and all catalytic-signature mutants had similar NAD$^+$ binding constants to the wild-type enzyme. The greatest change in NAD$^+$ binding was seen when the STS motif was replaced with ATA, yet the difference is only a 5-fold increase in K_d which does not indicate a significant alteration. This is unlike the large changes in enzymatic activity as a result of substituting these same catalytic residues with Ala.

3.2.6 Photox colocalization with actin *in vivo*

To study Photox-actin interactions within the cell, fluorescence microscopy of yeast cells expressing GFP-Photox E353A/E355A was used to observe the possible co-localization with actin (Figure 3.10). Visualization of actin using rhodamine-phalloidin resulted in images that could be overlaid with those depicting the GFP-Photox signal. Yellow regions of overlapping intensity indicate that Photox is co-localized with actin within the cell. Some areas where co-localization is not seen may be due to intracellular
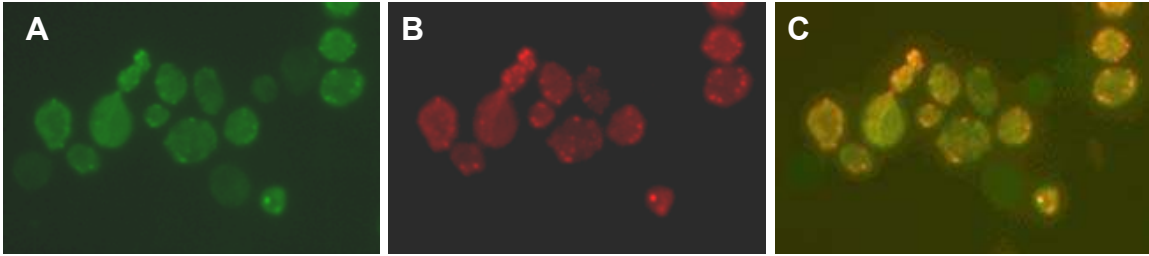
69

Figure 3.10 **Photox co-localization with actin.** Fluorescent images of yeast (W303a) expressing GFP-Photox and stained with rhodamine-phalloidin. (A) GFP-Photox expression, (B) Rhodamine-phalloidin staining of F-actin, (C) Overlay of (A) and (B) where areas of yellow indicate co-localization.

Photox association with monomeric G-actin, which would not have been labeled by rhodamine-phalloidin.

3.2.7 Photox homology modeling

Due to limited solubility, Photox proved recalcitrant to X-ray crystallography. Thus, we employed a homology modeling approach to understand the structure-function relationships of Photox and its interactions with NAD^+ and actin. A model of the Photox catalytic domain (Figure 3.11) was built based on the 1.9 Å X-ray structure of NAD^+-bound SpvB from *Salmonella typhimurium* (PDB:2GWL), and spans 200 residues (209-408) in length (Visschedyk et al, 2010). High identity (61%) between the catalytic domains of these two proteins allowed for reliable and accurate modeling (Figure 3.12). Importantly, there are no insertions or deletions in the catalytic domain sequence alignment of these two proteins, and Photox includes a homologous region to the 30-residue segment previously unique to SpvB (residues 232-262 of Photox). Quality assessment of this model estimated a Global Distance Test-Total Score of 45.62. This score is an estimated measure of the position difference between Cα atoms in theoretical and experimental models. Values >40 indicate the correct fold, and those >84 imply reliable use in molecular replacement (Giorgetti et al, 2005). The score of 45.62 is respectable, indicating the correct fold for Photox modeled on SpvB.

3.2.8 The Photox catalytic domain

The catalytic domain of Photox is predicted to be an α/β protein which includes two anti-parallel β-sheets and separate α and β regions characteristic of the ADP-ribosylation
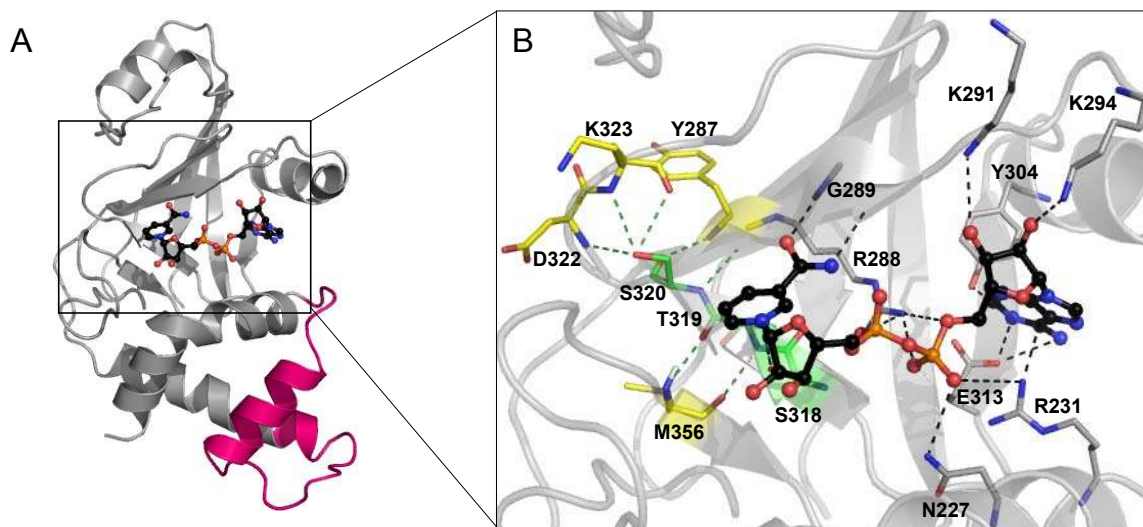
Figure 3.11 Structural model of Photox in complex with NAD⁺. (A) Cartoon representation of Photox (grey) with NAD⁺ (ball-and-stick, coloured by atom, carbon in black). The structure of Photox was modeled on SpvB-NAD⁺ (PDB: 2GWL). The insertion domain, previously unique to SpvB is highlighted in pink. (B) Interactions of Photox with NAD⁺. Predicted hydrogen bonds are indicated by dashed lines. Participating Photox residues are shown in stick format (grey). Residues which further stabilize the active site through hydrogen bonds with the STS motif (green) are shown in yellow.

Figure 3.12 Sequence alignment of Photox with SpvB. Full-length Photox aligned with full-length SpvB using the Expresso alignment software on the T-Coffee server (Armougam et al, 2006). The colour spectrum indicates areas of high identity or conservation (red) to poor identity or conservation (green). Dashed lines indicate gap regions in one sequence with respect to the other. Sequences inside the purple brackets were used for the homology model of Photox.

fold (SCOP code d.166.1.1). As with other members of this toxin family, NAD^+ binding is expected to occur through both hydrogen bonds and hydrophobic interactions. Fourteen hydrogen bonds are predicted between Photox and NAD^+, and are illustrated in Figure 3.11.

The active site is further stabilized by the STS motif which forms a scaffold of hydrogen-bonded residues. Ser-318 binds Glu-355, while Thr-319 forms hydrogen bonds to an adjacent β-sheet to maintain active site integrity, and Ser-320 orients the ARTT loop, including Glu-353 (Figure 3.11). These proposed interactions help to explain the observed decreases in activity after replacement of signature mART catalytic residues with Ala as reported above. Gly-289 was not substituted because this model indicates that its main chain atoms are involved in interactions within the active site, and any residue would be expected to have a similar effect. Ala replacement of those residues indicated in Figure 3.11, but not substituted in this study are also expected to negatively affect mART activity to varying degrees based on conservation among C2- and C3-like mARTs.

3.2.9 A model of Photox in complex with actin

The Photox homology model was further assembled into a complex (Figure 3.13) with actin based on the recent Iota-actin 2.81 Å X-ray structure (PDB ID: 3BUZ) (Tsuge et al, 2008). In the proposed complex, 22 Photox residues interact with 27 actin residues over an approximately 1,300 $Å^2$ area. Photox, like other mARTs, likely recognizes actin through the region B active site loop (residues 238-254), the PN loop (residues 321-329) and the ARTT loop (residues 344-354) (Sun et al, 2004). Iota was further found to
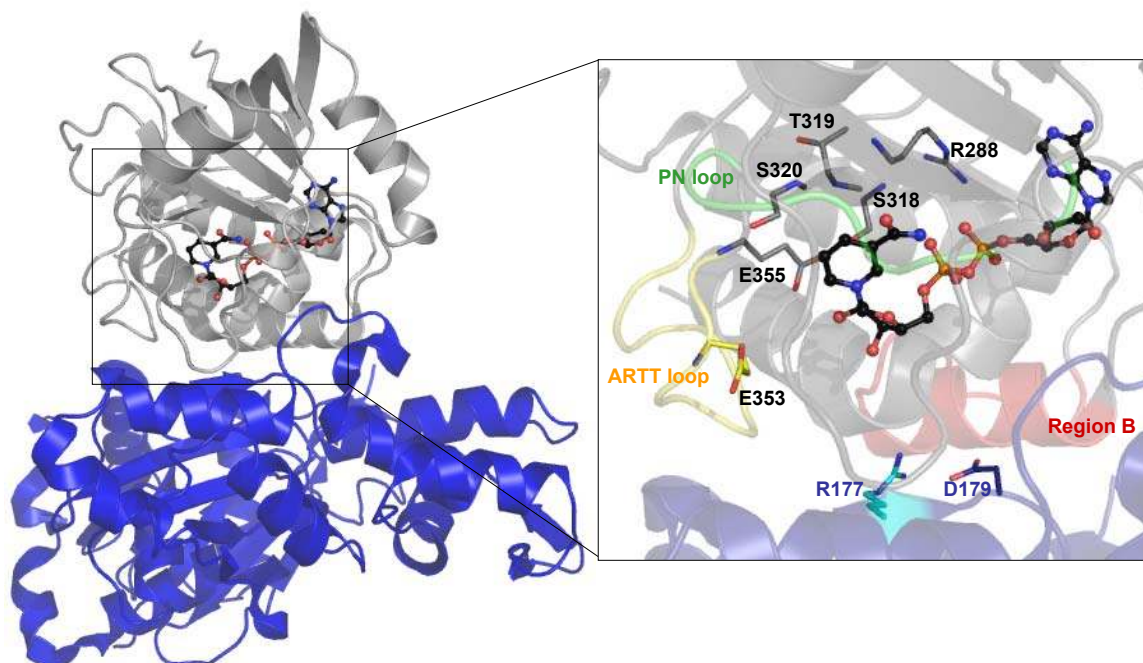
Figure 3.13 Structural model of Photox-actin-NAD$^+$ Michaelis complex. (A) Cartoon representation of Photox (grey), actin (blue) and NAD$^+$ (\ball-and-stick, coloured by atom, carbon in black). The structure of Photox was superimposed on Iota toxin in an Iota-actin complex (PDB: 3BUZ) using Coot. Inset: Important active-site residues of the Photox-actin complex with NAD$^+$ (black, ball-and-stick, coloured by atom) in the active site. Catalytically important residues are shown in stick representation, colored by atom and Arg177 (cyan) and Asp179 (blue) of actin are shown in stick representation. Important loops are in cartoon and colored yellow (ARTT loop), and green (PN loop), and the region B active site loop is seen behind the actin in red.

recognize its protein substrate through loop I of the N domain and another loop between α9 and β10; however, these residues are not conserved. Given the similarities in substrate specificity, one might predict that Photox would use a similar recognition motif, but further studies would be required for confirmation. Interestingly, only three residues along the Iota-actin interface are different in α- and β/γ-actin (M/L 176, A/C 272, and Y/F 279) (Tsuge et al, 2008). Mutagenesis studies of these residues may elucidate why some actin-targeting mARTs selectively ADP-ribosylate β/γ-actin only, while others are non-specific.

The authors of the Iota-actin structure complex proposed a common S_N1 alleviated-strain reaction mechanism for the actin-targeting mART toxins whereby an oxocarbenium intermediate is formed following the cleavage of the nicotinamide moiety from NAD^+. Finally, the nucleophilic attack on Arg-177 of the target actin leaves the ADP-ribose group covalently bound to this protein (Tsuge et al, 2008). Based on the similarities in structure and substrate identification, it is proposed that Photox would follow a similar mechanism (Figure 3.14). In this regard, Glu355 is poised to hydrogen bond to the nicotinamide-ribose, while phosphate electrostatic interactions hold the NAD^+ in a conformation favouring oxocarbenium cation formation. Tyr223 is in place to possibly assist bond rotation about the nicotinamide-phosphate single bond, to likely reposition the nicotinamide ribose. Actin Asp179 may stabilize the nicotinamide ribose, and Photox Glu353 is in range to stabilize actin Arg177 so it can proceed with nucleophilic attack of the oxacarbenium cation.
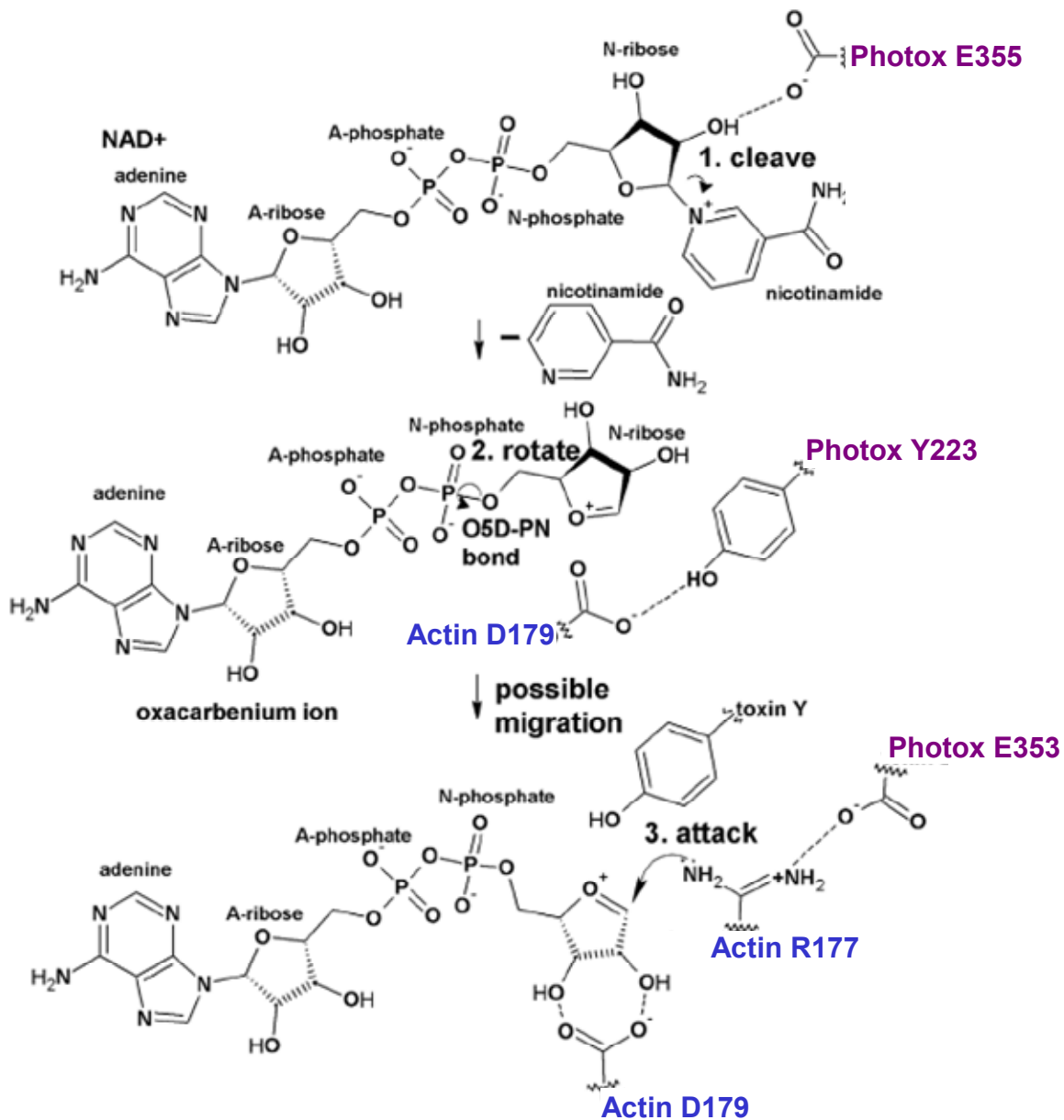
Figure 3.14 Proposed reaction mechanism for the mono-ADP-ribosylation of actin by Photox. First, the universally conserved primary catalytic Glu, E355 holds the NAD$^+$ in a conformation that favours the oxacarbenium ion intermediate. Second, Y223 may induce the rotation of the ribose ring to alleviate strain and bring the electrophile in closer proximity to the nucleophile. Finally, D179 stabilizes the ribose group, the secondary catalytic Glu, E353, stabilizes the target R177, and this R177 attacks the oxacarbenium ion resulting in covalent modification (modified from Fieldhouse et al, 2010).

3.2.10 Steric hindrance by ADP-ribosylation of actin

Using the Holmes model of filamentous actin, it has been previously shown (Margarit et al, 2006) that the location of the ADP-ribosylation site on actin, Arg177, is at an important region of inter-subunit interactions. Crystal structures of ADP-ribosylated actin monomers reveal no large structural changes due to this modification, so it has been suggested that polymerization is impeded by steric hindrance, and not by allosteric changes (Margarit et al, 2006). Recently, high resolution fiber diffraction studies have resulted in the Oda model (Oda et al, 2009), which adapts important details of the Holmes model of filamentous actin. Inspection of the current Oda model reveals few differences in the interaction of nearby intersubunit residues with Arg177. As a result, we suggest that the proposed change in actin structure should not present large changes for studies of actin-targeting mARTs. The ADP-ribose moiety is approximately 12 Å in length, so its addition at Arg177 may result in a reduction of actin polymerization due to steric hindrance. Residues involved in inter-subunit interactions in the Holmes model and previously predicted to be affected by the ADP-ribosylation include Glu-195, Ser-199, Phe-200 and Val-201 (Margarit et al, 2006). A search for near neighbours of Arg-177 in the Oda trimer reveals 17 residues of the adjacent actin subunit within 12 Å. Residues 187-202, and Glu-205 from the lower subunit are all within range to be affected by a 12 Å modification (Figure 3.15). Interestingly, a structure of ADP-ribosylated actin does not show the ADP-ribose modification, so it is presumed that it may possess a high degree of mobility (Margarit et al, 2006). Although there is a pocket adjacent to Arg177 that can accommodate phalloidin (1.5-fold larger than ADP-ribose) to stabilize filaments, perhaps the mobility of the ADP-ribose modification indicates that it does not remain bound in
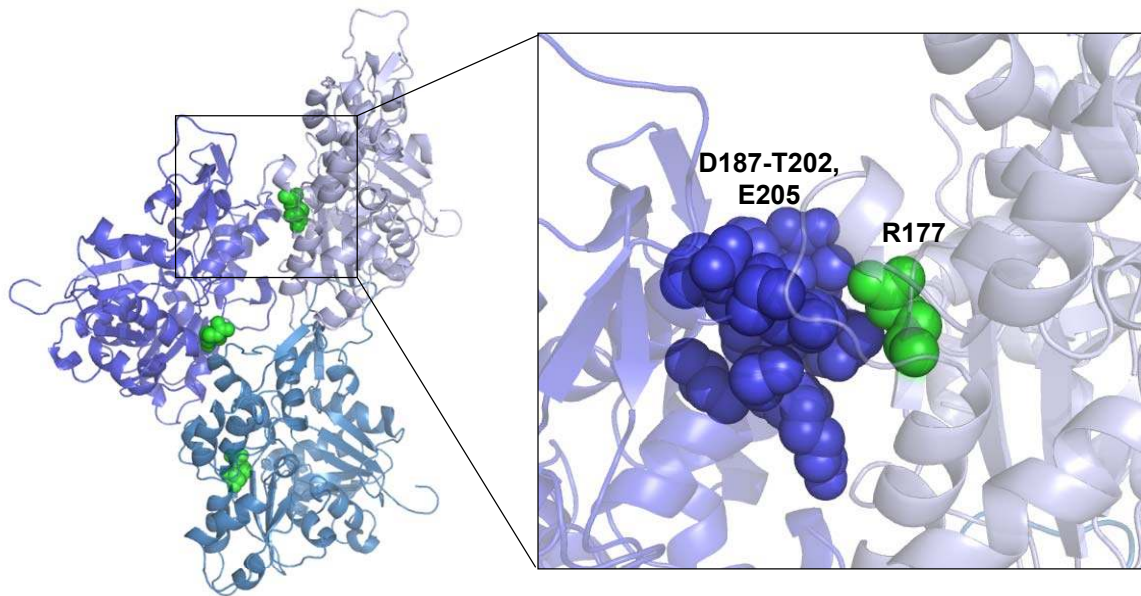
Figure 3.15 Model of actin polymer. Oda model of an F-actin trimer (Oda et al, 2009). Distinct actin subunits are shown in shades of blue. Arg177, site of ADP-ribosylation, is indicated by green spheres. Inset: Residues at the subunit interface. Arg177 is shown in green spheres, residues within 12 Å are displayed as blue spheres and include D187-T202 and E205.   .

this pocket, but is mobile enough to be creating steric clashes at the interface of actin subunits, thus preventing polymerization. Furthermore, a previous study has shown that actin with an ADP-ribose modification at Arg-177 can still form F-actin filaments, when incorporated with unmodified actin monomers in equal ratio in the presence of 2 mM MgCl$_2$ (Ballweber et al, 2001). However, the rate is decreased by approximately 25-fold, and ADP-ribosylated monomers are incorporated only at a minimal ratio of 4:1 of native to modified actin, indicating that in this case, the modification is not an absolute preventor of actin polymerization, but rather a severe hindrance. Perhaps, in this instance, the filament is able to form when the ADP-ribose is held in the pocket where phalloidin generally binds. A high-resolution structure of the F-actin filament would elucidate the mechanism of this polymerization deficiency, and clarify these hypotheses.

3.2.11 Structural comparison with other mARTs

Photox varies considerably from SpvB in domain organization. Unlike the single-domain SpvB, Photox includes an additional N-terminal domain from residue 1 to approximately residue 185. The Photox N-terminal domain is presently an enigma, as it is predicted to be highly disordered by GeneSilico. A BLAST search did not identify any homology or sequence similarity to the B component of other actin-targeting mARTs indicating that Photox may not function in the typical binary fashion. Based on the predicted disorder, it is possible that this domain may participate in chaperone binding in a secretion system, or perhaps entry of the toxin into the host cell, but details are not yet known. Genetic neighbourhood evidence collected from the STRING 8.0 database suggests interactions may occur between *plu0822* (encoding Photox) and *plu0826*

(encoding a VgrG-type protein) within *P. luminescens*. VgrG is thought to penetrate target cells during type VI secretion to serve as a translocator or an effector (Pukatzki et al, 2007), presenting the possibility that Photox may also infect cells via type VI secretion. Futher studies will be required to characterize the mechanism of cellular entry of this new mART toxin.

Structural details may also provide some insight into substrate specificity. Based on the structure of the Iota-actin complex, Tsuge et al. (2008) listed only three residues found at the toxin-actin interface that differ in muscle and non-muscle actin. One of these, Tyr-279 of actin, interacts with Tyr-62 on loop I of Iota toxin, which was shown to be an essential residue for mART activity (Tsuge et al, 2008). Interestingly, a structure-based sequence alignment at this position reveals a Tyr residue for each of Iota toxin, SpvB, CDTa, and Sa, but a threonine residue in C2 toxins. Therefore, this residue may play an important role in discrimination between actin isoforms, as C2 toxins are unique in their inability to modify α-skeletal muscle actin. Unfortunately, the N-terminal region of Photox could not be modeled accurately, and a sequence alignment at this position did not reveal any meaningful conclusions, but it would be expected to share the conserved Tyr motif.

3.3 CONCLUSION

Photox was identified as a novel mART toxin using a variety of *in silico* techniques. A thorough biochemical characterization confirmed that it is indeed a new member of the actin-targeting subgroup of mART bacterial enzymes. Mono-ADP-ribosylation of actin by Photox is comparable to that of other actin-targeting mARTs, and

as with other mART enzymes, Arg177 of actin is the specific site of modification. Structural modeling indicates that Photox is closely related to SpvB of *Salmonella enterica*, so it is not surprising that Photox shares SpvB's lack of glycohydrolase activity and 30-residue insertion segment. Furthermore, Photox is non-specific with respect to ADP-ribosylation of various actin isoforms, differentiating it from the C2 group of actin-targeting mART toxins. This characterization of a novel actin-targeting mART enzyme expands our knowledge of this family of toxic proteins and will be useful in the generation of effective and broad-spectrum inhibitors against these toxins.

CHAPTER 4 - CERTHRAX: THE ANTHRAX COUSIN WITH A KILLER TWIST

4.1 OVERVIEW

4.1.1 Abstract

The mART family of toxins is produced by pathogenic bacteria that contribute to many diseases in humans. Using a bioinformatic strategy, we identified Certhrax, the first anthrax-like mART toxin from the pathogenic G9241 strain of *B. cereus*. This enzyme was shown to be 60 times more toxic to mammalian cells than anthrax LF from *Bacillus anthracis*. Substitution of catalytic residues shows that the mART function is responsible for toxicity, and the protein binds NAD$^+$ with high affinity (K_d = 52.3 ± 12.2 μM). We report the 2.2 Å Certhrax X-ray crystal structure, highlighting its structural similarity with anthrax LF. We determined the crystal structures of Certhrax in complex with two potent inhibitors (P6, K_d = 1.7 ± 0.2 μM, K_i = 1.8 ± 0.4 μM; and PJ34, K_d = 5.8 ± 2.6 μM, K_i = 9.6 ± 0.3 μM). As with other toxins in this family, the phosphate-nicotinamide loop moves toward the NAD$^+$ binding site when the inhibitor is bound. These results indicate that Certhrax may be important in the pathogenesis of *B. cereus* strain G9241.

4.1.2 Introduction to anthrax toxin

Bacillus anthracis is infamous as the causative agent of anthrax which gained notoriety in 2001 after spores were sent through the U.S. Postal Service, infecting 22 people and killing five (Jernigan et al, 2001), and remains in the public eye as a potential bioterrorist threat. Inhalation anthrax is often fatal, as diagnosis is often not possible until the disease has progressed too far for antibiotic treatment to be effective. Anthrax toxin consists of three individually nontoxic proteins. Namely, the PA is recruited to form heptamers on cell surface receptors, which can then bind anthrax LF or edema factor (EF) to form a bipartite toxin. Endocytosis delivers the proteins to an endosome, where LF or EF can be translocated to the cytoplasm under acidic conditions. Once inside the cell, anthrax LF, which is a zinc metalloprotease, cleaves and inactivates mitogen-activated protein kinase kinases (MAPKK) to interfere with cell signaling (Duesbery et al, 1998, Tonello & Montecucco, 2009, Vitale et al, 1998). Anthrax EF, which is a calcium- and calmodulin-dependent adenylyl cyclase, catalyses the production of cAMP and also affects cell signaling and ion fluxes (Drum et al, 2002, Shen et al, 2005). Two plasmids, pXO1 and pXO2 are essential for anthrax toxicity. pXO1 contains genes for PA, LF and EF, while pXO2 encodes a poly-γ-D-glutamic acid capsule that participates in virulence by evading the host immune system (Candela & Fouet, 2006, Drysdale et al, 2005). These plasmids were thought to distinguish *B. anthracis* from other *Bacillus* species until recently, when related *Bacillus cereus* strains were found to contain similar plasmids.

4.1.3 Introduction to *Bacillus cereus*

B. cereus is a Gram-positive, spore-forming, rod-shaped bacterium, widely found in soil, dust, water and the hospital environment. It has been widely accepted as a causative agent of emetic and diarrheal food poisoning. Since most *B. cereus* isolates are harmless, it is often dismissed as a nosocomial pest due to its ubiquitous nature. However, in immunocompromised patients, *B. cereus* may cause a number of illnesses including septicemia, cutaneous infections, pneumonia, and periodontal disease (Bottone, 2010). In recent years, more severe *B. cereus* infections have been reported in otherwise healthy individuals, involving overwhelming sepsis and sometimes fatal pulmonary infections resembling anthrax respiratory disease (Avashia et al, 2007, Hoffmaster et al, 2006, Miller et al, 1997). As a result, this bacterium is now gaining attention as a *bona fide* human pathogen. *B. cereus* G9241, a strain associated with severe pneumonia in previously healthy patients, has been well characterized and shown to harbour a nearly complete pXO1 plasmid, similar to that of *B. anthracis* (Hoffmaster et al, 2004).

4.1.4 *In silico* identification of Certhrax

In silico analysis using bioinformatics tools has revealed a putative novel mART toxin, which we have named Certhrax, in the *B. cereus* G4291 strain (Fieldhouse et al, 2010). The 476-residue Certhrax protein is found on the pBC218 plasmid of this strain. This two-domain protein consists of a predicted PA-binding domain and mART domain. Specifically, the C-terminal mART domain shares up to 34% sequence identity with C2- and C3-like mART toxins. Primary structure alignment with other members of the mART

family indicates that Certhrax includes all of the crucial catalytic residues necessary for ADP-ribosyltransferase activity. Figure 4.1A compares active-site residues of the Certhrax mART domain with sequences of other mART toxins. It is evident that the classic mART catalytic Arg in region 1, known to aid in NAD^+-binding, the STS motif in Region 2 that forms the scaffold for the active site, and the catalytic Glu-x-Gln motif in Region 3 crucial for activity, are all present in Certhrax.

Certhrax also shares 31% identity and 51% similarity with anthrax LF from *B. anthracis* and has similar domain organization, which is highlighted in Figure 4.1B. Each protein contains a PA-binding domain and a mART domain; however, the latter is missing critical catalytic residues and is inactive in anthrax LF. In addition, the C-terminus of anthrax LF harbors an insertion in the mART domain and a zinc metalloprotease domain which confers its toxic effects. Both of these are absent in Certhrax, suggesting that the two toxins, while sharing some common structure and cell entry mechanism, do not share the same mechanism of lethality (target protein). In this chapter, we characterize Certhrax as a novel mART enzyme using a variety of biochemical techniques.

4.2 RESULTS

4.2.1 Overexpression and purification of Certhrax

Full-length Certhrax was over-expressed in Rosetta cells and purified at a yield of approximately 4 mg/L culture using immobilized metal affinity chromatography. The purity level was visualized by SDS-PAGE as seen in Figure 4.2 and the protein was positively identified by Western blot analysis using an anti-His tag antibody.

A

Toxin, *Organism*	Region 1	Region 2	Region 3
Certhrax, *B. cereus*	LIVY**R**RVS(39)	NYM**STS**LVQ(33)	YPG**Q**U**E**MLI
Iota, *C. perfringens*	LIVY**R**RSG(36)	NFI**STS**IGS(31)	YAG**E**Y**E**VLL
C2, *C. botulinum*	LIAY**R**RVD(42)	SFS**STS**LKS(30)	FQD**E**Q**E**ILL
Cholera, V. cholerae	DKLY**R**ADS(47)	GYV**STS**ISL(40)	HPD**E**Q**E**VSA
Pertussis, *B. pertussis*	ATVY**R**YDS(36)	AFV**STS**SSR(66)	ATY**Q**S**E**YLA

B

B. anthracis
Anthrax Lethal Factor

| Protective antigen (PA) | | PA-binding | mART (inactive) | Insertion | Zn^{2+} metalloprotease |

B. cereus
Certhrax

| Protective antigen (PA) | | PA-binding | mART (active) |
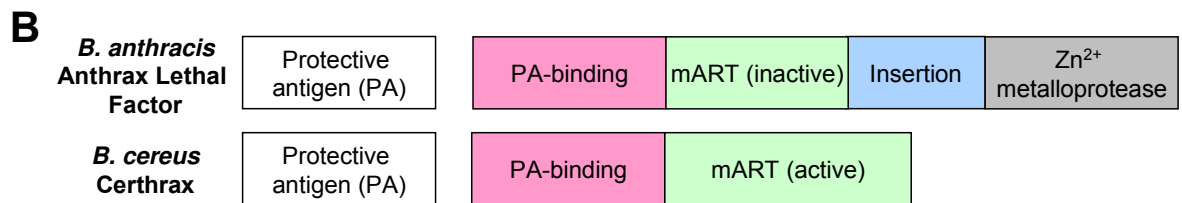
Figure 4.1. *In silico* **identification of Certhrax as a mono-ADP-ribosyltransferase.** (A) Sequence alignment of Certhrax with several other mART toxins. Characteristic active-site residues are shown to be conserved in region 1 (catalytic Arg, orange), region 2 (STS motif, green) and region 3 (catalytic QxE/ExE motif, magenta). (B) Domain organization of *B. anthracis* anthrax LF (top) as compared to *B. cereus* Certhrax (bottom). Each toxin contains a separate PA protein (white), a PA-binding domain (pink), a mART domain (green). Anthrax LF includes an additional insert domain (blue) and a zinc metalloprotease domain (grey). Domain colors correspond to structural images in Figure 4.5 and 4.6.
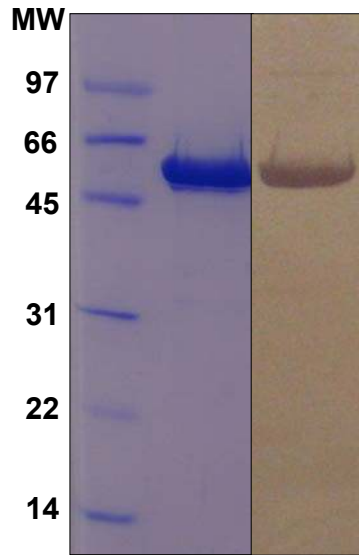
Figure 4.2. **Purification of Certhrax.** SDS-PAGE gel and anti-His tag Western blot showing purified Certhrax. *Lane 1*, molecular weight standards (BioRad) in kDa, *lane 2*, purified Certhrax, *lane 3*, Western blot, purified Certhrax.   .

4.2.2 Certhrax is lethal to cells and gains entry via PA

Mammalian cells were treated with Certhrax to ascertain cytotoxicity. Based on the similarity to anthrax LF, and the homologous PA-binding domain, we predicted that Certhrax would also require PA for cell entry. RAW264.7 cells were selected for Certhrax infection assays since they have classically been used as the host target cells for anthrax LF toxin, and a PA-resistant cell line is available (Klimpel et al, 1992, Quinn et al, 1991). An infection assay using RAW264.7 cells with varying concentrations of Certhrax (0-100,000 pg/mL) in the presence of 100 ng/mL PA gave an LD_{50} of 98.6 ± 4.6 pg/mL (Figure 4.3A) as measured by a 3-(4,5-dimethylthiazol-2-yl)-2,5-diphenyltetrazolium bromide (MTT) colorimetric assay 72 h post-infection. In the absence of PA, cell growth was not impaired, and little cytotoxicity was observed, even at 10 ng/mL (100-fold the Certhrax LD_{50} dose). This indicates that, like anthrax LF, Certhrax is not toxic in the absence of PA (Singh et al, 1989). To further corroborate this result, R3D cells, which lack the PA receptor, were treated with Certhrax (Figure 4.3B). They did not show significant lethality until treated with extremely high doses of Certhrax, even in the presence of PA, supporting the finding that Certhrax achieves cell entry in a similar fashion to anthrax, via a PA-mediated mechanism. Similar studies with anthrax LF gave an LD_{50} of 6.1 ng/mL (Quinn et al, 1991) using the same RAW264.7 cell line and identical concentration of PA. Comparison with the LD_{50} of Certhrax indicates that Certhrax is 60-fold more toxic towards the RAW264.7 cell line than its infamous counterpart.
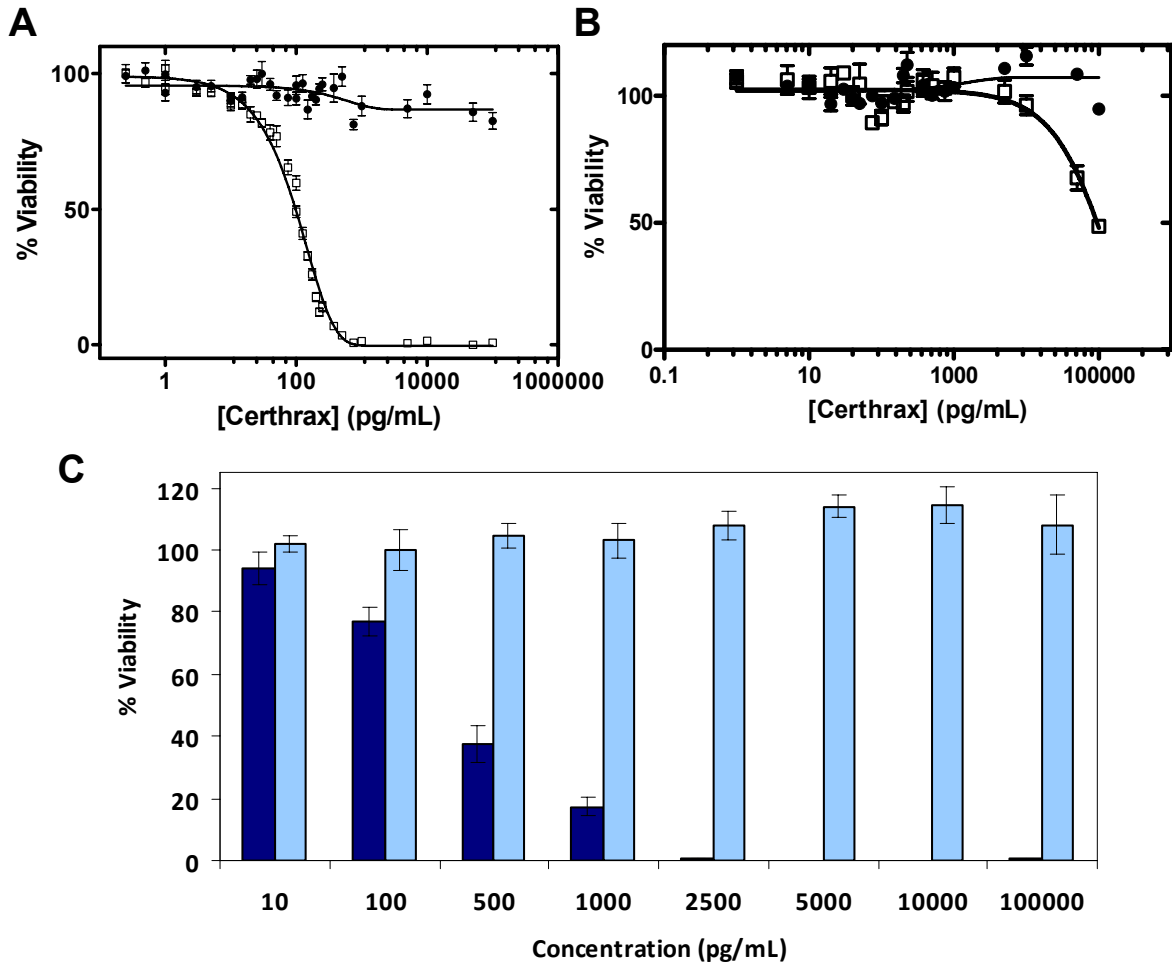
Figure 4.3. Certhrax cytotoxicity. (A) LD_{50} curve of Certhrax with RAW264.7 cells in the presence (squares) and absence (circles) of 100 ng/mL PA, and increasing concentrations of Certhrax. (B) Similar LD_{50} experiment to that in (A), using R3D cells lacking the PA receptor in the presence (squares) and absence (circles) of 100 ng/mL PA, and increasing concentrations of Certhrax. (C) Effect of Certhrax on mouse macrophage cell growth as indicated by percent viability of cells 72 h following addition of 100 ng/mL PA and increasing concentrations of wild type Certhrax (dark blue) or Q/E mutant Certhrax (light blue) where the catalytic Gln and Glu have each been replaced with Ala. In (A) and (B), the Certhrax concentrations ranged 0-100,000 pg/mL and in (A)-(C), cell viability was measured using an MTT colorimetric assay (described in the Experimental Procedures section).

91

4.2.3 Certhrax is a novel bacterial mART enzyme

The infection assay was then used to evaluate the mART activity of the C-terminal domain of Certhrax. A catalytically inactive Certhrax in which both the hallmark Gln429 and Glu431 residues were substituted with Ala (QxE variant) was prepared. Proper folding was monitored by measuring the maximum wavelength of intrinsic tryptophan emission, which was 339 nm for both wild type and QxE Certhrax. The lethality of this QxE variant was compared with wild-type Certhrax activity (Figure 4.3C). While 2.5 ng/mL of Certhrax was enough to kill 100% of RAW264.7 cells, the catalytically inactive Certhrax was much less toxic, since the cells remained ~100% viable even at a 100 ng/mL concentration. This indicates that these active-site residues are required for the mART activity, and the mART enzymatic activity is responsible for the observed growth-defective phenotype in mouse fibroblasts.

4.2.4 Confocal microscopy imaging of cell entry

In order to visualize the host cell entry of Certhrax, RAW264.7 cells, in the presence of 100 ng/mL PA, were treated with Certhrax covalently labeled with a fluorophore, DyLight488. Cells were infected with Certhrax for various times before being fixed and imaged using confocal microscopy (Figure 4.4A-I). At 5 min post-infection (Figure 4.4D), a weak fluorescence signal was seen, indicating that Certhrax had entered the cells. By 10 min post-infection (Figure 4.4E) Certhrax started to localize in specific regions and was no longer evenly dispersed throughout the cell. Concurrent DAPI staining showed that the Certhrax was extranuclear in its cellular location. After 20 min (Figure 4.4F), the toxin aggregated to form specific punctate regions within the cell,

92
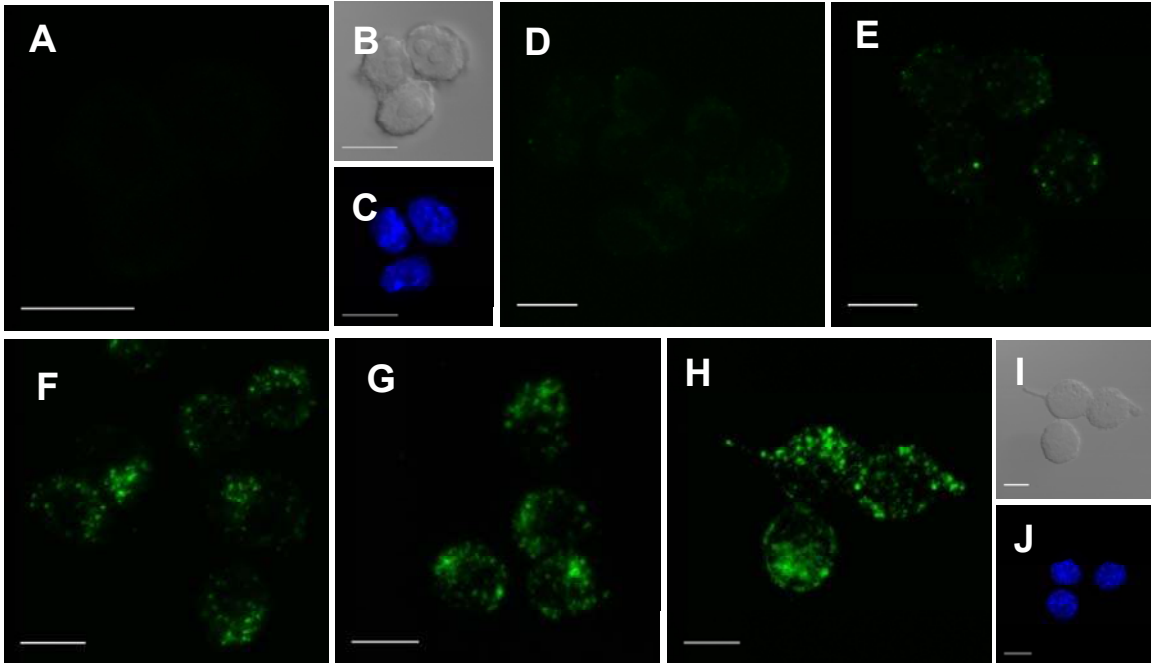
Figure 4.4. Certhrax host cell entry. (A)-(J) Fluorescence confocal microscopy of Certhrax infection of RAW264.7 cells. Cells were fixed and stained with DAPI at varying time points post-infection with DyLight488 fluorophore-labeled Certhrax in the presence of 100 ng/mL PA. (A) 0 min, (D) 5 min, (E) 10 min, (F) 20 min, (G) 1 h, (H) 24 h post-infection. (B) and (I) show cells under DIC at 0 min and 24 h, respectively, while (C) and (J) illustrate DAPI staining at 0 min and 24 h, respectively. Scale bar is 10 μm.

which increased in intensity until 1 h had elapsed (Figure 4.4G). This correlates with previous images of anthrax LF infection (Zornetta et al, 2010), where LF is not uniformly distributed throughout the cell, but seems to coalesce with certain cellular organelles.

By 24 h post-infection (Figure 4.4H), the signal remained similar to that after 1 h. Certhrax, like anthrax LF, requires PA for cell entry (Abrami et al, 2003, Abrami et al, 2008, Zornetta et al, 2010), so we expect that the two toxins may follow a similar pathway of cell entry. However Certhrax does not appear to behave identically to anthrax LF once inside the cell. By 90 min post-infection with anthrax LF, Zornetta et al. (2010) observed a small amount of weak punctate staining, predominately cytoplasmic. This is in stark contrast to Certhrax which continues to show intense non-uniform staining even up to 24 h after treatment without an apparent loss in fluorescence intensity. Notably, although anthrax LF and EF also enter cells in an identical manner via the PA receptor, they are each localized in different parts of the cell by 90 min post-treatment. Considering that its mechanism of killing and toxicity are unique, it is not surprising that Certhrax also shows cellular localization distinct from that of anthrax LF. Extensive microscopy studies with numerous antibodies for sub-cellular markers at a variety of timepoints would give more insight into the cellular entry pathway of Certhrax.

4.2.5 NAD$^+$ glycohydrolase activity of Certhrax

NAD$^+$ glycohydrolase activity is present as a secondary enzymatic activity in most mART enzymes and represents the first step of the mART reaction, where OH$^-$ serves as the nucleophile in the absence of a target protein (amino acid nucleophile) (Jorgensen et al 2008). In the absence of a natural protein substrate for mART enzymatic

activity, NAD^+ glycohydrolase activity of Certhrax was characterized using an established fluorescence-based assay (Armstrong & Merrill, 2001). Certhrax NAD^+ glycohydrolase activity exhibited Michaelis-Menten behaviour where the kinetic parameters (Table 4.1) indicate a strong glycohydrolase activity for Certhrax ($K_M = 41.6 \pm 10.9$ µM, $k_{cat} = 8.7 \pm 1.0$ min^{-1}). While some mART enzymes do not exhibit glycohydrolase activity, those that do are generally not as active as Certhrax. For example, Certhrax glycohydrolase activity is more than 300-fold higher than that of exotoxin A from *Pseudomonas aeruginosa* ($k_{cat} = 0.0278 \pm 0.0083$ min^{-1}) (Yates & Merrill, 2005). The addition of the natural protein substrate to the fluorescence assay should lead to a sharp increase in the activity observed, since mART activity is usually 3-4 orders of magnitude higher than the residual glycohydrolase activity of these enzymes. However, the addition of various concentrations of classical C2- and C3-like mART substrates, including purified α-skeletal actin and RhoA, resulted in no change in the activity observed, indicating that these are not substrates for Certhrax, unlike for C2-like and C3-like toxins.

4.2.6 Certhrax NAD^+ binding

A tryptophan fluorescence quenching assay was used to quantify NAD^+-binding by titrating NAD^+ with Certhrax. The dissociation constant, K_d, for Certhrax with NAD^+, 52.3 ± 12.2 µM, indicates a binding affinity for the substrate comparable to that of other mARTs (Table 4.1). For example, the actin-targeting Photox from *Photorhabdus luminscens* has a K_d of 11.2 ± 0.3 µM (Visschedyk et al, 2010), while C3 from *Clostridium botulinum* has a K_d of 60 ± 6 µM (Menetrey et al, 2002).

TABLE 4.1

Kinetic parameters of Certhrax glycohydrolase activity

Parameter	Certhrax
K_M (μM)	41.6 ± 10.9
v_{max} (μM min^{-1})	8.7 ± 4.2
k_{cat} (min^{-1})	8.7 ± 4.2
k_{cat}/K_M (M^{-1} min^{-1})	2.09×10^5
$K_{d\,(NAD+)}$ (μM)	52.3 ± 12.2

Kinetic parameters were determined as described in Experimental Procedures. All measurements represent the mean $\pm$ S.E. of at least 6 replicates, from at least three independent experiments.

4.2.7 Crystal structure of full-length Certhrax

The structure of full-length Certhrax was determined at 2.2 Å in the apo-(substrate-free) form (Table 4.2). As shown in Figure 4.5A, the Certhrax structure includes a PA-binding domain (residues 1-242, pink) at the N-terminus and a mART domain (residues 24-476, green) with α/β topology at the C-terminus. Superposition with the structure of anthrax LF (PDB: 1J7N, Figure 4.5B) illustrates tertiary structural similarity in the mART domain (r.m.s.d. = 4.022 Å over 153 Cα atoms). However, a closer look at important catalytic residues of Certhrax highlights their absence in anthrax LF (Figure 4.5C), which renders its mART domain inactive. The PA-binding domain of each toxin also superimposes closely (r.m.sd. = 1.692 Å over 164 Cα atoms); however the mART and PA domains are twisted with respect to one another when comparing Certhrax with anthrax LF. This N-terminal domain consists of a 12-helix bundle alongside a four-stranded β-sheet. Several regions of anthrax LF domain 1 have been shown to play a role in PA binding, and are relatively conserved in Certhrax as well (Melnyk et al, 2006). Specifically, the region of maximal homology between anthrax EF and LF has previously been shown to play a role in PA-binding (Gupta et al, 2001). Structural alignment shows that this region is also highly conserved in Certhrax (Figure 4.5D) where the sequence Val110-Lys116 in Certhrax differs by only a single amino acid from the homologous sequence Val147-Lys153 in anthrax LF, and aligns closely in tertiary structure. This supports our *in vivo* data showing that Certhrax gains entry to host cells via PA in a similar fashion to anthrax LF and EF.

TABLE 4.2

Crystallographic data and refinement statistics for *B. cereus* Certhrax structures

	Certhrax (cat. domain + PJ34)	Certhrax (full-length)	Certhrax (full-length + P6)
Diffraction data			
X-Ray Source	Rigaku FR-E	CLS beamline 08ID[1]	CLS beamline 08ID
Wavelength [Å]	1.5418	0.9762	0.9762
Unit cell parameters (Å)	$a = 31.9$	$a = 61.37$	$a = 61.31$
	$b = 70.2$	$b = 95.49$	$b = 100.29$
	$c = 98.7$	$c = 190.65$	$c = 191.09$
Space group	$P2_12_12_1$	$P2_12_12_1$	$P2_12_12_1$
Resolution range (Å)[a]	57.2 – 1.8 (1.9 – 1.8)	40 – 2.20 (2.28 – 2.20)	48.50 - 1.96 (2.03 - 1.96)
Data completeness (%)	98.7 (97.0)	98.2 (96.0)	99.14 (98.0)
R_{sym} (%)[b]	6.6 (42.9)	10.4 (69.8)	6.0 (89.6)
Redundancy	3.6	6.8	5.6
Average $I/\sigma(I)$	41.1 (4.2)	25.8 (2.2)	19.7 (2.3)
Refinement statistics			
Molecular replacement program	MOLREP[2]	PHASER[3]	PHASER
Molecular replacement model	PDB entry 3BW8	Certhrax$_c$ and Certhrax N-terminal domain structure (unpublished)	Certhrax$_{FL}$
R_{work} (%)[c]/R_{free} (%)[d]	20.9/25.7	24.2/28.8	18.9/22.8
No. of atoms			
Protein	1,628	6,735	7,301
Ligand	22		52
Water	163	26	493
R.M.S.D. from ideal			
bond length (Å)	0.010	0.012	0.015
bond angles (°)	1.179	1.3	1.069
Mean B-factors (Å^2)	14.10	59.90	44.6
Ramachandran plot (%)			
Favoured	99.0	98.4	97.7
Outliers	0.0	0.0	0.3

[a]Values in parentheses are for the highest resolution shell.

[b] $R_{sym} = \sum |(I\text{-}<I>)|/\sum(I)$, where I is the observed intensity.

[c] $\sum ||F_{obs}|\text{-}|F_{calc}||/\sum|F_{obs}|$, where $|F_{obs}|$ and $|F_{calc}|$ are observed and calculated structure factor amplitude.

[d]The R_{free} value was calculated with a random 5% subset of all reflections excluded from refinement.

Table 4.2 references: [1]Grochulski et al, 2011; [2] Vagin & Teplyakov, 2010; [3]McCoy et al, 2007.
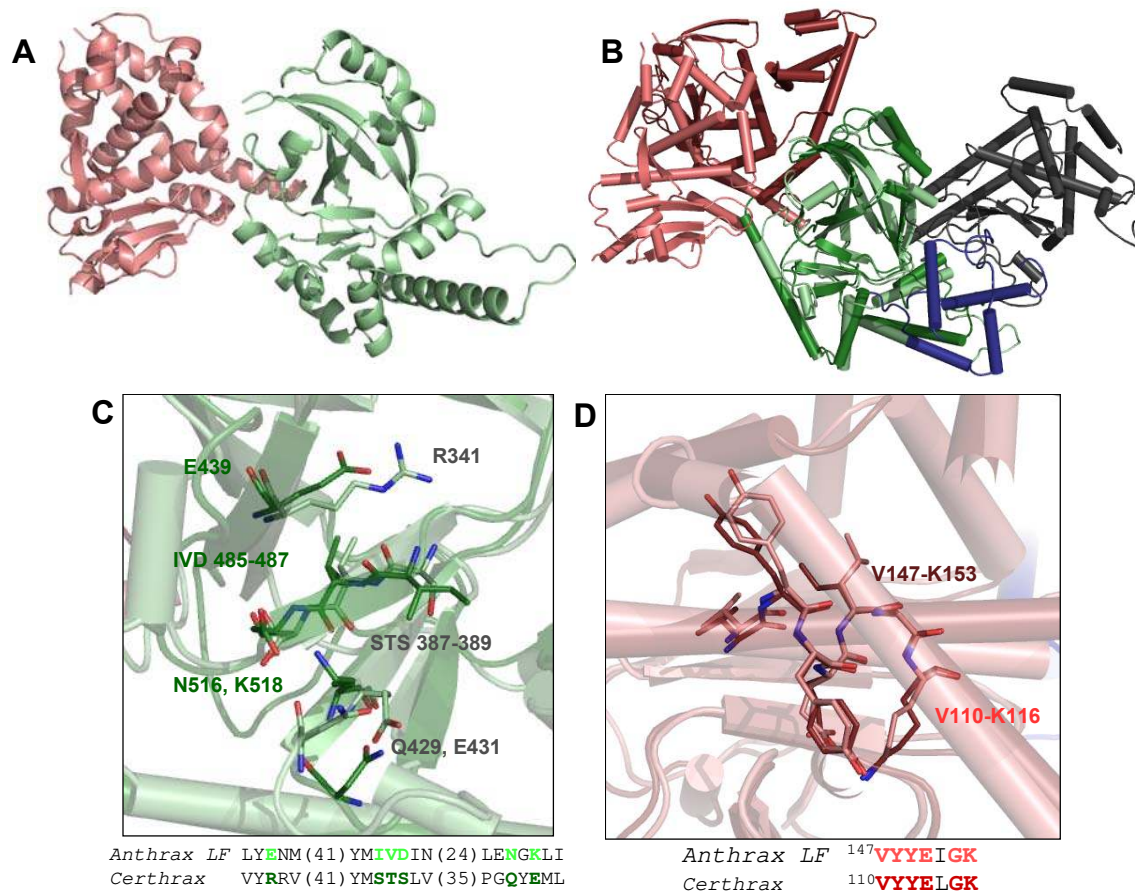
Figure 4.5. Structure of full-length Certhrax compared with anthrax lethal factor.
(A) Crystal structure of full-length Certhrax (no ligand bound). PA-binding domain in pink, mART domain in green, shown in cartoon representation. (B) Superposition of Certhrax (pale pink and green) with anthrax LF (bold red, green, blue and grey), aligned with respect to the mART domains. Domains colored as in Figure 4.1B with the additional anthrax LF insertion domain and zinc metalloprotease domain in blue and grey, respectively. (C) Structural alignment of hallmark active-site residues in the Certhrax mART domain (light green), and aligned residues of anthrax LF (dark green). Highlighted region shown in stick format, and in text beneath. (D) Structural alignment of residues important for PA binding (Lacy et al, 2002) in Certhrax (pink) and anthrax LF (red). Highlighted residues shown in stick representation are shown in text sequence beneath.

4.2.8 The Certhrax catalytic domain

In the catalytic domain, Certhrax is similar to other mART toxins (Figure 4.6). The ARTT loop (residues 424-430) connects β-strands β5 and β6, as in Iota toxin and C3bot (Han et al, 2001, Tsuge et al, 2003) and includes the QxE catalytic motif. The secondary Glu/Gln residue of mARTs, located two residues upstream from the primary catalytic Glu, may play a role in substrate recognition (Vogelsgesang & Aktories, 2006). In actin-targeting toxins that attach ADP-ribose to an Arg residue, this secondary position is a Glu (Laing et al, 2011). In the case of Certhrax, as in the Rho GTPase targeting enzymes that modify an Asn residue, a conserved Gln is present at this position. Additionally, an aromatic (Tyr) residue lies in the middle of the loop in Certhrax, and is conserved among actin- and Rho GTPase-targeting mARTs, and the mammalian Ecto-ARTs, and is also thought to play a role in substrate binding (Holbourn et al, 2006). The STS motif is found on a β-strand and forms a scaffold for the active site. These three residues (387-389) participate in ten hydrogen bonds with other sites within the protein including catalytic residues Arg341 and Gln429, and adjacent β-strands, to stiffen the active site. The PN loop (390-404) connects β-strands β3 and β4, and begins immediately following the STS motif. In the absence of NAD^+, the PN loop is pulled away from the active site, which is not uncommon, and it contains conserved aromatic and Arg residues as seen in actin-targeting and C3-like mARTs, which are known to contribute to NAD^+ binding (Menetrey et al, 2002, Tsuge et al, 2003). In alignment with other C3-like and actin-targeting mARTs, Certhrax contains an α-helix that interacts with NAD^+ in the active site, and includes the conserved sequence (Y-$X_{6/7}$-IN-X_2-L). This sequence is not observed in the toxins of other mART subgroups.
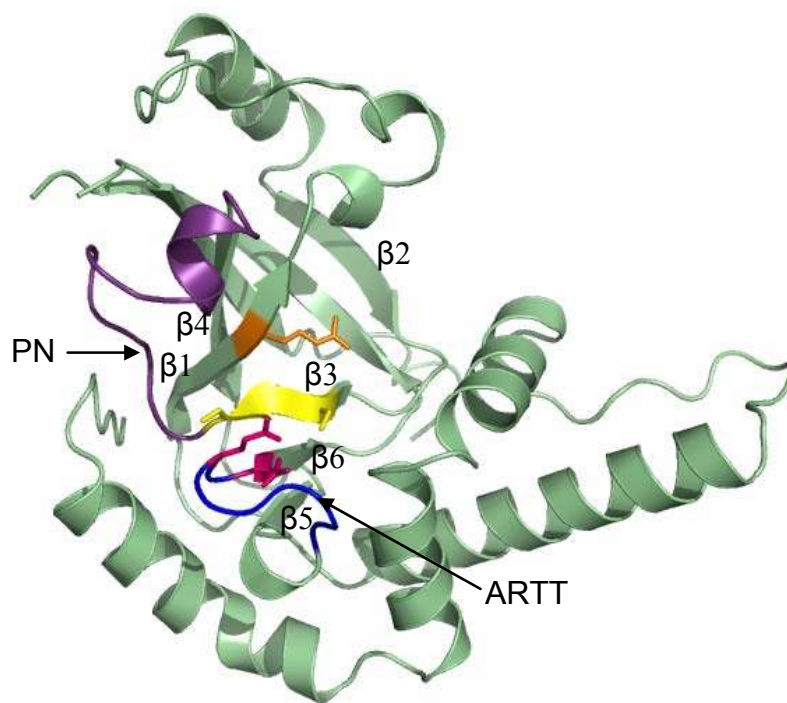
Figure 4.6. Catalytic domain of full-length Certhrax. The C-terminal mART domain of Certhrax shown in pale green, in cartoon format. Hallmark catalytic residues are shown in stick representation in orange (R341), magenta (Q429, E431), and yellow (STS motif 387-389). The PN loop is highlighted in purple, and the ARTT loop in blue.

4.2.9 Inhibition of Certhrax mART activity

A number of small molecule compounds were tested for inhibitory properties against Certhrax (Table 4.3). Several of these have previously been identified as poly-ADP-ribosyltransferase inhibitors (P1, P3 and P6), while others were discovered through a virtual screen for inhibitors against another mART toxin, cholix (V23, V30; Turgeon et al, 2011). Derivatives of P6 (P6C, P6D, P6F and P6G) were synthesized (Sinova, Ic.) in an attempt to improve and elucidate the properties of inhibitor binding and toxin inhibition. Those inhibitors showing the most promise were further characterized using fluorescence-based assays to determine the K_d and IC$_{50}$ for each compound (Table 4.4). Notably, inhibitor P6 shows the most promise as a lead compound for further development ($K_d = 1.7 \pm 0.2$ μM, $K_i = 1.8 \pm 0.4$ μM). This compound differs by only a single oxygen atom from P6D, which is a weaker inhibitor ($K_d = 3.0 \pm 0.3$ μM, $K_i = 22.5 \pm 0.4$ μM). Likewise, P6F and P6G differ by a hexameric ring being exchanged for a chloride ion, with a substantial difference in inhibition due to this change (P6F: $K_d = 3.1 \pm 0.3$ μM, $K_i = 3.6 \pm 0.3$ μM; P6G: $K_d = 2.2 \pm 0.3$ μM, $K_i = >295$ μM). These inhibitors are competitive inhibitors against the NAD$^+$ substrate for this mART toxin family and inhibition plots of two of the best inhibitors, P6F and PJ34, are shown in Figure 4.7. Experimental K_i values were calculated from the data in Figure 4.7 for PJ34 and P6F (14.7 and 2.7 μM, respectively), and correlate well with the calculated K_i values for these inhibitors (9.6 and 3.6 μM, respectively).

To determine whether these inhibitors also have potential *in vivo,* the effectiveness of the most potent inhibitor, P6, was determined in RAW264.7 cells by measuring the EC$_{50}$ at a lethal concentration of Certhrax. The EC$_{50}$ of P6 in the presence

TABLE 4.3

Chemical structures and characteristics of small molecule inhibitors tested against Certhrax
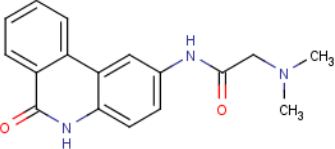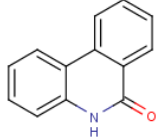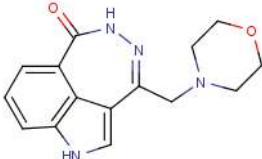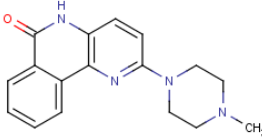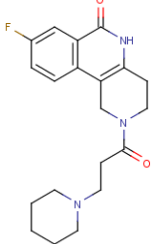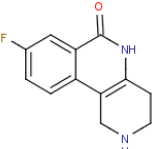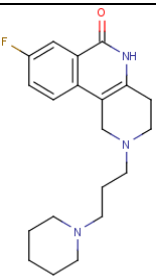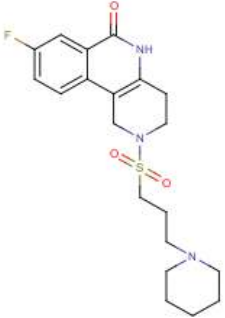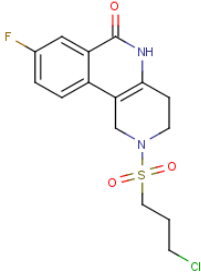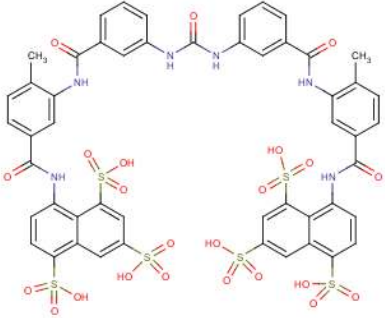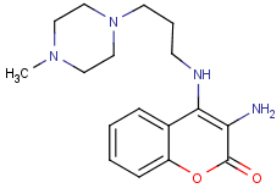
Inhibitor	Chemical structure	Characteristics
PJ34		LogP[a] = 1.87 LogD[b] (5.5) = 0.21 LogD (7.4) = 1.67 MW = 295.34
PJ97A		LogP = 2.74 LogD (5.5) = 2.74 LogD (7.4) = 2.74 MW = 195.22
P1		LogP = 0.61 LogD (5.5) = 0.48 LogD (7.4) = 0.60 MW = 284.31
P3		LogP = 2.46 LogD (5.5) = 0.30 LogD (7.4) = 2.00 MW = 294.35
P6		LogP = 1.13 LogD (5.5) = -2.21 LogD (7.4) = -0.81 MW = 357.42
P6C		LogP = 0.54 LogD (5.5) = -2.44 LogD (7.4) = -0.89 MW = 332.23
P6D		LogP = 1.86 LogD (5.5) = -2.47 LogD (7.4) = -0.50 MW = 343.45

TABLE 4.3 continued

P6F		LogP = 0.73 LogD (5.5) = -2.12 LogD (7.4) = -0.36 MW = 407.51
P6G		LogP = 0.53 LogD (5.5) = 0.53 LogD (7.4) = 0.53 MW = 358.82
Suramin		LogP = 5.58 LogD (5.5) = -8.68 LogD (7.4) = -8.68 MW = 1297.28
V23		LogP = -0.13 LogD (5.5) = -3.07 LogD (7.4) = -1.34 MW = 316.40
V30		LogP = 1.15 LogD (5.5) = 1.15 LogD (7.4) = 1.13 MW = 313.40

[a]LogP is the calculated $\log_{10}$(partition coefficient), where partition coefficient is [compound]$_{octanol}$/[compound]$_{water}$.
[b]LogD pH profiles represent the calculated $\log_{10}$(distribution coefficient), where distribution coefficient is [microspecies]$_{octanol}$/[microspecies]$_{water}$ including ionized and non-ionized microspecies.
Partition coefficients and MW were calculated using ChemAxon software, available at:
(http://intro.bio.umb.edu/111-112/OLLM/111F98/newclogp.html).

TABLE 4.4

Binding and inhibition constants of 12 small molecule
compounds with full-length Certhrax

Inhibitor	K_d (μM)[a]	IC_{50} (μM)[b]	K_i (μM)[c]
P6	1.7 ± 0.2	6.1 ± 1.2	1.8 ± 0.4
P3	3.3 ± 0.4	7.2 ± 2.6	2.1 ± 0.8
Suramin	1.9 ± 0.7	10.6 ± 1.5	3.1 ± 0.4
P6F	3.1 ± 0.3	12.1 ± 1.1	3.6 ± 0.3
P1	1.3 ± 0.2	13.0 ± 2.7	3.9 ± 0.8
PJ97A	1.6 ± 0.6	16.8 ± 1.6	5.0 ± 0.5
PJ34	5.8 ± 2.6	32.3 ± 1.1	9.6 ± 0.3
P6D	3.0 ± 0.3	76.1 ± 1.2	22.5 ± 0.4
V30	0.4 ± 0.3	87.1 ± 1.3	25.8 ± 0.4
P6C	6.8 ± 1.0	121 ± 1.7	35.9 ± 0.5
V23	0.4 ± 0.2	380 ± 3.3	112.4 ± 1.0
P6G	2.2 ± 0.3	>1000	>295

[a] K_d values represent the mean ± S.E. from at least three independent
experiments with at least 9 replicates.
[b] IC_{50} values represent the mean ± S.E. from at least three independent
experiments with at least 6 replicates.
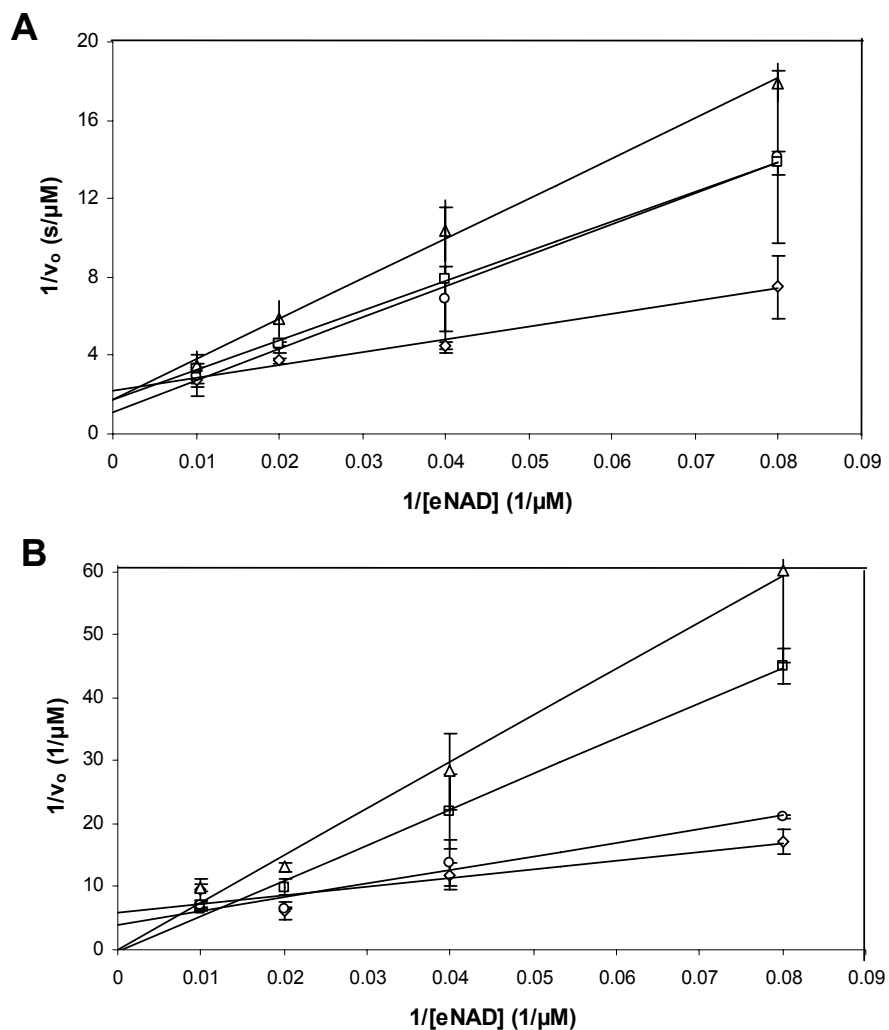
Figure 4.7 Inhibition of Certhrax glycohydrolase activity. Shown are Lineweaver-Burk plots for Certhrax in the presence of various concentrations of inhibitors PJ34 (A) or P6F (B). The glycohydrolase activity of Certhrax was measured with 0 (circles), 6 (squares), 12 (diamonds) and 24 (triangles) μM inhibitor. v_o indicates initial velocity. Error bars, S.E.

of 10 ng/mL toxin (500-fold the LD_{50}) was found to be 5.7 ± 1.2 μM. The maximal effective concentration was approximately 30 μM, which resulted in 90% cell viability. This indicates that the potency of P6 *in vitro* translates to *in vivo* efficacy. Given previous studies that have also shown P6 as a potent inhibitor against exotoxin A of *Pseudomonas aeruginosa* (Turgeon et al, 2011), we now have strong evidence that P6 is an ideal candidate for further development as a therapeutic agent, and that it may have broad-spectrum mART inhibition properties.

4.2.10 Crystal structure of the Certhrax-P6 complex

To further investigate the interactions of Certhrax with active site inhibitors, we determined the 1.96 Å structure of Certhrax in complex with inhibitor P6 (Figure 4.8). This compound is buried in a cleft between the β1 and β3 strands. The P6 phenanthridinone ring is barely exposed to solvent due to enclosure by the ARTT and PN loops. The inhibitor is specifically stabilized in the active site by hydrogen bonds with the Arg342 backbone, located immediately beside the catalytic Arg341, on the β1 sheet, Tyr284 on the α3 helix, and an arene-arene interaction with Tyr398 on the PN loop (Figure 4.8B). The hexameric ring at the opposite end of the inhibitor is flanked on one side by the α3 helix but is otherwise solvent-exposed. Not surprisingly, this end of the molecule is less ordered, with a higher crystallographic B-factor.

4.2.11 Crystal structure of the Certhrax$_{cat}$-PJ34 complex

In collaboration with researchers at the Structural Genomics Consortium in Toronto, we also determined the 1.8 Å structure of the mART domain of Certhrax
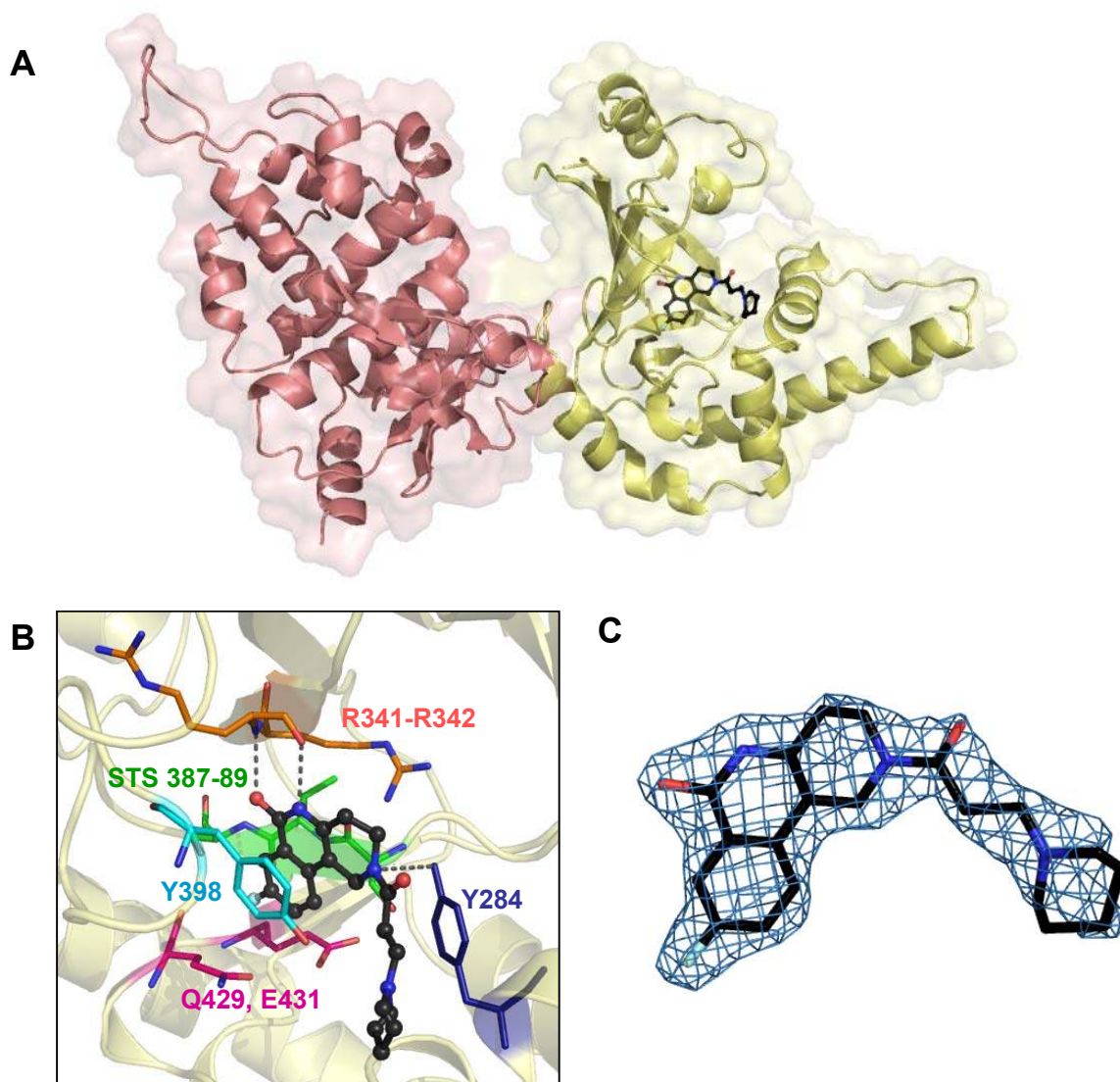
Figure 4.8 Structure of Certhrax with inhibitor P6 bound in the active site. (A) Full-length Certhrax (PA-binding domain, pink; mART domain, yellow) in complex with inhibitor P6 (black). (B) Interactions with P6 in the Certhrax active site. Important active site residues are shown in stick representation (including backbone atoms), and P6 in ball-and-stick (black). Tyr284 (blue) and backbone atoms of Arg342 (orange) form H-bonds with the inhibitor (dashed lines), while Tyr398 (cyan) is involved in aromatic interactions. Other active-site residues are shown in pink (QxE motif) and green (STS motif). (C) Electron density of P6 bound to Certhrax. Simulated annealing omit map around the inhibitor is shown in blue (contoured at 1σ).

(residues 242-468) in complex with inhibitor PJ34 (Figure 4.9). In this case, the inhibitor is bound in the active site by hydrogen bonds with Arg342 and a crystallographically ordered water molecule (Figure 4.9B, note that the N,N-dimethyl acetamide tail of PJ34 is disordered, and therefore was not included in the model).

Superposition of the mART domain of all three structures (Figure 4.10) shows that there are no large domain rearrangements due to inhibitor binding. The r.m.s.d. of the apo-catalytic domain with the P6-bound catalytic domain and with the PJ34-bound structure are 0.59 Å and 0.48 Å, respectively. Interestingly, comparison between the two inhibitor-bound structures gives a lower r.m.s.d. of 0.33 Å when the mART domains are superimposed. The higher similarity of inhibitor-bound structures is in part due to a conserved loop movement upon inhibitor binding. The PN loop, spanning residues 390-398, includes Tyr398 which forms an aromatic interaction with both inhibitor P6 and PJ34. At the furthest point, this loop moves 12 Å towards the active site to allow for the interaction. Comparison between the main chain atoms in the inhibitor-bound structures indicates that the PN loop position is conserved when an inhibitor is bound (r.m.s.d., 0.18 Å), but superposition with the apo-structure is significantly different (r.m.s.d. apo- and PJ34 structures, 2.68 Å; apo- and P6 structures, 2.59 Å) (Figure 4.10B). Other active-site residues including the STS motif, the catalytic Arg341, and the QxE motif, remain relatively unchanged despite inhibitor binding. This is in contrast to other mART enzymes which show structural changes, specifically in the ARTT loop upon substrate binding (Bell & Eisenberg, 1996, Li et al, 1996, Menetrey et al, 2002).
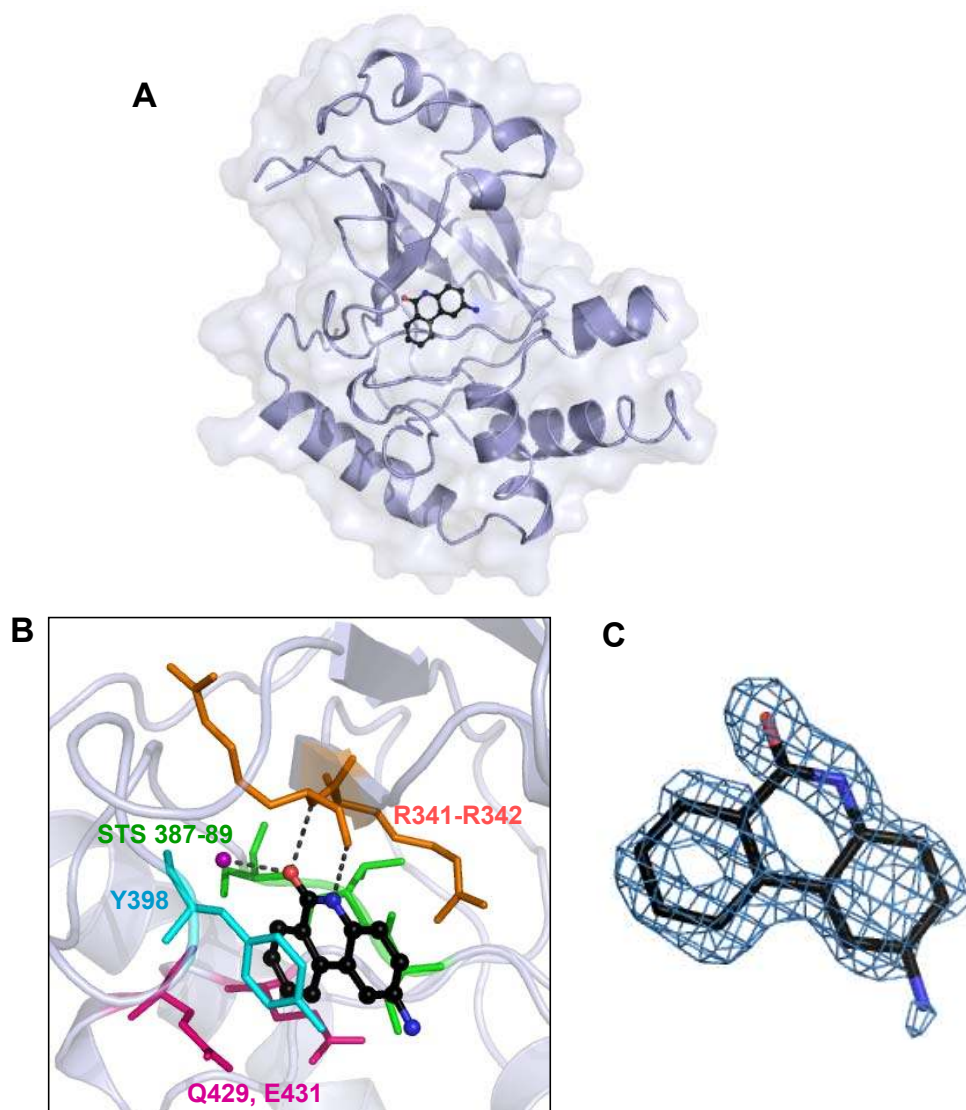
Figure 4.9 Structure of Certhrax with inhibitor PJ34 bound in the active site. (A) Catalytic mART domain of Certhrax (light blue) in complex with inhibitor PJ34 (black). (B) Interactions with PJ34 in the Certhrax active site. Important active-site residues are shown in stick representation, and PJ34 in ball-and-stick (black). Arg342 (orange) and a crystallographically ordered water (purple) form H-bonds with the inhibitor (dashed lines), while Tyr398 (cyan) is involved in aromatic interactions. Other active site residues are colored as in (Figure 4.8B). (C) Electron density of PJ34 bound to Certhrax. Simulated annealing omit map around the inhibitor is shown in blue (contoured at 0.9σ).
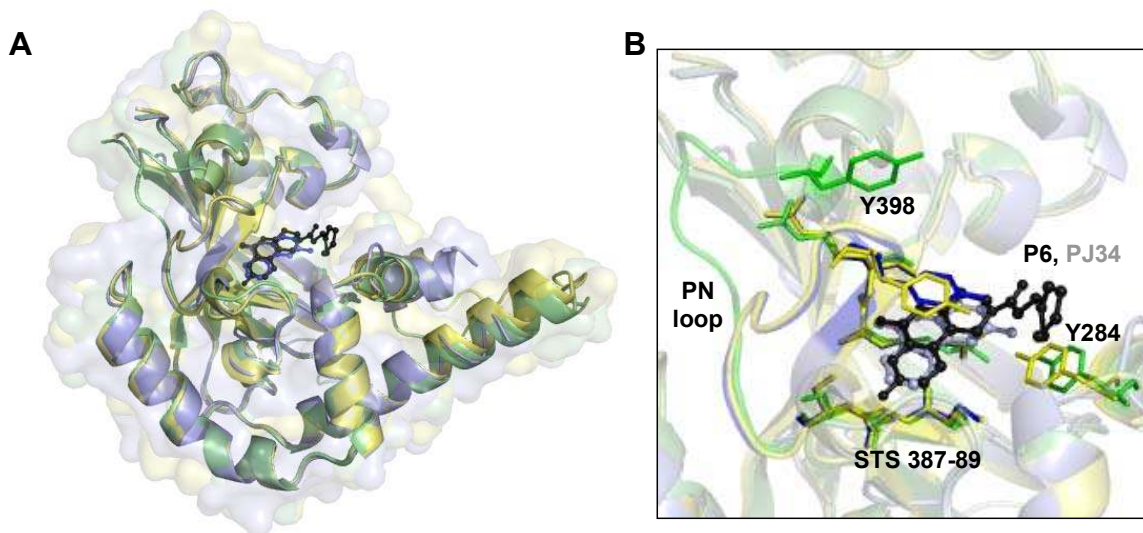
Figure 4.10 Certhrax mART domain with inhibitors bound. (A) Superposition of the Certhrax mART domain from three separate crystal structures including full-length apo-Certhrax (green), full-length Certhrax in complex with P6 (yellow), and Certhrax catalytic domain in complex with PJ34 (blue). (B) Superposition of active-site residues of three catatlytic domain structures, coloured as in (B). Active site residues are shown in stick representation, and Loop 389-398, including Tyr398, is also shown in colour. Inhibitors P6 (black) and PJ34 (grey) are illustrated in ball-and-stick representation.

4.3 DISCUSSION

In this study, we consider the activity of an enzyme from the pathogenic *B. cereus* strain G9241, which causes anthrax-like pneumonia in humans. Researchers are increasingly recognizing *B. cereus* as a dangerous human pathogen, and this strain is a prime example. In general, different species in the *B. cereus* group are defined by plasmid-encoded features. Here we identify Certhrax, which is encoded on the plasmid, pBC218, unique to strain G9241. Most clinical strains of *B. cereus*, including G9241, are often associated with pXO1-like plasmids, encoding homologs of the anthrax toxins (Rasko et al, 2007). However, a pXO2-like plasmid, carrying genes for capsule synthesis and generally required for anthrax disease, is absent. Previous studies have shown that G9241 produces a capsule, but it does not react to poly-D-Glu antibodies, as would be expected for a capsule produced by pXO2. Instead pBC218 and pBCXO1 each lead to the production of separate capsular material (polysaccharide and hyaluronic acid, respectively) to aid in evasion of the host immune response. Both plasmids contribute to anthrax-like disease in mice (Oh et al, 2011), and the ΔpBC218 mutant was found to be 20- to 80-fold less virulent than the wildtype strain. We suggest that Certhrax may contribute to the virulence of this plasmid in the pathogenic strain.

4.3.1 Possible evolution of Certhrax

It is difficult to say whether Certhrax or anthrax LF is the parental factor for the other toxin. Phylogenetic studies have shown that the *B. cereus* species group is actually a single species, although the nomenclature does not reflect this (Papazisi et al, 2011). *B. cereus* G9241 occurs earlier on a phylogenetic tree of the *B. cereus* group than *B.*

anthracis (Stenfors Arnesen et al, 2008), yet the genes involved in anthrax disease are carried by extrachromosomal plasmids, which play an important role in *Bacillus* diversity and allow for horizontal gene transfer. In general, a pathogenic species will lose (rather than gain) characteristics over time, but in this case, Certhrax is missing the metalloprotease domain as compared to anthrax LF, while anthrax LF lacks an active mART domain as compared to Certhrax, so this logic does not help to determine which toxin is the precursor of the other. In the case of an outbreak of anthrax-like infections, an understanding of the causative agents and the ability to identify a responsible strain will be crucial for timely disease control (Salter, 2011). Characterization of participating virulence factors is one important step in this understanding.

Structural alignment of Certhrax with other mART domains indicates that Certhrax aligns approximately as well with the inactive mART domain of anthrax LF (r.m.s.d., 3.9 Å) as with several other mART toxins (r.m.s.d., 1.9-2.5 Å). A primary difference is an 80-residue insertion domain in anthrax LF, which interrupts the mART domain (Pannifer et al, 2001). This helical bundle domain is required for anthrax LF activity (Quinn et al, 1991), but is not required in Certhrax, where the metalloprotease domain is absent. The missing catalytic residues required for mART activity in anthrax LF raise the question of whether Certhrax gained this function over time, and lost the insertion and zinc metalloprotease domain, or whether anthrax LF lost the mART activity and acquired an additional domain. Perhaps the evolution was driven by the redundancy of two highly potent mechanisms of toxicity in a single protein. Alternatively, these two toxins may simply represent two different approaches from a common ancestor to inactivate eukaryotic target proteins and disrupt host cell function.

4.3.2 Certhrax as part of a classic mART subgroup

Here, Certhrax is shown to gain entry to host cells via PA association, in a similar fashion to anthrax LF and EF. Yet, cytotoxicity studies with mammalian cells indicate that Certhrax is 60-fold more toxic than anthrax LF. Certhrax joins actin-targeting VIP2 and Rho GTPase-ribosylating C3cer as mART toxins originating from *B. cereus*. However, Certhrax is unique in its origin from the pathogenic G9241 strain. Certhrax shows some similarity in structure and function to both the actin- and Rho-targeting toxins, but does not clearly align with a single one of these subgroups of mART toxins. Structurally, Certhrax shares the same core fold in the catalytic domain as other mARTs This is reflected by its CATH code, 3.90.176.10, which matches that of other mART domains. (The CATH database classifies protein structures based on their class, architecture, topology and homology (Knudsen, & Wiuf (2010)). The Certhrax ARTT loop contains a secondary catalytic Gln residue as in Rho-targeting toxins, and an aromatic residue mid-loop that is conserved in both actin- and Rho-targeting mARTs. However, the large movement of the ARTT loop upon NAD$^+$ binding that is found in several other mART structures (Bell & Eisenberg, 1996, Li et al, 1996, Menetrey et al, 2002) does not occur upon binding of active site inhibitors in Certhrax. Furthermore, extensive attempts to identify the host protein target of Certhrax have so far been inconclusive. Typical mART substrates, such as eukaryotic elongation factor 2, actin, or RhoA are not modified by Certhrax. We propose that Certhrax may belong to a new class of mARTs, bridging the well-characterized C2- and C3-like mART families, but more intriguingly, also linking the mART toxins to anthrax LF. We are currently working with more exhaustive techniques to identify the natural substrate (see below).

4.3.3 Attempts to elucidate the protein substrate of Certhrax

Concurrent with this work, various techniques were used in attempt to identify the natural host substrate of Certhrax. Unfortunately, these techniques, which can successfully pull out actin as a substrate of Photox, failed to return any true positive results for Certhrax. Modified Western blots using biotinylated-NAD^+, pull-down assays using biotin-NAD^+ and a streptavidin column, and affinity columns with bound Certhrax were all futile. We expect that the natural protein substrate of Certhrax must be of relatively low abundance in host cells, making it difficult to identify. More rigorous high-throughput approaches will be necessary to elucidate its substrate(s); these are discussed further in Chapter 5.

4.3.4 Inhibition of Certhrax

Inhibition studies identified several compounds (competitive inhibitors of the NAD^+ substrate) that will be useful leads in the development of potent inhibitors against Certhrax. Specifically, inhibitor P6 binds and inhibits glycohydrolase activity with low micromolar affinity. Crystal structures of P6 and PJ34 in complex with Certhrax indicate that the inhibitors interact in a common fashion with residues within the binding/catalytic site, as would be expected for competitive inhibitors of the NAD^+ substrate. Specifically, hydrogen bonding with Arg342 and the movement of the PN loop allow an aromatic interaction with Tyr398. The rearrangement of side chains to facilitate this interaction has been seen upon NAD^+-binding to other mART toxins (Han et al, 1999, Menetrey et al, 2002). For example, crystal structures of the NAD^+-bound and free C3bot indicate that

115

upon NAD^+ binding, the primary catalytic Glu shifts (7 Å) to be in position to form H-bonds with the nicotinamide ribose. In addition, a Phe residue of the PN loop changes position to form a stacking interaction with NAD^+, as seen with Tyr398 of Certhrax. However in these examples, there was no large loop movement to correctly position the aromatic side chains, as seen with Certhrax. Analysis of the binding mechanisms in these toxin-inhibitors complexes will be invaluable contributions towards the development of potent therapeutics against Certhrax and related mART toxins. Moreover, since the active site of mART enzymes is reasonably conserved, a powerful inhibitor for Certhrax may be applicable to several other enzymes in this family. Translation of the inhibitory effects to a cell-based system indicate that the P6 inhibitor is not toxic to the cells, can pass through the cell membrane, and retain similar efficacy as demonstrated *in vitro* against the purified enzyme. Arising from these studies, P6 provides an excellent lead compound for the development of more potent inhibitors against Certhrax and other mART toxins.

During the initial stage of this work, the inhibitor suramin gained significant attention because crystals of full-length Certhrax were reproducibly obtained in the presence of this compound. Intriguingly, this compound shows relatively tight binding ($K_d = 1.9 \pm 0.7$), and inhibition of Certhrax ($K_i = 3.1 \pm 0.4$). However, suramin is not seen in the crystal structures, and extensive co-crystallization trials with suramin produced only apo-crystals. The role of suramin in crystallization and inhibition of full-length Certhrax remains an unanswered question.

4.4 CONCLUSION

Altogether, our observations contribute to the understanding of the toxicity of a pathogenic strain of *B. cereus*, G9241, and add a new member to the family of mART toxins. Continued work can lead to the development of more effective therapeutics that target these bacterial virulence factors, and more efficient disease control in the instance of an outbreak of anthrax-like disease.

CHAPTER 5 - CONCLUSION AND FUTURE

DIRECTIONS

5.1 PHOTOX AND CERTHRAX ARE IMPORTANT NEW MART TOXINS

Upon their discovery, antibiotics seemed destined to be the "magic bullet" that would rid the world of lethal bacterial infections. Unfortunately, it is evident that the targeted organisms are developing resistance even more quickly than new antibiotics can be identified. As a result, the pharmaceutical industry has lost some enthusiasm for antibiotic development, for fear that new antibiotics will be obsolete before substantial profit can be made. New approaches must be taken to combat bacterial infections in the face of a declining availability of effective antibiotics. The antivirulence approach elegantly disrupts the toxic virulence factors of an invading pathogen without placing direct evolutionary pressure on the organism itself. In this way, resistance should not be an imminent concern, while the organism's ability to promote infection should be limited. The mART family of toxins contributes to a wide range of diseases and, as such, makes an excellent target for antivirulence therapies.

Here we identified and characterized two new members of the mART family to further our understanding of these harmful enzymes. Photox and Certhrax were each identified through *in silico* methods by screening the genomes of recently sequenced pathogens and looking for the characteristic mART fold and conserved catalytic site residues. Their *in vivo* cytotoxicity in yeast, and the subsequent protection provided when the catalytic residues were altered, indicated that they were indeed novel mART family toxins worthy of further study.

Photox was successfully expressed and purified from *E. coli* inclusion bodies and was shown to covalently modify actin. Mass spectrometric analysis indicated that there was a single ADP-ribose modification at Arg177 of actin. This made Photox the newest

member of the C2-like subgroup of actin-targeting mART toxins. As with other actin-targeting mARTs, actin is the sole primary target of Photox. Using labeled NAD^+, Photox was found to modify α-skeletal actin and nonmuscle β- and γ-actin. Similarly, Iota, Sa, CDTa, and SpvB toxins modify each of these actin isoforms, but are in contrast with C2 which does not modify α-actin. A fluorescence-based assay was used to characterize the kinetic parameters of this new toxin. Photox mART activity exhibited Michaelis-Menten behaviour with respect to the actin and ε-NAD^+ substrates, with a similar rate of activity to Iota toxin. Unlike the binary actin-targeting toxins, Photox did not show glycohydrolase activity in the absence of a protein substrate, again showing similarity to SpvB. Photox shares highest primary sequence homology with SpvB, which also lacks glycohydrolase activity. The 35% identity between Photox and SpvB in the catalytic domain allowed for the creation of a structural model of Photox based on the SpvB crystal structure. While Photox proved recalcitrant to crystallography due to limited solubility, the structural model allowed for visualization of the active site components. All binary toxins include a B-subunit necessary for entry to a host cell. BLAST searches did not reveal a similar component in the *P. luminescens* genome, so we predict that Photox is a non-binary actin-targeting mART, like SpvB. Fluorescence microscopy imaging was used to visualize the colocalization of labeled Photox with actin. In the future, this technique may prove useful for other novel toxins, where the identity of the host protein substrate is unknown. It could also be used to study the time course of the reaction. The characterization of actin-targeting mART toxins such as Photox will aid in the development of effective therapeutics for this whole subgroup.

Certhrax was also successfully expressed and purified from *E. coli*. Like anthrax LF, Certhrax was found to require PA for host cell entry. This opens the door for potential development of inhibitors of PA function, which could stop both LF and Certhrax activity at the stage of receptor-protein interaction. While the host protein substrate of Certhrax remains unknown, it was found to have high glycohydrolase activity, which followed Michaelis-Menten behaviour with respect to the ε-NAD$^+$ substrate. Confocal microscopy was used in an effort to find clues about the host substrate. It was seen that Certhrax localizes to distinct regions within a cell by 10 minutes post-infection. Future studies with a more rigorous approach making use of many different antibodies and time points may provide more information. The crystal structure of full-length Certhrax was determined to 2.2 Å, and the toxin shows similarities to members of both the C2- and C3-like subgroups of mART toxins. Unfortunately, tests with classical substrates of these subgroups gave no sign of ADP-ribose modification using Certhrax. The close structural relationship with anthrax LF likely indicates that one of these toxic proteins likely evolved from the other. More importantly, the continued characterization of either one may translate to an increased understanding of the other. A number of small molecules were tested for inhibitory properties against Certhrax activity, and compound P6 showed the most promise as a lead compound for further development. Efforts are currently under way to increase the potency of this inhibitor, as evidenced by the P6 derivatives which have already been tested and presented in this work. The hope remains that a potent Certhrax inhibitor may also be useful against other mART toxins, which is possible since Certhrax already seems

to bridge both the C2- and C3-like mART subgroups. Interestingly, compound P6 has already been shown to inhibit cholix from *P. aeruginosa* in the DT group mARTs.

5.2 FUTURE DIRECTIONS

5.2.1 Protein substrate identification for new mART toxins

A number of possibilities exist for future studies with Photox, Certhrax, and other mART toxins to enhance our understanding of their mode of action. One of the major unanswered questions in the field is the problem of identifying a host protein substrate for new mART toxins. The natural protein substrate is necessary for more complete and physiologically relevant characterization of a toxin's activity and inhibition. Although many different strategies have already been used, none of them have been successful across a broad range of new toxins. The blot technique employing biotinylated NAD^+ and subsequent mass spectrometric analysis was effective for the identification of eEF2 as a substrate for cholix toxin (Jørgensen et al, 2008), and actin as a substrate for Photox. However, this same method applied to Certhrax was not successful. The mass spectrometric analysis of proteins identified by the blot is efficient only when they can be easily separated from background proteins. Repeated Certhrax blots with biotin-NAD^+ resulted in a number of false positives that were not shown to be Certhrax substrates in an *in vitro* assay. It is likely that the mass spectrometric analysis identified contaminating proteins that were actually higher in concentration in the sample than the *bona fide* substrate protein. It is clear that this blotting technique is useful only in cases where the substrate is in relatively high abundance in a cell lysate, as with eEF2 and actin.

The use of pull-down assays yielded similar negative results. Streptavidin columns were used to try to isolate biotin-ADP-ribosylated proteins from a cell lysate. The lysate treated with toxin and biotinylated-NAD$^+$ was passed through a streptavidin column in the hope that the modified substrate could be captured and identified by mass spectrometric analysis after SDS-PAGE separation. This technique successfully identified actin as a substrate for Photox, but was not effective with Certhrax. Similarly, the use of a column charged with toxin was unable to pull down toxin-substrate complexes with Certhrax. Brand new approaches are necessary to bypass this bottleneck in the characterization of novel mARTs.

A recent collaborative project with the group of Won-Ki Huh in South Korea employs a bimolecular fluorescence complementation assay (BiFC) (Sung & Huh, 2010) in the hopes of elucidating the Certhrax protein substrate. This assay relies on the interaction of two proteins tagged with non-fluorescent fragments of yellow fluorescent protein (YFP). Huh's group has gene-tagged all possible proteins in the yeast genome and can screen them for interactions with a tagged protein of interest such as Certhrax. A test screen with Photox successfully identified interactions with actin-related proteins. We expect that the identification of Certhrax substrate(s) may not be as straight-forward, given the expectation that they are in low abundance. Proteins showing positive interactions with Certhrax from this BiFC screen are currently being purified and tested *in vitro*.

To combat the problem of low abundance substrates in cell lysates, a high-throughput purification and testing approach in yeast may yield promising results. Proteins which show promise as putative mART targets based on historical mART targets or

bioinformatical analysis could be expressed and purified in a high-throughput fashion for efficient testing. This technique is currently under way in our lab through the purification of proteins in 96-well block in a high-throughput approach. Each of the purified proteins will be tested for activity with a mART toxin using a fluorescence-based plate reader assay. The individual expression and purification of each putative substrate should help to overcome the lack of detection due to natural low abundance in a cell lysate. Purifications of proteins showing positive results could then be scaled up. The small G-proteins represent an interesting group for this type of study as several are already known to be mART substrates. Limitations include the inability to assay membrane proteins, and eukaryotic proteins which cannot be easily expressed in *E. coli*.

Additionally, *in silico* tools are becoming increasingly more powerful, and may one day help in the prediction of substrates for novel mART toxins. As more protein structures are added to the Protein Data Bank, it becomes easier to model the structure of new proteins *in silico*. These structures will allow for comparison of novel mART toxins with existing structures and prediction of the important residues involved in substrate recognition. Furthermore, it may become easier in the future to predict protein-protein interactions using bioinformatics tools. Techniques to predict interactions based on known protein complexes are already in the early stages of development (Davis et al, 2007).

5.2.2 Residues involved in substrate recognition

A more thorough understanding of how mART toxins recognize their substrates would help to narrow down the proteins being considered as substrates and aid in the

search for these targets. The large actin-targeting mART subgroup presents a good opportunity to study toxin-substrate interactions. A crystal structure of the toxin-substrate complex is available (Tsuge et al, 2008), and with more than ten members in this subgroup, conserved residues can be studied with a lower frequency of false positive results. Mutagenesis studies with actin could be used to determine the precise roles in substrate recognition of conserved and non-conserved residues at the actin-toxin interface. Since α-skeletal and β/γ non-skeletal actin differ by only a few residues at the toxin-actin interface, specific attention to differences between actin isoforms as targets would give insight into recognition mechanisms of specific C2-like toxins. Focused mutagenesis studies of mART toxins could also be used to continue to build on the work that has been done to date with C2- and C3-like toxins, has shown that a single residue substitution (the secondary catalytic Glu/Gln) can lead to a reversal in substrate recognition from an Asn to an Arg target residue (Vogelsgesang & Aktories, 2006). In addition, a few toxins seem to bridge the C2- and C3-like subgroups of mART toxins, and may provide further insight into substrate recognition mechanisms. Specifically, SpyA is a hybrid between C2- and C3-like toxins (Coye & Collins, 2004). It modifies actin and has an ExE motif like the C2 toxins but is more structurally similar to the C3 toxins, in its small size (25 kDa), high pI (9.1), and 35% identity with other C3 toxins. An in-depth look at similarities and differences within each subgroup may shed light on which SpyA characteristics are responsible for target specificity. An expanded view of residues required for substrate interaction would allow for homologous residues in new mART toxins to be identified, hopefully easing the prediction of substrates for these new toxins.

5.2.1 Role of glycohydrolase activity

The glycohydrolase activity exhibited by many mART toxins presents another intresting avenue of study. While this activity may not hold as much physiological relevance as the mART activity itself, an understanding of which residues play a role will help in the description of transferase activity. A literature review of toxins exhibiting glycohydrolase activity, sequence and structure comparisons, and mutagenesis studies would shed light on which residues are involved. With this knowledge we could hopefully impart or remove glycohydrolase activity from a toxin without altering the mART activity, and could use this information to fill in some gaps in how the mART reaction proceeds. Specifically the role of an N-terminal (non-catalytic) domain of a toxin in glycohydrolase activity would be interesting to study, since most experiments focus solely on the active site residues or catalytic domain.

5.2.3 Mechanism of host cell entry

Not all mART toxins share a common mechanism for gaining entry to host cells. As a result, some toxins are difficult to study *in vivo* without direct intracellular expression. In cases where cell entry is well understood, such as with C2 or Certhrax, associated proteins can be purified and used to assist the host cell uptake of toxin. However, in cases such as Photox, where no obvious binding partner or translocation domain exists, such studies are not trivial. A more focused look at consensus sequences in non-catalytic toxin domains and domains of other well-characterized proteins may provide some clues. Furthermore, recent work by Fehrer et al (2010) indicates that even toxins without a

separate translocation domain may be specifically recognized by the cell to induce endocytosis. Additional studies in this area could determine which protein characteristics signal endocytosis, and if they apply to other mART toxins. Not only would the characterization of cell entry mechanisms allow for ease of use for *in vivo* studies, it may present an additional step in the infection pathway that could be targeted for antivirulence therapies.

5.3 POTENTIAL APPLICATIONS FOR PHOTOX AND CERTHRAX

The identification and characterization of novel mART toxins expands the list of potential applications. Photox presents the case for more work to be done in the area of agricultural applications. The close symbiosis of *P. luminescens* with the *Heterorhabditidae* nematode to destroy insect larvae may be of use for farmers desiring to control insect pests. *B. thuringensis* has been used for nearly a century as a bacterial means of insecticidal protection. Its high specificity makes it an environmentally friendly option, with low risks to humans, animals and beneficial insects. Transgenic cotton and corn crops expressing *B. thuringensis* genes are now common, but early signs of insect resistance suggest it is also time for some fresh options (Tabashnik et al, 2008). It is possible that Photox could one day be used in a similar fashion, either alone or in conjunction with current treatments. Like Photox, Certhrax also opens up avenues for further applications beyond the development of inhibitors or vaccines. Bioterrorism is a growing concern in the United States and throughout the world. The delivery of deadly anthrax spores by mail in 2001 sparked thoughts of possible future attacks of a similar nature. The efficient distribution of a deadly bacterial toxin could pose drastic

consequences if we are not prepared. Certhrax, as a closely related toxin to anthrax LF, can help us to understand the mode of action of LF. The study of new, related toxins may help us to be prepared with therapeutic treatments against potential bio-weapons. The characterization of new toxins in general will increase our understanding of bacterial weaponry, and hopefully aid in the prevention of future bacterial bioterrorism threats.

5.4 CONCLUDING REMARKS

Bacterial infections continue to be a major cause of death worldwide, especially in developing countries. Unfortunately, the dawn of antibiotics was not the infallible cure the world was hoping for. The scientific community continues to seek creative ways to impede the toxic effects of invading pathogens. Antivirulence approaches are showing promise in this regard. The continued identification and characterization of pathogenic virulence factors such as mART toxins will leave us better equipped to develop potent therapeutics against these toxic enzymes.

REFERENCES

Abrami L, Kunz B, Deuquet J, Bafico A, Davidson G, & van der Goot FG (2008) Functional interactions between anthrax toxin receptors and the WNT signalling protein LRP6. *Cell Microbiol* 10: 2509-2519

Abrami L, Liu S, Cosson P, Leppla SH, & van der Goot FG (2003) Anthrax toxin triggers endocytosis of its receptor via a lipid raft-mediated clathrin-dependent process. *J Cell Biol* **160**: 321-328

Adams PD, Afonine PV, Bunkoczi G, Chen VB, Davis IW, Echols N, Headd JJ, Hung LW, Kapral GJ, Grosse-Kunstleve RW, McCoy AJ, Moriarty NW, Oeffner R, Read RJ, Richardson DC, Richardson JS, Terwilliger TC, & Zwart PH (2010) PHENIX: a comprehensive Python-based system for macromolecular structure solution. *Acta Crystallogr D Biol Crystallogr* **66**: 213-221

Aktories K, Barmann M, Ohishi I, Tsuyama S, Jakobs KH, & Habermann E (1986) Botulinum C2 toxin ADP-ribosylates actin. *Nature* **322**: 390-392

Aktories K, Lang AE, Schwan C, & Mannherz HG (2011) Actin as target for modification by bacterial protein toxins. *FEBS J* **278**: 4526-4543

Aktories K, Rosener S, Blaschke U, & Chhatwal GS (1988) Botulinum ADP-ribosyltransferase C3. Purification of the enzyme and characterization of the ADP-ribosylation reaction in platelet membranes. *Eur J Biochem* **172**: 445-450

Aktories K, Weller U, & Chhatwal GS (1987) *Clostridium botulinum* type C produces a novel ADP-ribosyltransferase distinct from botulinum C2 toxin. *FEBS Lett* **212**: 109-113

Armougom F, Moretti S, Poirot O, Audic S, Dumas P, Schaeli B, Keduas V, & Notredame C (2006) Expresso: automatic incorporation of structural information in multiple sequence alignments using 3D-Coffee. *Nucleic Acids Res* **34**: W604-8

Armstrong S, Li JH, Zhang J, & Merrill AR (2002) Characterization of competitive inhibitors for the transferase activity of *Pseudomonas aeruginosa* exotoxin A. *J Enzyme Inhib Med Chem* **17**: 235-246

Armstrong S & Merrill AR (2001) Application of a fluorometric assay for characterization of the catalytic competency of a domain III fragment of *Pseudomonas aeruginosa* exotoxin A. *Anal Biochem* **292**: 26-33

Avashia SB, Riggins WS, Lindley C, Hoffmaster A, Drumgoole R, Nekomoto T, Jackson PJ, Hill KK, Williams K, Lehman L, Libal MC, Wilkins PP, Alexander J, Tvaryanas A, & Betz T (2007) Fatal pneumonia among metalworkers due to inhalation exposure to *Bacillus cereus* containing *Bacillus anthracis* toxin genes. *Clin Infect Dis* **44**: 414-416

Ballweber E, Galla M, Aktories K, Yeoh S, Weeds AG, & Mannherz HG (2001) Interaction of ADP-ribosylated actin with actin binding proteins. *FEBS Lett* **508**: 131-135

Barth H, Blocker D, Behlke J, Bergsma-Schutter W, Brisson A, Benz R, & Aktories K (2000) Cellular uptake of Clostridium botulinum C2 toxin requires oligomerization and acidification. *J Biol Chem* **275**: 18704-18711

Barth H, Preiss JC, Hofmann F, & Aktories K (1998) Characterization of the catalytic site of the ADP-ribosyltransferase *Clostridium botulinum* C2 toxin by site-directed mutagenesis. *J Biol Chem* **273**: 29506-29511

Bell CE & Eisenberg D (1997a) Crystal structure of diphtheria toxin bound to nicotinamide adenine dinucleotide. *Adv Exp Med Biol* **419**: 35-43

Bell CE & Eisenberg D (1997b) Crystal structure of nucleotide-free diphtheria toxin. *Biochemistry* **36**: 481-488

Bell CE & Eisenberg D (1996) Crystal structure of diphtheria toxin bound to nicotinamide adenine dinucleotide. *Biochemistry* **35**: 1137-1149

Bhakdi S, Bayley H, Valeva A, Walev I, Walker B, Kehoe M, & Palmer M (1996) Staphylococcal alpha-toxin, streptolysin-O, and *Escherichia coli* hemolysin: prototypes of pore-forming bacterial cytolysins. *Arch Microbiol* **165**: 73-79

Bishop AL & Hall A (2000) Rho GTPases and their effector proteins. *Biochem J* **348**: 241-255

Bjarnsholt T & Givskov M (2007) Quorum-sensing blockade as a strategy for enhancing host defences against bacterial pathogens. *Philos Trans R Soc Lond B Biol Sci* **362**: 1213-1222

Bottone EJ (2010) *Bacillus cereus*, a volatile human pathogen. *Clin Microbiol Rev* **23**: 382-398

Candela T & Fouet A (2006) Poly-gamma-Glu in bacteria. *Mol Microbiol* **60**: 1091-1098

Chambers HF & Deleo FR (2009) Waves of resistance: *Staphylococcus aureus* in the antibiotic era. *Nat Rev Microbiol* **7**: 629-641

Chardin P, Boquet P, Madaule P, Popoff MR, Rubin EJ, & Gill DM (1989) The mammalian G protein RhoC is ADP-ribosylated by *Clostridium botulinum* exoenzyme C3 and affects actin microfilaments in Vero cells. *EMBO J* **8**: 1087-1092

Chen VB, Arendall WB, 3rd, Headd JJ, Keedy DA, Immormino RM, Kapral GJ, Murray LW, Richardson JS, & Richardson DC (2010) MolProbity: all-atom structure validation for macromolecular crystallography. *Acta Crystallogr D Biol Crystallogr* **66**: 12-21

Cheng Y & Prusoff WH (1973) Relationship between the inhibition constant (K1) and the concentration of inhibitor which causes 50 per cent inhibition (I50) of an enzymatic reaction. *Biochem Pharmacol* **22**: 3099-3108

Choudhary S, Mathew M, & Verma RS (2011) Therapeutic potential of anticancer immunotoxins. *Drug Discov Today* **16**: 495-503

Coye LH & Collins CM (2004) Identification of SpyA, a novel ADP-ribosyltransferase of *Streptococcus pyogenes*. *Mol Microbiol* **54**: 89-98

Crowley PJ & Martini LG (2001) Enhancing oral absorption in animals. *Curr Opin Drug Discov Devel* **4**: 73-80

Daborn PJ, Waterfield N, Silva CP, Au CP, Sharma S, & Ffrench-Constant RH (2002) A single *Photorhabdus* gene, makes caterpillars floppy (mcf), allows *Escherichia coli* to persist within and kill insects. *Proc Natl Acad Sci USA* **99**: 10742-10747

Davis FP, Barkan DT, Eswar N, McKerrow JH, & Sali A (2007) Host pathogen protein interactions predicted by comparative modeling. *Protein Sci* **16**: 2585-2596

de Castro E, Sigrist CJ, Gattiker A, Bulliard V, Langendijk-Genevaux PS, Gasteiger E, Bairoch A, & Hulo N (2006) ScanProsite: detection of PROSITE signature matches and ProRule-associated functional and structural residues in proteins. *Nucleic Acids Res* **34**: W362-5

Domenighini M & Rappuoli R (1996) Three conserved consensus sequences identify the NAD-binding site of ADP-ribosylating enzymes, expressed by eukaryotes, bacteria and T-even bacteriophages. *Mol Microbiol* **21**: 667-674

Drum CL, Yan SZ, Bard J, Shen YQ, Lu D, Soelaiman S, Grabarek Z, Bohm A, & Tang WJ (2002) Structural basis for the activation of anthrax adenylyl cyclase exotoxin by calmodulin. *Nature* **415**: 396-402

Drysdale M, Heninger S, Hutt J, Chen Y, Lyons CR, & Koehler TM (2005) Capsule synthesis by *Bacillus anthracis* is required for dissemination in murine inhalation anthrax. *EMBO J* **24**: 221-227

Duchaud E, Rusniok C, Frangeul L, Buchrieser C, Givaudan A, Taourit S, Bocs S, Boursaux-Eude C, Chandler M, Charles JF, Dassa E, Derose R, Derzelle S, Freyssinet G, Gaudriault S, Medigue C, Lanois A, Powell K, Siguier P, Vincent R et al (2003) The genome sequence of the entomopathogenic bacterium *Photorhabdus luminescens*. *Nat Biotechnol* **21**: 1307-1313

Duesbery NS, Webb CP, Leppla SH, Gordon VM, Klimpel KR, Copeland TD, Ahn NG, Oskarsson MK, Fukasawa K, Paull KD, & Vande Woude GF (1998) Proteolytic inactivation of MAP-kinase-kinase by anthrax lethal factor. *Science* **280**: 734-737

Egelman EH (2001) Actin allostery again? *Nat Struct Biol* **8**: 735-736

Ehlers RU (2001) Mass production of entomopathogenic nematodes for plant protection. *Appl Microbiol Biotechnol* **56**: 623-633

Emsley P, Lohkamp B, Scott WG, & Cowtan K (2010) Features and development of Coot. *Acta Crystallogr D Biol Crystallogr* **66**: 486-501

Etienne-Manneville S & Hall A (2002) Rho GTPases in cell biology. *Nature* **420**: 629-635

Evans HR, Sutton JM, Holloway DE, Ayriss J, Shone CC, & Acharya KR (2003) The crystal structure of C3stau2 from *Staphylococcus aureus* and its complex with NAD. *J Biol Chem* **278**: 45924-45930

Evans P (2006) Scaling and assessment of data quality. *Acta Crystallogr D Biol Crystallogr* **62**: 72-82

Fahrer J, Kuban J, Heine K, Rupps G, Kaiser E, Felder E, Benz R, & Barth H (2010) Selective and specific internalization of clostridial C3 ADP-ribosyltransferases into macrophages and monocytes. *Cell Microbiol* **12**: 233-247

Fauci AS (2001) Infectious diseases: considerations for the 21st century. *Clin Infect Dis* **32**: 675-685

Fehr D, Burr SE, Gibert M, d'Alayer J, Frey J, & Popoff MR (2007) *Aeromonas* exoenzyme T of *Aeromonas salmonicida* is a bifunctional protein that targets the host cytoskeleton. *J Biol Chem* **282**: 28843-28852

Fernandes P (2006) Antibacterial discovery and development-the failure of success? *Nat Biotechnol* **24**: 1497-1503

ffrench-Constant RH & Bowen DJ (2000) Novel insecticidal toxins from nematode-symbiotic bacteria. *Cell Mol Life Sci* **57**: 828-833

Field M, Rao MC, & Chang EB (1989) Intestinal electrolyte transport and diarrheal disease (2). *N Engl J Med* **321**: 879-883

Fieldhouse RJ & Merrill AR (2008) Needle in the haystack: structure-based toxin discovery. *Trends Biochem Sci* **33**: 546-556

Fieldhouse RJ, Turgeon Z, White D, & Merrill AR (2010) Cholera- and anthrax-like toxins are among several new ADP-ribosyltransferases. *PLoS Comput Biol* **6**: e1001029

Fischer-Le Saux M, Viallard V, Brunel B, Normand P, & Boemare NE (1999) Polyphasic classification of the genus *Photorhabdus* and proposal of new taxa: *P. luminescens* subsp. *luminescens* subsp. nov., *P. luminescens* subsp. *akhurstii* subsp. nov., *P. luminescens* subsp. *laumondii* subsp. nov., *P. temperata* sp. nov., *P. temperata* subsp. *temperata* subsp. nov. and *P. asymbiotica* sp. nov. *Int J Syst Bacteriol* **49 Pt 4**: 1645-1656

Fu ZQ, Guo M, Jeong B, Tian F, Elthon TE, Cerny RL, Staigers D, & Alfano JR (2007) A type III effector ADP-ribosylates RNA-binding proteins and quells plant immunity. *Nature* **447**: 284-289

Fujihara H, Walker LA, Gong MC, Lemichez E, Boquet P, Somlyo AV, & Somlyo AP (1997) Inhibition of RhoA translocation and calcium sensitization by in vivo ADP-ribosylation with the chimeric toxin DC3B. *Mol Biol Cell* **8**: 2437-2447

Galloway TS, Tait RM, & van Heyningen S (1987) Photolabelling of cholera toxin by NAD$^+$. *Biochem J* **242**: 927-930

Genth H, Gerhard R, Maeda A, Amano M, Kaibuchi K, Aktories K, & Just I (2003) Entrapment of Rho ADP-ribosylated by *Clostridium botulinum* C3 exoenzyme in the Rho-guanine nucleotide dissociation inhibitor-1 complex. *J Biol Chem* **278**: 28523-28527

Gill DM & Meren R (1978) ADP-ribosylation of membrane proteins catalyzed by cholera toxin: basis of the activation of adenylate cyclase. *Proc Natl Acad Sci USA* **75**: 3050-3054

Ginalski K, Elofsson A, Fischer D, & Rychlewski L (2003) 3D-Jury: a simple approach to improve protein structure predictions. *Bioinformatics* **19**: 1015-1018

Giorgetti A, Raimondo D, Miele AE, Tramontano A (2005) Evaluating the usefulness of protein structuremodels for molecular replacement. *Bioinformatics* **21**: 72-6

Gouet P, Courcelle E, Stuart DI, & Metoz F (1999) ESPript: analysis of multiple sequence alignments in PostScript. *Bioinformatics* **15**: 305-308

Grochulski P, Fodje MN, Gorin J, Labiuk SL, & Berg R (2011) Beamline 08ID-1, the prime beamline of the Canadian Macromolecular Crystallography Facility. *J Synchrotron Radiat* **18**: 681-684

Gulke I, Pfeifer G, Liese J, Fritz M, Hofmann F, Aktories K, & Barth H (2001) Characterization of the enzymatic component of the ADP-ribosyltransferase toxin CDTa from *Clostridium difficile*. *Infect Immun* **69**: 6004-6011

Gupta P, Singh A, Chauhan V, & Bhatnagar R (2001) Involvement of residues 147VYYEIGK153 in binding of lethal factor to protective antigen of *Bacillus anthracis*. *Biochem Biophys Res Commun* **280**: 158-163

Han S, Arvai AS, Clancy SB, & Tainer JA (2001) Crystal structure and novel recognition motif of rho ADP-ribosylating C3 exoenzyme from *Clostridium botulinum*: structural insights for recognition specificity and catalysis. *J Mol Biol* **305**: 95-107

Han S, Craig JA, Putnam CD, Carozzi NB, & Tainer JA (1999) Evolution and mechanism from structures of an ADP-ribosylating toxin and NAD complex. *Nat Struct Biol* **6**: 932-936

Hentzer M, Wu H, Andersen JB, Riedel K, Rasmussen TB, Bagge N, Kumar N, Schembri MA, Song Z, Kristoffersen P, Manefield M, Costerton JW, Molin S, Eberl L, Steinberg P, Kjelleberg S, Hoiby N, & Givskov M (2003) Attenuation of *Pseudomonas aeruginosa* virulence by quorum sensing inhibitors. *EMBO J* **22**: 3803-3815

Herman IM (1993) Actin isoforms. *Curr Opin Cell Biol* **5**: 48-55

Hochmann H, Pust S, von Figura G, Aktories K, & Barth H (2006) *Salmonella enterica* SpvB ADP-ribosylates actin at position Arg-177-characterization of the catalytic domain within the SpvB protein and a comparison to binary clostridial actin-ADP-ribosylating toxins. *Biochemistry* **45**: 1271-1277

Hoffmaster AR, Hill KK, Gee JE, Marston CK, De BK, Popovic T, Sue D, Wilkins PP, Avashia SB, Drumgoole R, Helma CH, Ticknor LO, Okinaka RT, & Jackson PJ (2006) Characterization of *Bacillus cereus* isolates associated with fatal pneumonias: strains are closely related to *Bacillus anthracis* and harbor *B. anthracis* virulence genes. *J Clin Microbiol* **44**: 3352-3360

Hoffmaster AR, Ravel J, Rasko DA, Chapman GD, Chute MD, Marston CK, De BK, Sacchi CT, Fitzgerald C, Mayer LW, Maiden MC, Priest FG, Barker M, Jiang L, Cer RZ, Rilstone J, Peterson SN, Weyant RS, Galloway DR, Read TD et al (2004) Identification of anthrax toxin genes in a *Bacillus cereus* associated with an illness resembling inhalation anthrax. *Proc Natl Acad Sci USA* **101**: 8449-8454

Holbourn KP, Shone CC, & Acharya KR (2006) A family of killer toxins. Exploring the mechanism of ADP-ribosylating toxins. *FEBS J* **273**: 4579-4593

Hung DT, Shakhnovich EA, Pierson E, & Mekalanos JJ (2005) Small-molecule inhibitor of *Vibrio cholerae* virulence and intestinal colonization. *Science* **310**: 670-674

Inoue S, Sugai M, Murooka Y, Paik SY, Hong YM, Ohgai H, & Suginaka H (1991) Molecular cloning and sequencing of the epidermal cell differentiation inhibitor gene from *Staphylococcus aureus*. *Biochem Biophys Res Commun* **174**: 459-464

Irving AT, Wang D, Vasilevski O, Latchoumanin O, Kozer N, Clayton AH, Szczepny A, Morimoto H, Xu D, Williams BR, & Sadler AJ (2012) Regulation of actin dynamics by protein kinase R control of gelsolin enforces basal innate immune defense. *Immunity* **36**: 795-806

Jernigan JA, Stephens DS, Ashford DA, Omenaca C, Topiel MS, Galbraith M, Tapper M, Fisk TL, Zaki S, Popovic T, Meyer RF, Quinn CP, Harper SA, Fridkin SK, Sejvar JJ, Shepard CW, McConnell M, Guarner J, Shieh WJ, Malecki JM et al (2001) Bioterrorism-related inhalational anthrax: the first 10 cases reported in the United States. *Emerg Infect Dis* **7**: 933-944

Jones TA, Zou JY, Cowan SW, & Kjeldgaard M (1991) Improved methods for building protein models in electron density maps and the location of errors in these models. *Acta Crystallogr A* **47**: 110-119

Jorgensen R, Merrill AR, & Andersen GR (2006) The life and death of translation elongation factor 2. *Biochem Soc Trans* **34**: 1-6

Jorgensen R, Merrill AR, Yates SP, Marquez VE, Schwan AL, Boesen T, & Andersen GR (2005) Exotoxin A-eEF2 complex structure indicates ADP ribosylation by ribosome mimicry. *Nature* **436**: 979-984

Jorgensen R, Purdy AE, Fieldhouse RJ, Kimber MS, Bartlett DH, & Merrill AR (2008) Cholix toxin, a novel ADP-ribosylating factor from *Vibrio cholerae*. *J Biol Chem* **283**: 10671-10678

Just I, Geipel U, Wegner A, & Aktories K (1990) De-ADP-ribosylation actin by *Clostridium perfringens* Iota-toxin and *Clostridium botulinum* C2 toxin. *Eur J Biochem* **192**: 723-727

Just I, Mohr C, Schallehn G, Menard L, Didsbury JR, Vandekerckhove J, van Damme J, & Aktories K (1992) Purification and characterization of an ADP-ribosyltransferase produced by *Clostridium limosum*. *J Biol Chem* **267**: 10274-10280

Just I, Selzer J, Jung M, van Damme J, Vandekerckhove J, & Aktories K (1995) Rho-ADP-ribosylating exoenzyme from *Bacillus cereus*. Purification, characterization, and identification of the NAD-binding site. *Biochemistry* **34**: 334-340

Kabsch W (2010) Xds. *Acta Crystallogr D Biol Crystallogr* **66**: 125-132

Kabsch W, Mannherz HG, Suck D, Pai EF, & Holmes KC (1990) Atomic structure of the actin:DNase I complex. *Nature* **347**: 37-44

Katada S, Hirokawa T, Oka Y, Suwa M, & Touhara K (2005) Structural basis for a broad but selective ligand spectrum of a mouse olfactory receptor: mapping the odorant-binding site. *J Neurosci* **25**: 1806-1815

Katada T & Ui M (1982) ADP ribosylation of the specific membrane protein of C6 cells by islet-activating protein associated with modification of adenylate cyclase activity. *J Biol Chem* **257**: 7210-7216

Kauppi AM, Nordfelth R, Uvell H, Wolf-Watz H, & Elofsson M (2003) Targeting bacterial virulence: inhibitors of type III secretion in *Yersinia*. *Chem Biol* **10**: 241-249

Klimpel KR, Molloy SS, Thomas G, & Leppla SH (1992) Anthrax toxin protective antigen is activated by a cell surface protease with the sequence specificity and catalytic properties of furin. *Proc Natl Acad Sci USA* **89**: 10277-10281

Knudsen M, & Wiuf C (2010) The CATH database. *Hum Genomics* **4**: 207-12

Kurowski MA & Bujnicki JM (2003) GeneSilico protein structure prediction meta-server. *Nucleic Acids Res* **31**: 3305-3307

Lacy DB, Mourez M, Fouassier A, & Collier RJ (2002) Mapping the anthrax protective antigen binding site on the lethal and edema factors. *J Biol Chem* **277**: 3006-3010

Laing S, Unger M, Koch-Nolte F, & Haag F (2011) ADP-ribosylation of arginine. *Amino Acids* **41**: 257-269

Lang AE, Schmidt G, Schlosser A, Hey TD, Larrinua IM, Sheets JJ, Mannherz HG, & Aktories K (2010) *Photorhabdus luminescens* toxins ADP-ribosylate actin and RhoA to force actin clustering. *Science* **327**: 1139-1142

Lesnick ML, Reiner NE, Fierer J, & Guiney DG (2001) The *Salmonella* spvB virulence gene encodes an enzyme that ADP-ribosylates actin and destabilizes the cytoskeleton of eukaryotic cells. *Mol Microbiol* **39**: 1464-1470

Li M, Dyda F, Benhar I, Pastan I, & Davies DR (1996) Crystal structure of the catalytic domain of *Pseudomonas* exotoxin A complexed with a nicotinamide adenine dinucleotide analog: implications for the activation process and for ADP ribosylation. *Proc Natl Acad Sci USA* **93**: 6902-6906

Margarit SM, Davidson W, Frego L, & Stebbins CE (2006) A steric antagonism of actin polymerization by a S*almonella* virulence protein. *Structure* **14**: 1219-1229

Masignani V, Balducci E, Di Marcello F, Savino S, Serruto D, Veggi D, Bambini S, Scarselli M, Arico B, Comanducci M, Adu-Bobie J, Giuliani MM, Rappuoli R, & Pizza M (2003) NarE: a novel ADP-ribosyltransferase from *Neisseria meningitidis*. *Mol Microbiol* **50**: 1055-1067

McCoy AJ, Grosse-Kunstleve RW, Adams PD, Winn MD, Storoni LC, & Read RJ (2007) Phaser crystallographic software. *J Appl Crystallogr* **40**: 658-674

McGuffin LJ, Street SA, Bryson K, Sorensen SA, & Jones DT (2004) The Genomic Threading Database: a comprehensive resource for structural annotations of the genomes from key organisms. *Nucleic Acids Res* **32**: D196-9

Melnyk RA, Hewitt KM, Lacy DB, Lin HC, Gessner CR, Li S, Woods VL Jr, & Collier RJ (2006) Structural determinants for the binding of anthrax lethal factor to oligomeric protective antigen. *J Biol Chem* **281**: 1630-1635

Menetrey J, Flatau G, Stura EA, Charbonnier JB, Gas F, Teulon JM, Le Du MH, Boquet P, & Menez A (2002) NAD binding induces conformational changes in Rho ADP-ribosylating *Clostridium botulinum* C3 exoenzyme. *J Biol Chem* **277**: 30950-30957

Miller JM, Hair JG, Hebert M, Hebert L, Roberts FJ,Jr, & Weyant RS (1997) Fulminating bacteremia and pneumonia due to *Bacillus cereus*. *J Clin Microbiol* **35**: 504-507

Murshudov GN, Skubak P, Lebedev AA, Pannu NS, Steiner RA, Nicholls RA, Winn MD, Long F, & Vagin AA (2011) REFMAC5 for the refinement of macromolecular crystal structures. *Acta Crystallogr D Biol Crystallogr* **67**: 355-367

Murzin AG, Brenner SE, Hubbard T, & Chothia C (1995) SCOP: a structural classification of proteins database for the investigation of sequences and structures. *J Mol Biol* **247**: 536-540

Nagahama M, Sakaguchi Y, Kobayashi K, Ochi S, & Sakurai J (2000) Characterization of the enzymatic component of Clostridium perfringens Iota-toxin. *J Bacteriol* **182**: 2096-2103

Nemoto Y, Namba T, Kozaki S, & Narumiya S (1991) Clostridium botulinum C3 ADP-ribosyltransferase gene. Cloning, sequencing, and expression of a functional protein in *Escherichia coli*. *J Biol Chem* **266**: 19312-19319

Nordfelth R, Kauppi AM, Norberg HA, Wolf-Watz H, & Elofsson M (2005) Small-molecule inhibitors specifically targeting type III secretion. *Infect Immun* **73**: 3104-3114

Oda T, Iwasa M, Aihara T, Maeda Y, & Narita A (2009) The nature of the globular- to fibrous-actin transition. *Nature* **457**: 441-445

Oh SY, Budzik JM, Garufi G, & Schneewind O (2011) Two capsular polysaccharides enable *Bacillus cereus* G9241 to cause anthrax-like disease. *Mol Microbiol* **80**: 455-470

Ohishi I (1987) Activation of botulinum C2 toxin by trypsin. *Infect Immun* **55**: 1461-1465

O'Neal CJ, Jobling MG, Holmes RK, & Hol WG (2005) Structural basis for the activation of cholera toxin by human ARF6-GTP. *Science* **309**: 1093-1096

Otterbein LR, Graceffa P, & Dominguez R (2001) The crystal structure of uncomplexed actin in the ADP state. *Science* **293**: 708-711

Otto H, Tezcan-Merdol D, Girisch R, Haag F, Rhen M, & Koch-Nolte F (2000) The spvB gene-product of the *Salmonella enterica* virulence plasmid is a mono(ADP-ribosyl)transferase. *Mol Microbiol* **37**: 1106-1115

Otwinowski Z & Minor W (1997) Processing of X-ray Diffraction Data Collected in Oscillation Mode. In *Methods in Enzymology,* Carter CWJ & Sweet R,M. (eds) pp 307-326. Academic Press: New York

Palumbi SR (2001) Humans as the world's greatest evolutionary force. *Science* **293**: 1786-1790

Pannifer AD, Wong TY, Schwarzenbacher R, Renatus M, Petosa C, Bienkowska J, Lacy DB, Collier RJ, Park S, Leppla SH, Hanna P, & Liddington RC (2001) Crystal structure of the anthrax lethal factor. *Nature* **414**: 229-233

Papazisi L, Rasko DA, Ratnayake S, Bock GR, Remortel BG, Appalla L, Liu J, Dracheva T, Braisted JC, Shallom S, Jarrahi B, Snesrud E, Ahn S, Sun Q, Rilstone J, Okstad OA, Kolsto AB, Fleischmann RD, & Peterson SN (2011) Investigating the genome diversity of *B. cereus* and evolutionary aspects of *B. anthracis* emergence. *Genomics* **98**: 26-39

Pastan I, Hassan R, FitzGerald DJ, & Kreitman RJ (2007) Immunotoxin treatment of cancer. *Annu Rev Med* **58**: 221-237

Paterson HF, Self AJ, Garrett MD, Just I, Aktories K, & Hall A (1990) Microinjection of recombinant p21rho induces rapid changes in cell morphology. *J Cell Biol* **111**: 1001-1007

Perieteanu AA, Visschedyk DD, Merrill AR, & Dawson JF (2010) ADP-ribosylation of cross-linked actin generates barbed-end polymerization-deficient F-actin oligomers. *Biochemistry* **49**: 8944-8954

Peterson JW & Ochoa LG (1989) Role of prostaglandins and cAMP in the secretory effects of cholera toxin. *Science* **245**: 857-859

Plotkin SA & Plotkin SL (2011) The development of vaccines: how the past led to the future. *Nat Rev Microbiol* **9**: 889-893

Popoff MR & Boquet P (1988) Clostridium spiroforme toxin is a binary toxin which ADP-ribosylates cellular actin. *Biochem Biophys Res Commun* **152**: 1361-1368

Projan SJ (2003) Why is big Pharma getting out of antibacterial drug discovery? *Curr Opin Microbiol* **6**: 427-430

Pukatzki S, Ma AT, Revel AT, Sturtevant D, & Mekalanos JJ (2007) Type VI secretion system translocates a phage tail spike-like protein into target cells where it cross-links actin. *Proc Natl Acad Sci USA* **104**: 15508-15513

Quinn CP, Singh Y, Klimpel KR, & Leppla SH (1991) Functional mapping of anthrax toxin lethal factor by in-frame insertion mutagenesis. *J Biol Chem* **266**: 20124-20130

Rappuoli R, Black S, & Lambert PH (2011) Vaccine discovery and translation of new vaccine technology. *Lancet* **378**: 360-368

Rasko DA, Rosovitz MJ, Okstad OA, Fouts DE, Jiang L, Cer RZ, Kolsto AB, Gill SR, & Ravel J (2007) Complete sequence analysis of novel plasmids from emetic and periodontal *Bacillus cereus* isolates reveals a common evolutionary history among the *B. cereus*-group plasmids, including *Bacillus anthracis* pXO1. *J Bacteriol* **189**: 52-64

Richard JF, Petit L, Gibert M, Marvaud JC, Bouchaud C, & Popoff MR (1999) Bacterial toxins modifying the actin cytoskeleton. *Int Microbiol* **2**: 185-194

Robbins JB, Schneerson R, Trollfors B, Sato H, Sato Y, Rappuoli R, & Keith JM (2005) The diphtheria and pertussis components of diphtheria-tetanus toxoids-pertussis vaccine should be genetically inactivated mutant toxins. *J Infect Dis* **191**: 81-88

Rubin EJ, Gill DM, Boquet P, & Popoff MR (1988) Functional modification of a 21-kilodalton G protein when ADP-ribosylated by exoenzyme C3 of *Clostridium botulinum*. *Mol Cell Biol* **8**: 418-426

Sack RB (2011) The discovery of cholera-like enterotoxins produced by *Escherichia coli* causing secretory diarrhoea in humans. *Indian J Med Res* **133**: 171-180

Sakurai J, Nagahama M, Hisatsune J, Katunuma N, & Tsuge H (2003) *Clostridium perfringens* Iota-toxin, ADP-ribosyltransferase: structure and mechanism of action. *Adv Enzyme Regul* **43**: 361-377

Salter SJ (2011) You cannot *B. cereus*. *Nat Rev Microbiol* **9**: 83

Schleberger C, Hochmann H, Barth H, Aktories K, & Schulz GE (2006) Structure and action of the binary C2 toxin from *Clostridium botulinum*. *J Mol Biol* **364**: 705-715

Schmitt CK, Meysick KC, & O'Brien AD (1999) Bacterial toxins: friends or foes? *Emerg Infect Dis* **5**: 224-234

Schwan C, Stecher B, Tzivelekidis T, van Ham M, Rohde M, Hardt WD, Wehland J, & Aktories K (2009) *Clostridium difficile* toxin CDT induces formation of microtubule-based protrusions and increases adherence of bacteria. *PLoS Pathog* **5**: e1000626

Sehr P, Joseph G, Genth H, Just I, Pick E, & Aktories K (1998) Glucosylation and ADP ribosylation of Rho proteins: effects on nucleotide binding, GTPase activity, and effector coupling. *Biochemistry* **37**: 5296-5304

Sekine A, Fujiwara M, & Narumiya S (1989) Asparagine residue in the rho gene product is the modification site for botulinum ADP-ribosyltransferase. *J Biol Chem* **264**: 8602-8605

Sept D & McCammon JA (2001) Thermodynamics and kinetics of actin filament nucleation. *Biophys J* **81**: 667-674

Shen Y, Zhukovskaya NL, Guo Q, Florian J, & Tang WJ (2005) Calcium-independent calmodulin binding and two-metal-ion catalytic mechanism of anthrax edema factor. *EMBO J* **24**: 929-941

Stenfors Arnesen LP, Fagerlund A, & Granum PE (2008) From soil to gut: *Bacillus cereus* and its food poisoning toxins. *FEMS Microbiol Rev* **32**: 579-606

Suarez G, Sierra JC, Erova TE, Sha J, Horneman AJ, & Chopra AK (2010) A type VI secretion system effector protein, VgrG1, from *Aeromonas hydrophila* that induces host cell toxicity by ADP ribosylation of actin. *J Bacteriol* **192**: 155-168

Sun J, Maresso AW, Kim JJ, & Barbieri JT (2004) How bacterial ADP-ribosylating toxins recognize substrates. *Nat Struct Mol Biol* **11**: 868-876

Sung MK & Huh WK (2010) *In vivo* quantification of protein-protein interactions in *Saccharomyces cerevisiae* using bimolecular fluorescence complementation assay. *J Microbiol Methods* **83**: 194-201

Tabashnik BE, Gassmann AJ, Crowder DW, & Carriere Y (2008) Insect resistance to Bt crops: evidence versus theory. *Nat Biotechnol* **26**: 199-202

Talbot GH, Bradley J, Edwards JE,Jr, Gilbert D, Scheld M, Bartlett JG, & Antimicrobial Availability Task Force of the Infectious Diseases Society of America (2006) Bad bugs need drugs: an update on the development pipeline from the Antimicrobial Availability Task Force of the Infectious Diseases Society of America. *Clin Infect Dis* **42**: 657-668

Tonello F & Montecucco C (2009) The anthrax lethal factor and its MAPK kinase-specific metalloprotease activity. *Mol Aspects Med* **30**: 431-438

Tsuge H, Nagahama M, Nishimura H, Hisatsune J, Sakaguchi Y, Itogawa Y, Katunuma N, & Sakurai J (2003) Crystal structure and site-directed mutagenesis of enzymatic components from *Clostridium perfringens* Iota-toxin. *J Mol Biol* **325**: 471-483

Tsuge H, Nagahama M, Oda M, Iwamoto S, Utsunomiya H, Marquez VE, Katunuma N, Nishizawa M, & Sakurai J (2008) Structural basis of actin recognition and arginine ADP-ribosylation by *Clostridium perfringens* Iota-toxin. *Proc Natl Acad Sci U S A* **105**: 7399-7404

Turgeon Z, White D, Jorgensen R, Visschedyk D, Fieldhouse R, Mangroo D, & Merrill AR (2009) Yeast as a tool for characterizing mono-ADP-ribosyltransferase toxins. *FEMS Lett* **300**: 97-106

Turgeon Z, Jorgensen R, Visschedyk D, Edwards PR, Legree S, McGregor C, Fieldhouse RJ, Mangroo D, Schapira M, & Merrill AR (2011) Newly discovered and characterized antivirulence compounds inhibit bacterial mono-ADP-ribosyltransferase toxins. *Antimicrob Agents Chemother* **55**: 983-991

Unnikrishnan M, Rappuoli R, & Serruto D (2012) Recombinant bacterial vaccines. *Curr Opin Immunol* **24**: 337-342

Vagin A, & Teplyakov A (2010) Molecular replacement with MOLREP. *Acta Crystallogr. D Biol. Crystallogr*. **66**: 22-25

Van Ness BG, Howard JB, & Bodley JW (1980) ADP-ribosylation of elongation factor 2 by diphtheria toxin. NMR spectra and proposed structures of ribosyl-diphthamide and its hydrolysis products. *J Biol Chem* **255**: 10710-10716

Vandekerckhove J, Schering B, Barmann M, & Aktories K (1987) *Clostridium perfringens* Iota toxin ADP-ribosylates skeletal muscle actin in Arg-177. *FEBS Lett* **225**: 48-52

Vandekerckhove J & Weber K (1978) At least six different actins are expressed in a higher mammal: an analysis based on the amino acid sequence of the amino-terminal tryptic peptide. *J Mol Biol* **126**: 783-802

Vilches S, Wilhelms M, Yu HB, Leung KY, Tomas JM, & Merino S (2008) *Aeromonas hydrophila* AH-3 AexT is an ADP-ribosylating toxin secreted through the type III secretion system. *Microb Pathog* **44**: 1-12

Visschedyk DD, Perieteanu AA, Turgeon ZJ, Fieldhouse RJ, Dawson JF, & Merrill AR (2010) Photox, a novel actin-targeting mono-ADP-ribosyltransferase from *Photorhabdus luminescens*. *J Biol Chem* **285**: 13525-13534

Visschedyk D, Rochon A, Tempel W, Dimov S, Park HW, & Merrill AR. (2012) Certhrax toxin, an Anthrax related ADP-ribosyltransferase from *Bacillus cereus*. *J Biol Chem*, [ePub ahead of Print], PMID 22992735.

Vitale G, Pellizzari R, Recchi C, Napolitani G, Mock M, & Montecucco C (1998) Anthrax lethal factor cleaves the N-terminus of MAPKKs and induces tyrosine/threonine phosphorylation of MAPKs in cultured macrophages. *Biochem Biophys Res Commun* **248**: 706-711

Vogelsgesang M & Aktories K (2006) Exchange of glutamine-217 to glutamate of *Clostridium limosum* exoenzyme C3 turns the asparagine-specific ADP-ribosyltransferase into an arginine-modifying enzyme. *Biochemistry* **45**: 1017-1025

Wallner B, Larsson P, & Elofsson A (2007) Pcons.net: protein structure prediction meta server. *Nucleic Acids Res* **35**: W369-74

Waterfield NR, Bowen DJ, Fetherston JD, Perry RD, & ffrench-Constant RH (2001) The tc genes of *Photorhabdus*: a growing family. *Trends Microbiol* **9**: 185-191

Waterfield NR, Ciche T, & Clarke D (2009) *Photorhabdus* and a host of hosts. *Annu Rev Microbiol* **63**: 557-574

Wegner A & Aktories K (1988) ADP-ribosylated actin caps the barbed ends of actin filaments. *J Biol Chem* **263**: 13739-13742

Weigt C, Just I, Wegner A, & Aktories K (1989) Nonmuscle actin ADP-ribosylated by botulinum C2 toxin caps actin filaments. *FEBS Lett* **246**: 181-184

Weldon JE & Pastan I (2011) A guide to taming a toxin--recombinant immunotoxins constructed from *Pseudomonas* exotoxin A for the treatment of cancer. *FEBS J* **278**: 4683-4700

West RE Jr, Moss J, Vaughan M, Liu T, & Liu TY (1985) Pertussis toxin-catalyzed ADP-ribosylation of transducin. Cysteine 347 is the ADP-ribose acceptor site. *J Biol Chem* **260**: 14428-14430

Wiegers W, Just I, Muller H, Hellwig A, Traub P, & Aktories K (1991) Alteration of the cytoskeleton of mammalian cells cultured in vitro by *Clostridium botulinum* C2 toxin and C3 ADP-ribosyltransferase. *Eur J Cell Biol* **54**: 237-245

Wilde C, Chhatwal GS, Schmalzing G, Aktories K, & Just I (2001) A novel C3-like ADP-ribosyltransferase from *Staphylococcus aureus* modifying RhoE and Rnd3. *J Biol Chem* **276**: 9537-9542

Wilde C, Just I, & Aktories K (2002) Structure-function analysis of the Rho-ADP-ribosylating exoenzyme C3stau2 from *Staphylococcus aureus*. *Biochemistry* **41**: 1539-1544

Wilde C, Vogelsgesang M, & Aktories K (2003) Rho-specific *Bacillus cereus* ADP-ribosyltransferase C3cer cloning and characterization. *Biochemistry* **42**: 9694-9702

Wilkinson P, Waterfield NR, Crossman L, Corton C, Sanchez-Contreras M, Vlisidou I, Barron A, Bignell A, Clark L, Ormond D, Mayho M, Bason N, Smith F, Simmonds M, Churcher C, Harris D, Thompson NR, Quail M, Parkhill J, & Ffrench-Constant RH (2009) Comparative genomics of the emerging human pathogen *Photorhabdus asymbiotica* with the insect pathogen *Photorhabdus luminescens*. *BMC Genomics* **10**: 302

Wilson BA, Reich KA, Weinstein BR, & Collier RJ (1990) Active-site mutations of diphtheria toxin: effects of replacing glutamic acid-148 with aspartic acid, glutamine, or serine. *Biochemistry* **29**: 8643-8651

Wolf K, Betts HJ, Chellas-Gery B, Hower S, Linton CN, & Fields KA (2006) Treatment of *Chlamydia trachomatis* with a small molecule inhibitor of the *Yersinia* type III secretion system disrupts progression of the chlamydial developmental cycle. *Mol Microbiol* **61**: 1543-1555

Yamaguchi T, Hayashi T, Takami H, Ohnishi M, Murata T, Nakayama K, Asakawa K, Ohara M, Komatsuzawa H, & Sugai M (2001) Complete nucleotide sequence of a *Staphylococcus aureus* exfoliative toxin B plasmid and identification of a novel ADP-ribosyltransferase, EDIN-C. *Infect Immun* **69**: 7760-7771

Yates SP, Jorgensen R, Andersen GR, & Merrill AR (2006) Stealth and mimicry by deadly bacterial toxins. *Trends Biochem Sci* **31**: 123-133

Yates SP & Merrill AR (2005) Characterization of oxidized nicotinamide adenine dinucleotide (NAD$^+$) analogues using a high-pressure-liquid-chromatography-based NAD$^+$-glycohydrolase assay and comparison with fluorescence-based measurements. *Anal Biochem* **340**: 41-51

Yates SP, Taylor PL, Jorgensen R, Ferraris D, Zhang J, Andersen GR, & Merrill AR (2005) Structure-function analysis of water-soluble inhibitors of the catalytic domain of exotoxin A from *Pseudomonas aeruginosa*. *Biochem J* **385**: 667-675

Zhou GC, Parikh SL, Tyler PC, Evans GB, Furneaux RH, Zubkova OV, Benjes PA, & Schramm VL (2004) Inhibitors of ADP-ribosylating bacterial toxins based on oxacarbenium ion character at their transition states. *J Am Chem Soc* **126**: 5690-5698

Zornetta I, Brandi L, Janowiak B, Dal Molin F, Tonello F, Collier RJ, & Montecucco C (2010) Imaging the cell entry of the anthrax oedema and lethal toxins with fluorescent protein chimeras. *Cell Microbiol* **12**: 1435-1445